Nano Materials Science xxx (xxxx) xxx

Contents lists available at ScienceDirect

Nano Materials Science

journal homepage: www.keaipublishing.com/cn/journals/nano-materials-science/

Recent engineering strategies for enhancing C_{2+} product formation in copper-catalyzed CO_2 electroreduction

Muhammad Shakir Hussain [a], Sheraz Ahmed [b], Muhammad Irshad [a], Syeda Sidra Bibi [a], Muhammad Asif [c], Farooq Sher [d,*], Muhammad Kashif Khan [a,c,**]

[a] School of Chemical Engineering, Sungkyunkwan University, 2066, Seobu-Ro, Jangan-Gu, Suwon, Gyeong Gi-Do, 16419, Republic of Korea
[b] SKKU Advanced Institute of Nano Technology (SAINT), 2066, Seobu-Ro, Jangan-Gu, Suwon, Gyeong Gi-Do, 16419, Republic of Korea
[c] School of Mechanical Engineering, Sungkyunkwan University, 2066, Seobu-Ro, Jangan-Gu, Suwon, Gyeong Gi-Do, 16419, Republic of Korea
[d] Department of Engineering, School of Science and Technology, Nottingham Trent University, Nottingham, NG11 8NS, United Kingdom

ARTICLE INFO

Keywords:
Electroreduction
Cu-based catalysts
C_2 products
Structural engineering
Operando techniques

ABSTRACT

The conversion of carbon dioxide (CO_2) into hydrocarbons through electrochemical CO_2 reduction reaction (eCO_2RR) shows a promising method to reduce CO_2 levels and decrease reliance on fossil fuels in the years to come. Copper-based electrocatalysts exhibit a pronounced inclination for C–C coupling, drawing considerable interest as a favored metal catalyst for generating C_{2+} products through CO_2RR. However, CO_2RR still has some obstacles including product selectivity, higher overpotential, low Faradic efficiency (FE), stability, and current density (CD). Therefore, advancement in this field enables us to comprehend the complex multi-proton electron transfer during C–C coupling and engineering strategies to improve FE and CD. Herein, this review presents some key features of Cu-based catalysts as an electrocatalyst for C_2 product formation while addressing the industrial challenges that hinder commercialization of CO_2RR. In addition, recent strategies on Cu-based catalysts, synthesis strategies, advanced characterizations, and mechanistic investigations via theoretical simulations have been presented. Furthermore, recent approaches towards the composition, oxidation states, and active facets have been presented. Thus, the most favorable mechanism and possible pathways to synthesize C_{2+} products have been explained using theoretical calculations.

1. Introduction

The prodigious contest of new technology, industrialization, and economic growth in 20th century has been perceived to be rapid energy consumption [1]. Fossil fuel is the major source of energy to fulfill the energy requirement globally [2–4]. With the advancements in unconventional crude oil upgrading [5,6] and utilization of other petroleum resources [7–9], environmental concerns are increasing rapidly [10]. The combustion of large-scale fossil fuels including heteroatom components (NO_x, SO_x, and particulate matter) and greenhouse emissions erupt into severe issues like global warming and climate change [11,12]. The atmospheric CO_2 concentrations surpassed 424 parts per million (ppm) in 2024, with projections indicating an anticipated rise to 600 ppm, increasing at an annual rate of 2.5 ppm [13].

Not only does this pose a threat to the natural equilibrium of ecosystems, but it also jeopardizes the survival of human beings on Earth. To diminish the increasing concentration of CO_2 in the atmosphere which contributes 2 to 4 times more than other gases including ozone, nitrous oxides, and aerosol [14], the various strategies for CO_2 reduction and conversion including thermochemical [15–21], photochemical [22,23], electrochemical [24–31], and photoelectrochemical [32,33] methods have been adopted to convert CO_2 into valuable chemicals to maintain the dynamic carbon balance. Considering these attractive strategies, the most effective way is eCO_2RR (Electrochemical CO_2 reduction reaction) under various reaction conditions (mild and high pressure), reusable electrolytes, and sustainable driving force through potential synergy using electricity [34]. Moreover, to reduce CO_2 emissions, several other techniques like solid oxide fuel cells [35], water splitting [36], and biomass conversion [37,38] were also employed for the production of renewable energy to mitigate the dependency on fossil fuels.

CO_2 exhibits chemical inertness with a linear C=O bond energy of 750 kJ/mol, demanding significantly higher energy compared to other

* Corresponding author.
** Corresponding author.
E-mail addresses: Farooq.Sher@ntu.ac.uk (F. Sher), kashifkhan@skku.edu (M.K. Khan).

https://doi.org/10.1016/j.nanoms.2024.09.001

Please cite this article as: M.S. Hussain et al., Recent engineering strategies for enhancing C_{2+} product formation in copper-catalyzed CO_2 electroreduction, Nano Materials Science , https://doi.org/10.1016/j.nanoms.2024.09.001

carbon bonds such as C–H (411 kJ/mol), C–C (336 kJ/mol), and C–O (327 kJ/mol) [39]. Therefore, overcoming the energy barrier to reduce CO_2 into desirable products via CO_2RR is challenging. Despite criticism of the practical applications of CO_2RR, the advances achieved in the field of eCO_2RR hold significant importance, and further exploration needs to be considered, along with the understanding of kinetics and thermodynamic mechanisms. Secondly, the competition between hydrogen evolution reaction (HER) and CO_2RR, owing to their similar reduction potential, the insights into the mechanism behind the design of an efficient catalyst for the suppression of HER should be considered. Finally, the tremendous challenge to achieve the desired product through various eCO_2RR pathways with the highest FE (faradaic efficiency) is the main concern in eCO_2RR. In addition, the multiple protons coupled electrns are required to produce C_2 and C_{2+} products, resulting in complex reaction pathways [40]. Due to the complex reaction mechanism, the products are significantly influenced by the sensitivity of the electrocatalytic reaction conditions including electrolyte concentration [34], overpotential [41], pH [42,43], catalyst morphology [43], particle size [40], electrode potential [42,44], additives [45], electrolyte cation [46], and reactor design [28], respectively, which is critical for the progress in the development of CO_2RR.

The development of various materials for the electrocatalytic reduction of CO_2 is summarized in Fig. 1. From the 1950s to the 1990s, the CO_2RR was conducted on various transition metal-based catalysts (copper, zinc, and non-transition metal mercury, etc.), which resulted in the formation of CO_2 to formate [47–54]. Later from 1990 to 2000, the CO_2RR was studied over various metal catalysts including Pt, Au, Co, Ni, and Cu which yielded low selectivity toward C_2 products [55–62]. In late 2003, the selectivity towards C_2 and C_{2+} products was further improved using various crystal structures of copper [63,64]. In 2004, a drastic increase in the FE (63%) of ethylene was observed using Cu catalyst, which revolutionized the history of copper catalyst towards C_2 hydrocarbons [65]. From 2005 to 2015, the FE of C_{2+} hydrocarbons was further improved from 40 to 60% due to catalyst engineering strategies [31, 66–84]. From 2016 to 2024, the advancement involved in the revolution of copper catalysts toward C_2 products, reveals their significance in the field of hydrocarbons via CO_2RR [34,43,85–100]. Considering the revolutionary evolution from CO_2RR to C_2, based on structural optimization [101], theoretical calculations [81,82,102], and operando characterization techniques [103], FE and CD (current density) have been greatly enhanced. Previously, several review articles [13,104,105] for CO_2RR have been published but their area of interest in particular studies was related to the catalyst chemistry [106–109], reaction mechanism [102,110], product selectivity, morphological effect [111–113], material design [114], and fundamentals of CO_2RR [40]. Furthermore, numerous reviews have focused on the immobilization of molecular catalysts onto electrode surfaces for CO_2RR, catering to the specific interests of readers [115,116]. Considering the importance of eCO_2RR, a comprehensive review particularly considering the importance of all the aspects towards the advancement of FE and CD is required for complete understanding.

In the literature, several reviews have been published to produce C_{2+} products over the Cu-based electrocatalysts. Recently, Chen et al. focused on the progress of flow cells for CO_2RR to C_{2+} products and elaborated on the design principles of CO_2RR to C_{2+} products, the architectures, and the types of flow cells used to enhance the electrochemical performance [117]. In addition, the main strategies for optimizing flow cells (including cathode, anode, ion exchange membrane, and electrolyte) to generate C_{2+} products were described. Another review categorizes Cu-based materials into different groups including Cu metal, Cu oxides, Cu alloys, and Cu SACs, Cu heterojunctions based on their catalytic applications in electrochemical and photochemical for the production of C_{2+} products [118]. Hao et al. explained the recent utilization of in situ/operando characterization methods and ab initio molecular dynamics calculations in tracking structural reconstruction, discovering active sites, and unveiling the reaction mechanisms [119]. Similarly, Cui et al. suggested and highlighted the possible reaction pathways and strategies for CO_2RR, and summarized the progress using in-situ techniques for the elucidation of the mechanism [120]. Jun et al. summarized recent efforts to fine-tune the oxidation state of Cu to increase carbon capture and produce specific C_{2+} compounds to greatly expedite the advancement in the catalyst designs [121]. Furthermore, techno-economic analysis and reaction mechanism during CO_2RR to selectively produce C_2H_4 was briefly illustrated by Carroll et al. [122]. To examine the progress in the acidic media during CO_2RR and focus on reaction environment strategies such as electrocatalyst design, electrode modification, and electrolyte engineering to promote CO_2RR was explained by Zeng et al. [123]. Moreover, insights into the reaction mechanisms via in situ/operando

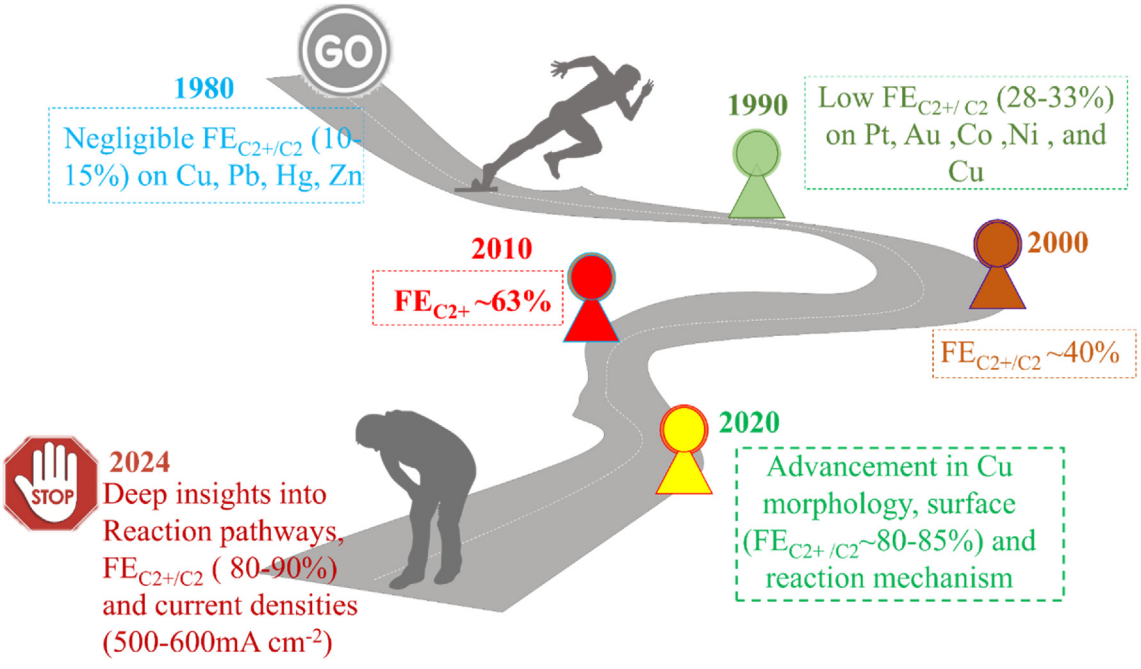

Fig. 1. Timeline for the development of C_2 and C_{2+} products from CO_2RR on Cu-based catalyst.

techniques and theoretical calculations were discussed, along with critical challenges and future directions in acidic CO_2RR technology. Yesupatham et al. discussed the catalyst design strategies, unique structural/morphological features, and product selectivity of diverse copper-based catalysts [124]. Therefore, above mentioned papers on the electrochemical CO_2 reduction to C_{2+} products primarily focus on the reaction parameters including reaction environment, morphology, bimetallic catalysts, reactor configuration, and DFT calculations. However, there is still a lack of research that covers all the fundamental aspects and summarizes them in one article for beginners.

This overview presents a comprehensive exploration of advancements in eCO_2RR over the past few decades, particularly focused on electrocatalytic strategies using copper catalysts. This review delves into catalyst engineering and effective strategies, encompassing metal oxide/metal interactions, oxygen vacancy generation, grain boundary formation, and various aspects of Cu catalysts. It underscores the relationship between interfacial engineering and Cu facets, highlighting their pivotal role in facilitating the production of C_2 products like ethylene, ethanol, and ethane which is crucial for industrial applications. Similarly, high energy density products C_2 (Ethylene, ethanol, and ethane) are demanding products due to their global demand but they have complicated reaction pathways. Furthermore, the review also presents reaction mechanism involved in the formation of C_2 products and their intermediates, vital for comprehending the eCO_2RR process. Given the propensity for C–C coupling reactions over Cu catalyst, CO_2RR to valuable hydrocarbons and alcohols has garnered significant attention. Hence, this study exclusively focuses on elucidating the reaction mechanism, catalyst synthesis strategies, and associated challenges in commercializing eCO_2RR, along with prospects.

2. CO_2RR technologies for Cu-based electrocatalyst

The overall scheme for CO_2RR is presented in Fig. 2 which shows that the industrial revolution and fossil fuel consumption enhanced the CO_2 emissions into the environment exponentially in the last few decades. To overcome these emissions, the electrochemical technologies using various types of electrolyzers such as H-cells [125], MEA (membrane electrode assembly) cells [126,127], microfluidic cells [128], and photo electrocatalysis cells [129] have been widely studied and detailed are presented in Table 1 The laboratory scale electrolyzer which is widely studied to understand the electrochemical mechanism and the basics involved in the eCO_2RR is an H-type cell; while the most efficient electrolyzer designs that utilize gas diffusion electrodes to reduce ohmic losses and mass transfer issues is MEA electrolyzer. Electrocatalysts hold paramount importance in CO_2RR, with Cu and Cu-based catalysts standing out as among the most widely employed due to their intrinsic advantageous characteristics Tables 2-5.

The electrochemical reduction of CO_2 on Cu/Cu-based catalysts results in various products, showcasing their broad product versatility alongside enhanced reaction kinetics and low applied potential requirements [167]. Cu/Cu-based catalysts are primarily recognized for their moderate CO adsorption energy, rendering them exceptional for facilitating the formation of C_2 products, which serve as efficient C–C coupling intermediates. These C_2 products are ethylene, ethane, and ethanol, commonly used as fuel or chemical feedstock. Nonetheless, there remains a need to enhance both product selectivity and current density for industrial scalability. Improvements in these areas require a thorough comprehension of the complex catalyst engineering processes and principles behind eCO_2RR [167,168].

3. Potential of Cu-based electrocatalyst for CO_2RR

The products obtained after eCO_2RR and the number of electrons consumed in the formation of particular products along with their standard potential have been discussed [169]. In past decades, CO and formic acid have been particularly used owing to their techno-economic analysis and are kinetically favorable. On the other hand, variety of CO_2 reduction products, C_2 and C_{2+} products are especially desirable because of their high packing energy density, higher calorific value, and significance to industrial advancements. Notably, ethylene (C_2H_4) stands out as a primary product of copper-based catalysts in eCO_2RR, serving as a foundational feedstock for producing various valuable chemicals such as ethylene oxide, polyethylene, and PVP. Similarly, ethanol is the second most important chemical feedstock to produce ethane, glycol ether,

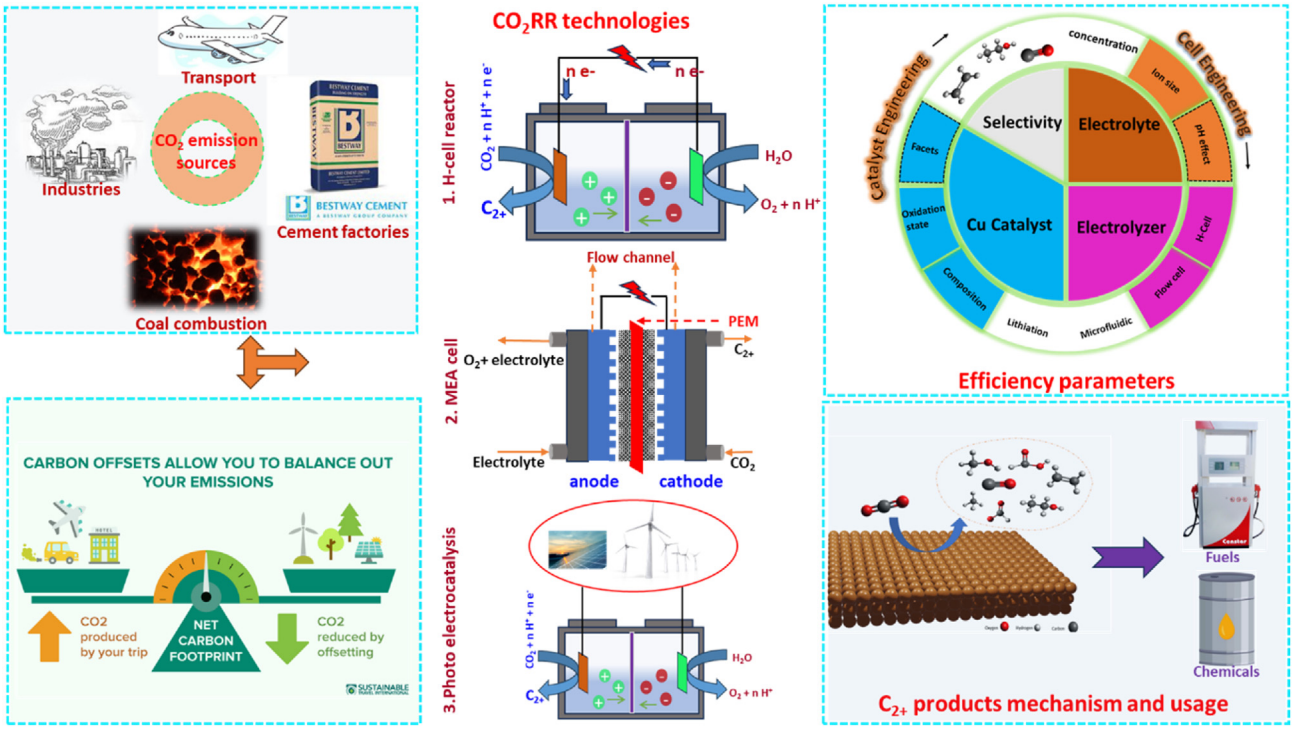

Fig. 2. Process flow diagram for CO_2RR into C_2 and C_{2+} products via various efficiency-dependent parameters.

Table 1
Electrochemical performance of recent Cu-based catalysts for C_{2+} products with their respective FE, CD, and potential at different electrolyte concentrations and reactor types.

Catalyst	Electrolyte	Potential (Vs RHE)	CD (mA cm^{-2})	Partial CD (mA cm^{-2})	FE_{C2+}	Reactor type	References
Cu-Pd bimetallic	1 M KCl	−1.15	200	225	75.6	Flow cell	[130]
Cu/Cu_2O	1 M KOH	−1.06	25	–	58.0	H cell	[131]
Cu_2O@CuBTC	0.1 M $KHCO_3$	−1.05	–	256	64.2	flow cell	[85]
CuO-ZrO_2		−1.50	–	200	82.3	flow cell	[132]
Cu_2O-Cu NCs	1 M KOH	−1.00	500	–	77.4	flow cell	[133]
$Cu@Cu_2O$		−1.08	15	–	79.0	H cell	[134]
Cu_xAl_y-OD	1 M KOH	−1.68	693	565	81.6	flow cell	[135]
Cu@Salen-PIL	1 M KOH	−0.80	–	263	80.9	flow cell	[136]
2.7% CuO_x -R	3 M KOH	−0.90	289	245	84.7	flow cell	[137]
$Cu_{100}Zn_{4.9}$	0.1 M CsI	−1.28	40	–	75.0	H cell	[138]
CuZn	1 M KOH	−1.17	140	–	80.0	H cell	[139]
Cu cavities	1 M KOH	−0.59	186	605	75.6	flow cell	[140]
Cu9Zn1	2 M KOH	−1.15	400	–	88.5	flow cell	[141]
Cu_2O@C/N	0.1 M $KHCO_3$	−0.90	–	245	75.9	flow cell	[142]
B-CuO	0.5 M $KHCO_3$	−1.00	30	–	55.7	flow cell	[137]
Cu2O/Cu	1 M KOH	−1.10	1003	–	80.4	flow cell	[143]
Cu_2O–xSe/Cu/NC	1 M KOH	−1.40	30.44	–	71.6	H cell	[144]
Cu@C	0.1 M CsI	−1.20	–	323	80.5	flow cell	[145]
CuNPs	1 M $KHCO_3$	−3.80	–	356	71.1	flow cell	[146]

Table 2
Summary of CO_2RR electrochemical performance on OD/HD single Cu-atom recently reported literature.

Catalysts	Products	Electrolyte	FE (%)	CD (mA/cm^2)	Potential (V vs RHE)	Reactor	Reference
Cu-Nanowires	Ethylene Ethanol	1.0 M KCl	60.0	50.0	−1.10	H-type	[147]
CuO ultra-thin nanoplate	Ethylene Ethanol	0.5 M KCl	84.0	200	−0.90	Flow cell	[148]
CuO/N_xC	Ethylene	0.1M $NaHCO_3$	36.0	140	−1.25	H-type	[93]
OD Cu	C_2/C_3	0.1 M $KHCO_3$	60.0	10.0	−1.00	H-type	[149]
B-OD Cu	C_{2+}	0.1M $KHCO_3$	48.0	33.4	−1.05	H-type	[93]
Cu oxides/ZnO	Ethylene	0.1M $KHCO_3$	91.0	7.50	−2.5 V vs. Ag/AgCl	H-type	[150]
Cu_2O NPs/C	C_2/C_3	0.1 M $KHCO_3$	74.0	16.0	−1.10	H-type	[91]
Cu_xO	C_2	2.0 M KOH	40.0	234	−1.17	Flow cell	[151]
Cu_2O/ILGS	Ethylene	0.1M $KHCO_3$	31.0	12.0	−1.15	H-type	[152]

Table 3
Summary of hetero-atomic Cu catalyst's electrochemical performance and their parameters.

Catalyst	Products	FE (%)	Electrolyte	Current Density (mA/cm^2)	Potential (Vs RHE)	Reactors	Reference
Cu/Ni tandem electrode	Ethylene Ethanol	62.0	1.0 M KOH	415	−0.70	Flow cell	[153]
CuO/Ni	Ethylene Ethanol	54.0 28.0	1.0 M KOH	1220.8	−3.0	Flow cell	[147]
F–Cu	Ethylene, Ethanol	70.0 20.0	1.0 M KOH	400	−0.97	Flow cell	[154]
Cu–CeO_2	Ethylene, Ethanol	42.0 20.0	0.1 M $KHCO_3$	20.0	−1.30	H-type	[155]
Cu–Au NWs	Ethylene Ethanol	43.0 20.0	0.1 M $KHCO_3$	12.1	−1.25	H-type	[156]
Ag–doped Cu	n-propanol	33.0	1.0 M KOH	4.50	−0.46	Flow cell	[152]
Pd–doped Cu	Alcohols	40.0	1.0 M KOH	277	−0.63	Flow cell	[157]
Cu–Ag	Acetaldehyde	50.0	0.1 M KOH	0.70	−0.53	H-type	[158]
Ag–Ru Co-doped Cu	n-propanol	36.0	1.0 M KOH	300	−2.60	Flow cell	[159]

amines, and esters [105,170]. Several studies suggested that Cu is the only transition metal that can produce C_1 hydrocarbon at a lower overpotential while C_{2+} products and oxygenates at a higher overpotential due to its moderate adsorption/desorption energies of *CO intermediate [147]. Furthermore, *CO adsorption on the Cu surface reduces the competitive HER due to blocking active sites, which alters the *H binding energy (Fig. 3a to b). Thus, CO poisoning of HER on the Cu catalyst enables Cu to be a promising candidate for C_{2+} and C_2 products in aqueous electrolytes. The classification of metal groups according to their specific product selectivity is determined by their binding energy for CO_2RR and HER intermediates, namely *H, *OCHO (adsorbed over catalyst via oxygen), *COOH (attached over catalyst via a carbon atom), and *CO. Copper catalysts possess a distinctive capability to yield C_{2+} products owing to their negative adsorption energy for *CO (−0.78 eV, by theoretical calculations) but positive adsorption energy for *H, facilitating the production of C_2 and C_{2+} products with greater ease, as depicted in Fig. 3.

The metals/metal alloys have been proven to be effective in selectivity and efficiency which can be modified through variation in the metal particle size, morphology, exposed surface/crystal facets, surface functionalization, controlling catalyst chemical states, porosity, or

Table 4
Summary of CO_2RR key performance indicators based on Cu nanocrystal catalyst.

Catalyst	Products	FE (%)	Electrolyte	Current density (mA/cm^2)	Potential (Vs RHE)	Reactors	Reference
Cu nanowire	Ethylene	60.0	1.0 M KCl	50.0	−1.10	H-cell	[147]
Cu	Ethanol Propanol	53.0 18.0	0.1 M $KHCO_3$	180	−3.50	H-cell	[88]
SW-Cu_2O	Ethylene Ethanol	60.0	1.0 M KCl	60.0	−1.50	H-cell	[160]
Cu single-atomic catalyst	C_2H_4	71.0	1.0 M KOH	16.5	−0.70	H-type	[89]
Cu-Cu dual-atomic catalyst	C_{2+}	91.0	0.1 M $KHCO_3$	90.0	−1.66	Flow cell	[161]
fragmented Cu	n-propanol	20.0	1.0 M $KHCO_3$	8.50	−0.45	H-type	[162]
Cu nanocavity	n-propanol	21.0	1.0 M KOH	7.80	−0.56	H-type	[163]
Ligand Cu_2O NCs	Ethylene C_{2+}	50.0 73.0	1.0 M KOH	250	−1.70	Flow cell	[164]
Multi Hollow Cu_2O	Ethylene	75.0 20.0	2.0 M KOH	342	−0.61	Flow cell	[165]
Cu NPs	Ethylene Ethanol	60.0 20.0	0.5 M KOH	300	−1.20	Flow cell	[166]

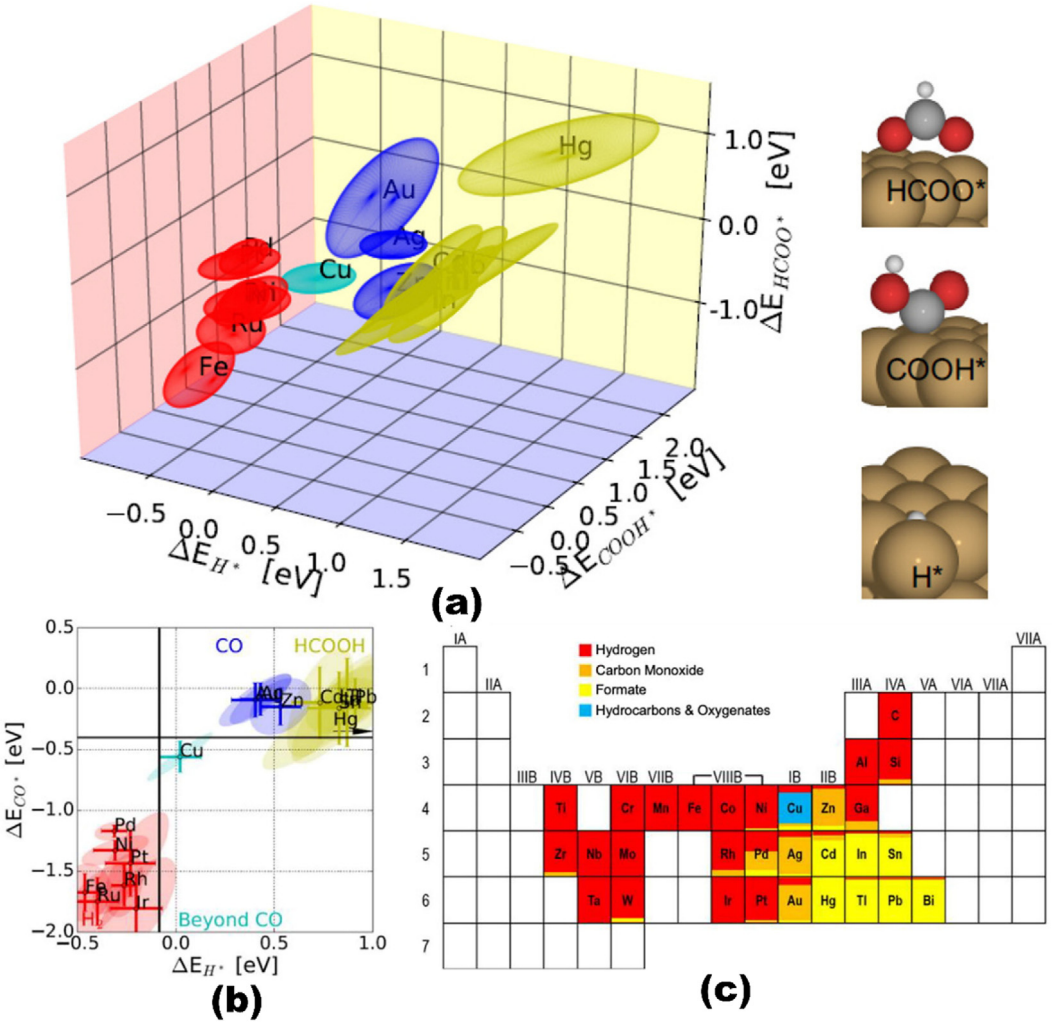

Fig. 3. CO_2RR to CO, H_2, and HCOOH for the proposed descriptors; (a) 3D description of the coupled binding energy ellipsoids concerning Au. Metals have been given color related to their specific products. Light pale (HCOOH), light violet (CO), red (H_2), and light Cyan (beyond CO*), (b) reaction intermediates (*CO and *H) binding energy on various metal electrodes, reproduced with permission from [171], Copyrights Wiley 2017 and (c) Periodic table highlighting the metal's efficiency for their favorable products during eCO_2RR, reproduced with permission from [66], Copyrights ACS ©2015.

creating heterostructure. Metals have poor selectivity for products with high energy densities and deactivate quickly owing to the oxidation of the metal-to-metal oxides. Hori et al. [172] investigated several metals to figure out the most suitable electrocatalyst. Metals such as Hg, Au, Pb, Zn, Cd, Sn, Ti, and In have been extensively employed for formate formation, whereas Ag, Pd, Ga, Ni, and Pt are primarily utilized for CO formation, as illustrated in Fig. 3c. However, CO_2 reduction to C_2 products or fuel is a difficult way because of complex reaction pathways. Thus, the

development of an efficient electrocatalyst having a desirable electronic configuration with larger FEs, and product selectivity at lower overpotential for long operation time is needed [173].

The strong CO* intermediate adsorption over the metal surface, leads to a quick deactivation of the catalyst, while the metal that adsorbs *CO weakly on its surface will desorb CO before it can react further with the intermediates; thus preventing the formation of C_2 species [62,174]. The strong reducing power of copper catalysts enables it to produce a wide range of product distribution with relatively low overpotential [175]. The high performance of eCO_2RR over Cu-based electrocatalysts was reported with $FE_{ethylene}$ greater than 75% with optimum stability [154, 176]. Cu-based catalysts mostly deactivate in acidic or neutral media in eCO_2RR due to HER [177]. It is widely acknowledged that Cu-based catalysts performed better in alkaline media and became particularly drawn to C_{2+} products. However, in an alkaline medium, CO_2 directly reacts with the alkaline medium and forms carbonate and bicarbonates which adds the additional expense of energy, materials, and regeneration of CO_2 [178].

Product selectivity can be enhanced using Cu-based catalysts which can controlled in many ways including grain boundary regulation [179], catalyst engineering [54,180–182], electrolyte selection (ionic, alkaline, or neutral) [179], dopant metals [183], various oxidation states [29], nitrogen-doping [184], and oxygen vacancies [185]. The unique behavior of Cu metal among various metals of the periodic table is the production of C_2, and C_{2+} hydrocarbons at appropriate current density with moderate FE; however, numerous factors still need to be investigated as depicted in Fig. 4. The only competitive reaction to C_{2+} products on Cu is hydrogen evolution reaction (HER) which could affect the product selectivity. However, HER could suppress with higher pressure CO_2RR or appropriate electrolytes with an anion exchange membrane. HER occurs more easily than CO_2RR products due to its lower thermodynamic potential. Similarly, a higher alkaline environment is more suitable for CO_2RR products, but it may cause catalyst degradation rapidly. Another dominant factor is catalyst degradation which occurs due to high current density, high alkaline electrolyte, and electrode flooding; thus, leading to catalyst delamination and catalyst instability. Secondly, C_{2+} product generation is comparatively challenging rather to C_1 products like CO and formate due to the multiple protons electrons transferred mechanism. Multiple protons electrons transfer is a complex reaction mechanism, due to which controlled reaction for a specific C_{2+} product selectivity become more complicated, such as ethylene, and ethanol each require 12 electrons whereas 14 electrons are required to produce ethane. Furthermore, catalyst engineering has had an enormous impact on the C_{2+} product generation such as oxygen vacancies, grain boundaries, surface morphology, catalyst composition, halide addition effect, and specific Cu facets. The mechanism behind the complex multi-proton-coupled electron transfer, which affects the catalytic activity and FE should be carefully investigated [31]. Previous studies have reported that C–C coupling is a fundamental and rate-determining step in C_2 species, which can be further verified by theoretical calculations revealing that Cu catalyst has moderate adsorption energy for *CO which makes it a strong candidate for C_{2+} product [186]. Lastly, overpotential and onset potential of CO_2RR are the most concerned terms regarding C_2 and C_{2+} products industrialization. Overpotential is the difference between thermodynamic and onset potential (applied potential). Overpotential is an extra potential that is being used for a specific product production due to ohmic losses. For instance, the thermodynamic potential of our C_2 products i.e., ethylene, ethanol, and ethane are 0.08, 0.09, and 0.14 V vs RHE, respectively. The most effective electrocatalyst is the one that could produce CO_2RR at a lower overpotential. Likewise other parameters, the C_1/C_2 pathways strongly depend on a range of applied potentials. For instance, *CO–CO dimerization pathway was confirmed to be more favorable at a low overpotential of Cu-based electrocatalysts, while *CO–COH was found to be energetically favorable at high overpotentials. These findings suggest the experimentally observed potential dependence of CH_4, C_2H_4, and C_2H_5OH. For instance, on Cu(100) surface, the lower energy barrier (0.69 vs 1.0 eV) favors C_2H_4 production over CH_4 generation via *CHO when the potential (U) is more positive than −0.6 V. This is achieved using C–C coupling through *CO–CO, followed by hydrogenation to *CO–COH [187]. Therefore, ethylene could be considered as a main product in this overpotential range. While in −0.6 to −0.8 V, adsorption of *H and *CO competes for surface active sites, resulting in a decreased amount of CO on the surface and thus leading to a lower rate of CO dimerization to ethylene. Furthermore, moving towards a more negative potential of −0.8 V, this site blocking does not affect the *CHO formation which can be formed via the Eley-Rideal (E-R) mechanism [188]. Thus, ethylene and methane synthesis share one intermediate, which is obvious from the subsequent appearance of ethylene and methane in this range of potential. This discussion indicates the importance of applied potential range and overpotential for a specific product generation [189]. Recently, CO_2RR in acidic electrolytes via gas diffusion electrode (GDE) employing copper-based ultrathin superhydrophobic microporous layer yielded 87% FE of C_{2+} with a partial current density of -1.6 A cm^{-2} [190]. In related work, Cu nanoparticles were utilized to produce multicarbon products (C_{2+}) in neutral electrolytes to a record value of 1.7 A cm^{-2}. The total FE for C_{2+} reached up to 76% at a current density of 1.6 A cm^{-2} [191]. Similarly, Yuan et al. focused on optimizing the reaction kinetics and product selectivity by modifying the hydrophobicity and pore size distribution of the microporous layer (MPL) of carbon fiber substrate. They succeeded in preparing ethylene with 0.697 A cm^{-2} partial current density and total C_{2+} products with 0.885 A cm^{-2} partial current density at −1.44 V vs. RHE potential [192]. These studies showed the highest reported C_{2+} products regarding their partial current density in the literature.

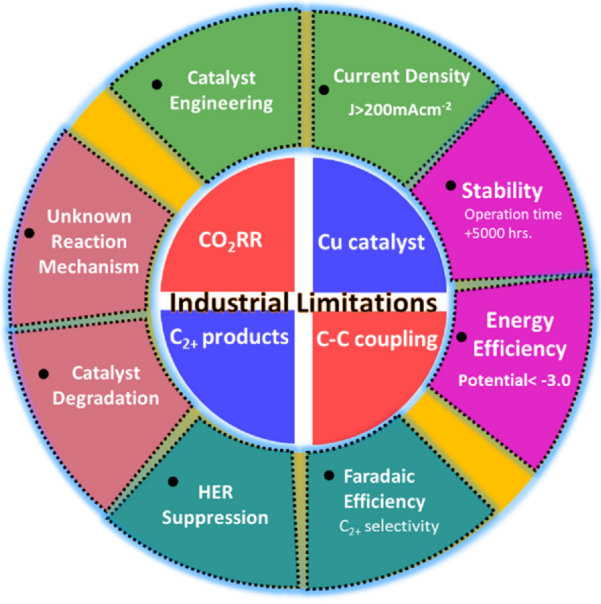

Fig. 4. Performance metrics of electrochemical reduction of CO_2 for industrial applications.

4. Copper catalyst engineering

4.1. Cu-based catalyst (OD–Cu)

The catalysts which consist of Cu as a cation and other elements as an anion are considered in this section. Mostly used anions are either oxygen or halides which have different catalytic activity and product selectivity due to sub-surface oxygen, intrinsic roughness of the surface, and grain boundaries. Although these catalysts have been used extensively for CO_2RR to hydrocarbons, and alcohol production. However, lower FE and

overpotential are their key issues of concern. The most widely used technique to regulate these issues is oxide-derived copper-based (OD-Cu) catalysts [193]. The product selectivity changes from ethylene to ethane as we increase the thickness from thinner to thicker. In addition, the size of Cu-NPs (Nanoparticles), surface coverage, and local pH are highly important for ethylene formation [75]. Moreover, as reported by Lee et al. [194], the utilization of OD–Cu catalysts promotes ethylene formation (FE = 40%) with a stability of 40 h at a lower potential (−1.08 V vs. RHE). This improved FE was attributed to the coexistence of Cu^0 and Cu^+ states following CO_2RR. The presence of these moieties contributes to enhanced selectivity and stability in product formation. The oxidation states of Cu exert a pivotal influence on CO_2RR, particularly regarding the adsorption of CO on an active Cu^+ surface, which shows better stability as compared to Cu^0. Additionally, the CO dimerization between Cu^0 and adjacent Cu^+ sites entails a moderate energy barrier, facilitating the creation of *OCCO intermediates over the catalyst surface. This phenomenon renders Cu-based catalysts well-suited for C–C coupling reactions, characterized by accelerated kinetics and thermodynamic feasibility towards C_2 products [195,196].

4.2. Oxide-derived Cu NPs (OD-Cu NPs)

Oxidized copper catalysts can be synthesized by various techniques like Cu_2O electrodeposition [75], sequential reduction [197], thermal treatment of metallic Cu in the air [198], and plasma treatment [55], which have significant potential to produce $FE_{ethylene}$ (60 % to 70%) and

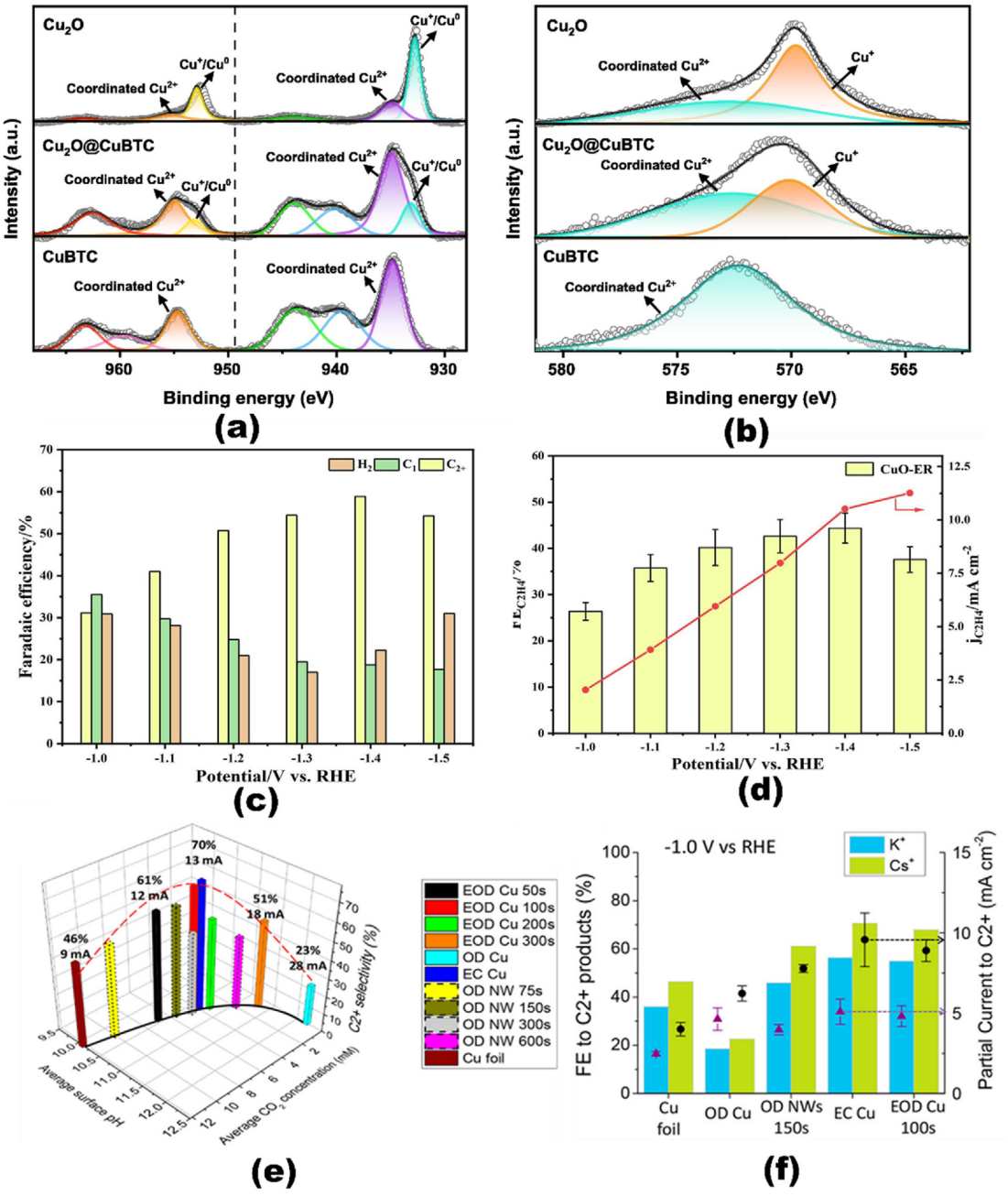

Fig. 5. (a) XPS of Cu 2p and, (b) Cu LMM Auger of Cu_2O, prepared by modifying reaction time [85], Copyrights Elsevier ©2023. (c) C_2H_4 Partial current density and FE on CuO-ER catalyst at various potentials, (d) FEs of H_2, and C_{2+} products on CuO-ER at different applied potentials, reproduced with permission from [185], Copyrights Elsevier ©2023. (e) Numerical simulation results of the averaged local and surface pH using various OD-Cu catalysts, (f) FEs, and partial CD towards C_{2+} products in K^+ & Cs^+ electrolyte at −1.0 V vs. RHE, Reproduced with permission from [195], Copyrights ACS ©2017.

other C_2 products with relatively higher current density (–250 mA cm^{-2}) [97]. Previous studies [71,74,94,97,199] demonstrated that grain boundaries, formation of low coordinated atoms, and the presence of Cu^{2+} sites in these OD-Cu base electrocatalysts could be the active species during eCO_2RR, which was further verified by the DFT calculation that the presence of a single Cu^{1+} site might not be able to improve FEs of the CO_2RR [200]. The OD-Cu catalysts are comparatively energy efficient as they exhibited lower onset potential and remarkable selectivity toward a specific product; particularly C_{2+} products as compared to methane. Apart from the grain boundaries of the catalyst, the manipulation between the oxidation states of Cu ($Cu^0/Cu^+/Cu^{2+}$) is believed to be important for ethylene production [201,202].

It has been observed that eCO_2RR and catalytic activity of the oxide-derived catalyst is better than the simple Cu owing to surface rupture and porosity of the former, resulting in enhanced CO_2 adsorption on the oxide-derived catalyst [69]. Most of the studies published in the literature investigated Cu and Cu_2O catalysts with different morphologies and characteristics, demonstrating that the presence of Cu_2O on the catalyst surface is a microcrystalline or rupture structure while Cu^0 has a flat surface (less conductive than Cu_2O), which is not effective. The oxide-derived catalyst has improved surface morphology, and intrinsic activity of eCO_2RR with suppressed HER. Cu_2O oxide-derived particles have higher FEs than electropolished Cu surfaces due to porosity and surface roughness [67]. Moreover, the former catalysts surface contains Cu^+, which promotes CO_2 activation [85]. In an alkaline environment, the active Cu^+ species is eventually reduced to Cu^0, which might impact the durability and selectivity of C_{2+} compounds (Fig. 5a to b); whereas Cu^+ is obvious in the synthesized catalyst which is reduced to Cu^0 after CO_2RR. Recently, a mixture of Cu^0/Cu^+ catalysts was prepared with a hydrothermal method under alkaline conditions. Their findings indicate that the presence of Cu^0/Cu^+ interfaces enhances crucial intermediate (*OCCOH) adsorption, thereby lowering the C–C coupling energy barrier and assisting the production of C_{2+} products (FE = 58.9%). At an optimal current density of −10.5 mA cm^{-2} at −1.40 V, FE of ethylene reached 44.5% (Fig. 5c to d). The catalyst's nanosheet structure helps to achieve a larger surface area of up to 15.1 m^2/g and exposes more active sites to CO_2 adsorption. The previously reported study showed that Cu^{2+} species are neither active sites in CO_2RR nor have a significant effect on C_{2+} product formation as compared to Cu^0/Cu^+. However, electrode surfaces containing lower oxidation states of Cu (Cu^+ and metallic Cu^0) have been reported to offer a higher yield of C_{2+} products [203–205]. The presence of an abundance of Cu^0/Cu^+ favors *CO adsorption density, resulting in high C_{2+} selectivity [206]. Further, theoretical examination was conducted to discover the synergistic impact of Cu^0 and Cu^+ by utilizing the density of states (DOS) model. The investigation shows that Cu_2O-Cu (100) has a reduced band gap energy (0.78 eV) compared to individual Cu_2O (1.25 eV), demonstrating the enhanced conductivity of combined Cu_2O-Cu [207].

In a subsequent study in 2023, Diao et al. [208] observed that annealed Cu catalyzed the conversion of CO_2 into ethylene and ethane at remarkably low potentials (−0.60 V). Contrarily, polycrystalline Cu produced C_2H_4 and CH_4 at higher potentials, yielding H_2 as the main product, with annealed Cu displaying low FE towards hydrocarbons. The deviation from the higher overpotential regime was attributed to mass transport constraints at elevated current densities (>10 mA cm^{-2}) and the electrode's inherent selectivity [80]. Similarly, Yanwei et al. [195] investigated the increasing pH effect on C_2 selectivity which leads to C–C coupling, whereas a decrease in CO_2 concentrations; lowered the C_2 selectivity (Fig. 5e). The average surface concentration of CO_2 was calculated using OD-Cu, electrochemical polished Cu, OD-NWs (oxide--derived nanowires), and electrochemical oxide derived Cu at −1.0 V and −0.70 V RHE which revealed their electrochemical performance towards C_{2+} products. Furthermore, the current density is directly proportional to the local pH value while inversely proportional to the CO_2 concentration as reported by Lum et al. It can be stated that the oxide-derived catalyst having a high pH value with a corresponding lower CO_2 concentration yields maximum current density (Fig. 5f). The product selectivity for OD NWs (Nanowires), EC Cu, Cu foil, OD Cu, and EOD Cu has been reported with the highest C_2 product selectivity observed for EOD Cu and EC Cu at 100 s. The maximum FE of the C_2 product (ethylene and ethanol) has been observed at −1.0 V (65%) and −0.90 V (45%) 195.

Several studies have corroborated that the mere presence of Cu^0 is not adequate for the generation of C_{2+} chemicals, whereas the presence of Cu^+ species on its surface is deemed an active prerequisite as we discussed earlier. Positively charged Cu^+ of *CO–Cu^+ species serve to mitigate the adverse effects induced by negatively charged species *CO_2–Cu^0 during CO_2RR. This positive charge is conducive to C–C coupling and dimerization, thereby suppressing HER and the formation of C_1 products [87,209,210]. Recent research has demonstrated that the stability and unique coexistence of Cu^+/Cu^0 is essential for the increased intermediate concentration [208,211]. However, an inadequate or excessive concentration of Cu^+/Cu^0 will lower the intermediate concentration. To overcome this issue Zhang et al. [85] presented a new strategy to regulate the intermediate concentration for balance achievement among the intermediates by tuning several parameters (*CO concentration, Cu^+ surface coverage, and cavity size, etc.) which were considered capable of producing C_2 products with FE (70.1%) at the current density of – 9.30 mA cm^{-2} (Fig. 6a and b). Similarly, by adjusting the electron transfer during the CO_2RR process, grain refining techniques have been employed to adjust the oxidation states of Cu-based catalysts. The effect of nanograin size was further investigated by Yang et al. [212], who claimed that a significant amount of active Cu nanograins yields better C_{2+} selectivity, particularly for 7.0 nm particle ensembles which exhibited sixfold higher than that of 18.0 nm Cu-NPs.

The C_2 selectivity remains optimum for Cu_2O at Cu-BTC heterostructure which behaves as a sacrifice template of Cu_2O octahedron (Fig. 6c), that enables higher C_{2+} products (FEs = 39.8% for C_2H_4, FE = 19% for C_2H_5OH, and FE = 5.4% for 1-propanol) [85]. It has been further confirmed [214] that the coexistence of Cu^+/Cu^0 significantly affects the electrochemical performance of the catalyst. The Cu_2O catalyst contains both Cu oxidations states Cu^+/Cu^0 and incorporated with various amounts of CNTs, which are highly conductive and thus caused the reduction peak toward the positive side (Fig. 6d). In addition, increasing CNTs decreased FE_{C2+} products at 800 mA cm^{-2} at fixed CD offering maximum value at Cu_2O/CNTs = 4 ratios (Fig. 6e). Gu et al. [215] reported higher FEs of C_{2+} products using CuO_x than Cu catalyst due to the formation of oxygen vacancies and its oxidation states in the later catalyst. The highest FE was observed for ethylene (at 63%, represented by the red column) in Fig. 6f at −1.40 V (vs. RHE) accompanied by HER (FE = 16%). The polarization curve illustrates the electrochemical performance in terms of kinetics. Pure Cu exhibits a lower onset potential of −0.50 V vs. RHE, attributed to the competing side reaction of hydrogen evolution (HER). In contrast, CuO_x-Vo catalyst exhibits a lower current density and a slightly higher onset potential of −0.60 V vs RHE than the Cu electrode. The difference may be explained by Cus greater electrical conductivity (Fig. 6g) [215]. In short, several researchers suggested that the long-term existence of Cu^+ species is important for the excellent catalytic activity of the catalyst and product selectivity. The synergetic effect of Cu^0 and Cu^{2+} sites in Cu catalysts is considered a significant parameter for higher FEs during the CO_2RR.

Several studies aimed to specify the active sites responsible for the remarkable catalytic properties of oxide-derived Cu and Cu-based catalysts. Chorkendorff and co-workers found strong CO binding sites in oxide-derived Cu catalysts as compared to polycrystalline Cu using temperature-programmed desorption (TPD) [67]. They assumed these strong binding sites could be grain boundaries observed in oxide-derived Cu catalysts. In related work, Kanan et al. explained grain boundaries are the active sites for the CO reduction to C_2 and C_3 products [217]. However, it is unclear whether all the grain boundaries are active or if only those grain boundaries with specific morphology for CO reduction to C_2 products. Yanwei et al. demonstrated with an isotopic labeling technique that oxide-derived Cu possesses a minimum of three types of active sites

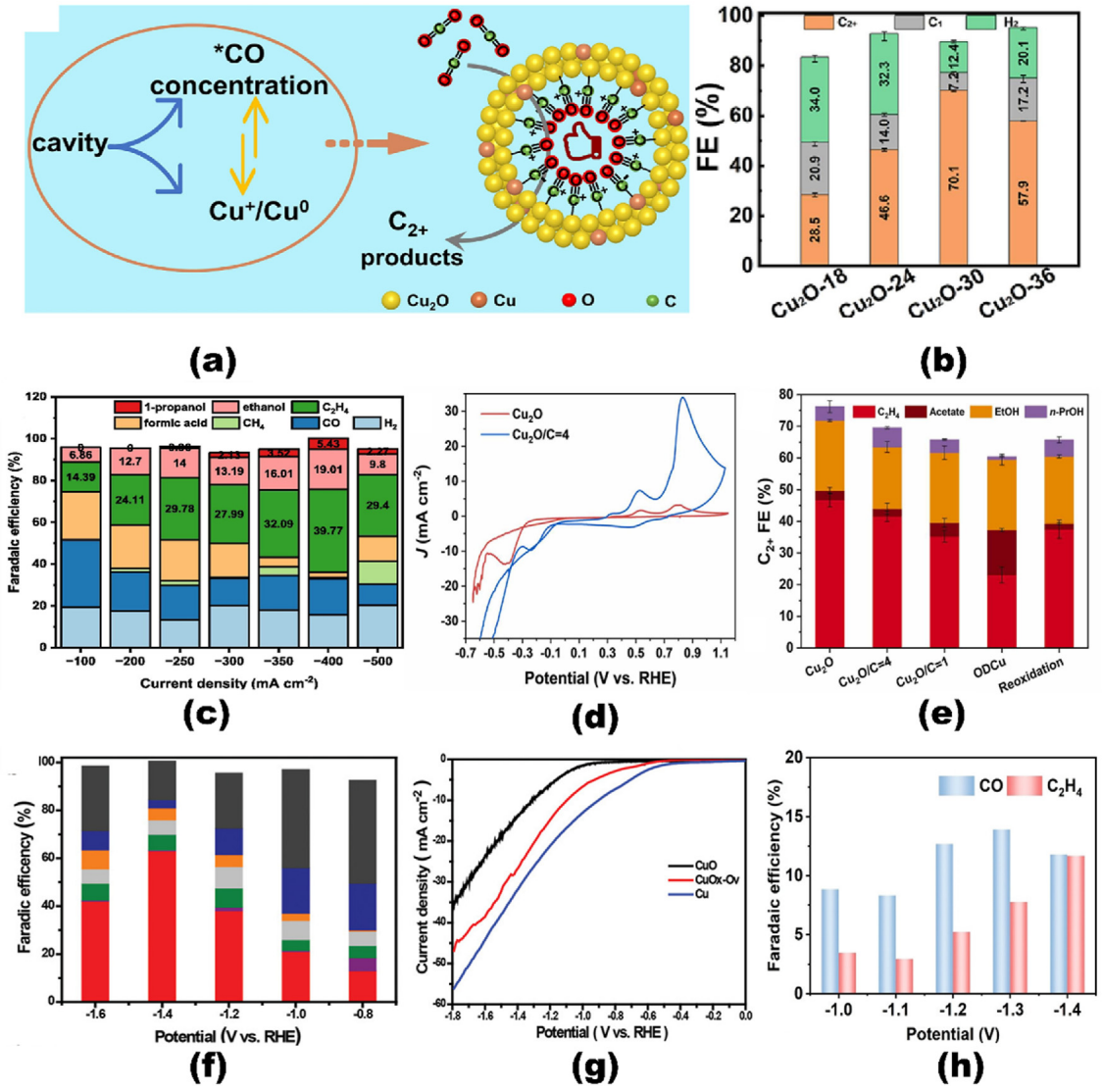

Fig. 6. (a) Schematics for Cu cavity contained Cu^{+}/Cu^{0}, and (b) FEs of C_{2+} over various Cu_2O catalysts [85,213], Copyrights Elsevier ©2023. (c) FEs of various products over Cu_2O@ CuBTC [85], Copyrights Elsevier ©2023. (d) Comparison of reduction-oxidation pattern between Cu_2O-2 and Cu_2O-2/CNTs, and (e) FEs C_{2+} of overall products of Cu_2O-2 based electrodes of CNTs (Carbon nanotubes) under 800 mA cm^{-2} [214], Copyrights Elsevier ©2023. (f) Overall FEs of C_{2+} products at numerous potentials for CuO_x-V_o catalyst, (g) Comparative LSV (linear sweep voltammetry) curves for CuO_x-Vo, CuO, and Cu in 0.1 M $KHCO_3$ [215], Copyrights Wiley ©2019 and (h) Chronoamperometry (CA) of Cu_2O–BN (Cu Boron nitride), and (i) FEs of CO_2RR products in CO_2-saturated 0.5 M $KHCO_3$ on Cu_2O-BN [216], Copyrights Wiley ©2022.

as shown in Fig. 7a, including selectively responsible for ethylene, acetate/ethanol, and 1-propanol, respectively. Contrarily, polycrystalline Cu, Cu (111), and Cu (100) do not have such kind of product-specific active sites [26].

Fig. 7b Shows isotopic composition of C_2 products produced by oxide-derived Cu catalysts at various applied potentials. The similar isotopic composition of ethanol and acetate regardless of the applied potential indicates that these products are generated from the same active sites. Secondly, the consistently higher ^{13}CO fraction of ethylene shows that ethylene is generated from a different active site. Finally, 1-propanol has a distinct ^{13}C fraction from ethylene or ethanol/acetate which strongly suggests that this product is produced by another active site [26]. Similarly, Yanwei et al. [149] synthesized ^{18}O enriched oxide-derived Cu catalyst by ^{18}O labeling technique (Fig. 7c). The oxide-derived Cu catalyst exhibited higher C_2/C_3 selectivity (60.1%) and lower selectivity towards C_1 products (6.5%) as compared to planar Cu catalysts as shown in Fig. 7d. They attributed the high C_2/C_3 product selectivity to high density of grain boundaries as previously reported by Kanan and co-workers. All these findings conclude that oxide-derived Cu catalysts show better C_2 product selectivity as well as current density than planar Cu foil or Cu catalysts due to either grain boundaries or residual oxygen [149].

4.3. Oxygen vacancy

Oxygen vacancies over the catalyst surface are perceived to enhance ethylene production by promoting the adsorption of *CO and *COH intermediates, subsequently facilitating the release of $*CH_2$, which is a crucial intermediate for C_{2+} products. The oxygen vacancies could be created with other oxygen-enriched compounds like ceria. Patra et al. [218] generated oxygen vacancies by introducing CeO_2 in the Cu catalyst and found that various calcination temperatures generate various oxygen vacancies that have different product selectivity. The porous structure of the bimetallic catalyst was demonstrated by HR-TEM subsequently leading to the polycrystalline nature of the catalyst. The single Cu atom and CeO_2 in HR–TEM is difficult to distinguish due to similar lattice spacing parameters (3.1 Å) [219]. The existence of the Ce^{3+} and oxygen

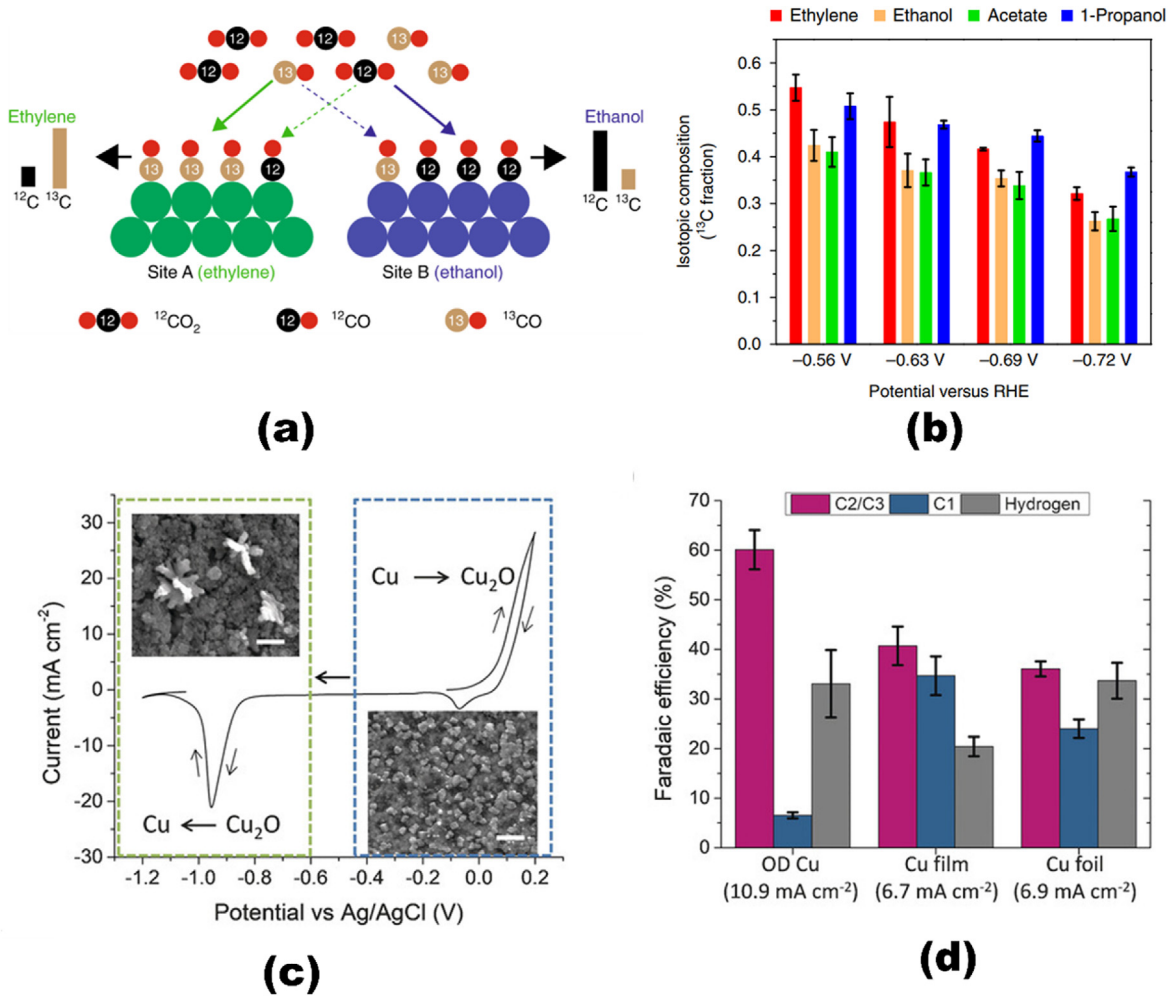

Fig. 7. (a) Hypothetical scenario of two types of active sites, site A and site B favors ethylene and ethanol formation respectively, (b) Isotopic composition of ethylene, ethanol, acetate and 1-propanol produced from $^{13}CO/^{12}CO$ gas mixture reduction at various potential on oxide derived Cu catalyst [26], Copyrights Springer Nature ©2019, (c) Generating of ^{18}O labeled OD Cu through electrochemical oxidation and reduction procedure and (d) C_2/C_3 Faradaic efficiency comparison for OD Cu, Cu film, and Cu foil. Reproduced with the permission from [149], Copyrights Wiley ©2018.

vacancies were attributed to the higher electrocatalyst performance using the Cu/CeO_2 catalyst; the oxidation states were further verified by XPS analysis. The various ceria oxidation states Ce^{3+} (A_s) and Ce^{4+} (A_L) were associated with three-fold and four-fold oxygen vacancies, respectively. The highest FEs of C_{2+} product for Cu-CeO_2 (4%) were obtained at −1.50 V (vs RHE). The number of oxygen vacancies from the O 1s spectra can be calculated from Eq. (1) [220,155]:

$$\text{Oxygen vacancy } (\%) = \frac{\frac{1}{2}A_s}{A_s + A_L} \times 100 \quad (1)$$

Similarly, Lim et al. [86] showed that CD and FE of Cu catalyst increased when 4.0% ceria is added to the catalyst due to the generation of oxygen vacancy. For example, it has been found that more unsaturated adsorption sites caused by oxygen vacancies improved the adsorption of *COH. In addition, DFT calculation indicates that CuO–V_o has lower adsorption energy for the intermediates than for a single CuO; which produces higher product selectivity and current density (low 3D Tafel plots) [215]. Regarding surface modification, lithiation is one of those techniques in which atomic scale spacing between two facets of Cu-NPs enables higher CO_2RR activity. The atomic spacings were created by inserting CuO_x-NPs into the electrochemical lithiation. The removal of lithium oxide from the NPs generates defects in NPs, which were verified by 3D tomography and STEM images [101]. The lithiation process is performed at various potentials resulting in different atomic spacings among the facets. This atomic space creation enhanced C–C coupling for the CO_2RR and improved ethylene and ethanol production by up to 80% which is higher than the normal copper catalyst.

4.4. Halide-derived Cu NPs catalyst (HD – Cu NPs)

These catalysts are derived from halides containing Cu cations and halide anions. It has been noted that Cu catalysts based on halides exhibit greater stability compared to oxide-derived catalysts. This stability is attributed to the significant electronegativity contrast between halides and oxygen [155]. Owing to this large electronegativity difference, stable Cu-halide compounds dissociate into more Cu^+ species which is considered a significant factor in the formation of C_{2+} products [147, 221]. Halide ions adsorbed on the catalyst surface increase its catalytic activity by surface reorganization as well as by modulation of catalyst oxidation states. The oxidation state of the catalyst active sites defines the ease of CO_2 activation [222]. It is well known that halogens have high electronegativity and tend to show distinctive electronic structures. A potential scenario is that the electrophilic atom in the substrate will be immediately contacted by the nucleophilic halogen atom, which will assist in activating important intermediates. On the other hand, the Cu surface's adsorption properties of halogen ions would promote the electron transfer from Cu to halogens, stabilizing the $Cu^{\delta+}$ species. For instance, Qiao et al. synthesized iodide-derived copper (ID-Cu), with a

trace amount of iodine species on Cu surface. The presence of negatively charged iodine species with positive Cu enhances the adsorption of intermediate thus leading to greater ethane selectivity of 72% at −1.6 V than oxide-derived copper catalyst (27%) [223]. However, halide ions can maneuver the activity and selectivity of Cu catalysts. The addition of Cl^- and Br^- yields CO selectivity whereas I^- ion addition results in methane formation up to 6 times compared without halide added electrolyte [224]. In a related work, it is observed that fluorine-doped Cu catalyst (F-Cu) yields significantly improved FE_{C2+} up to 70.4% at −0.97 V (vs RHE). This improvement was mainly attributed to *CO intermediate behavior on F-Cu catalyst which stabilized on fluorine-doped Cu catalyst for further C-C coupling instead of escaping as gaseous CO [225].

Hori et al. synthesized a single crystal (211) facet of Cu catalyst which reveals the formation of C_{2+} products (79.5%) particularly C_2H_4 having FE of 50.9% at −1.38 V and −5.0 mA cm^{-2}. However, the commercialization of single-crystal catalysts is very challenging owing to its complex and uneconomical synthesis procedure [63]. Similarly, at a current density of −40 mA cm^{-2}, with FE_{C2+} products is above 60%, as reported by Jiang et al. [221]. FE of C_{2+} products obtained at −1.1 V was 57%,

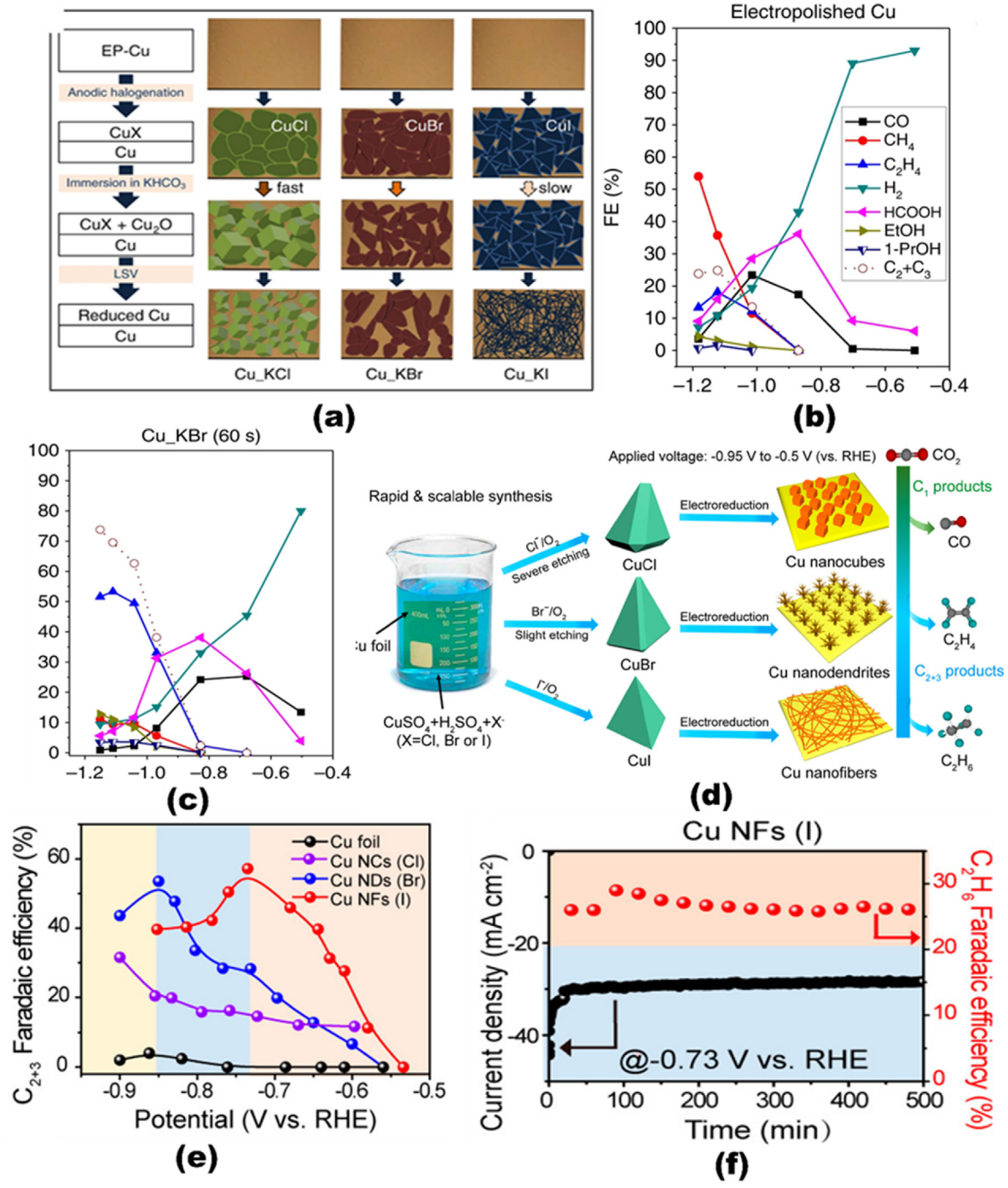

Fig. 8. (a) Anodic halogenation in different halogens, oxide formation was in $KHCO_3$ solution,(b) Effect of different potential to calculate the FE of the CO_2RR products over an electropolished Cu, (c) Cu-KBr at 60 s [227]. Copyrights Springer Nature ©2020, (d) Schematic illustration for the synthesis of CuCl, CuBr, and CuI nanostructures before and after reduction reaction, (e) Total FEs C_{2+} obtained at Cu foil, Cu nanocubes, Cu nano-dendrites, Cu nanofibers at different potentials, and (f) Stability of Cu NFs at −0.73 V vs. RHE [228], Copyrights ACS ©2019.

which is almost 4 times higher than Cu NWs under similar operating conditions [147]. The formation of C_{2+} products, especially ethylene, was further corroborated by DFT calculations, which showed that the adsorption of *COCOH species on Cu catalysts enhances ethylene formation while suppressing HER [147]. The generation of C_2 products is caused by anodic halogenation of Cu foil because it produces more active sites and surface roughness. These active sites can take the form of step atoms, under-coordinated atoms, or crystal grain boundaries [83]. The higher surface roughness might have negative effects on the performance if the halogenation time is too long due to an intense rough surface which increases the roughness factor resulting in the formation of HER. Therefore, the optimized roughness factor is calculated through the double-layer capacitance method which might be effective in considering the halogenation time [226]. To investigate the roughness factor and defect site, Kim et al. [227] synthesized high-density defect sites and rough Cu foil in cathodically halogenated (oxide is formed) in a $KHCO_3$ electrolyte to produce Cu-halogenated catalysts, which are subsequently reduced via an electrochemical reduction process (Fig. 8a). The respective Cu–X (where; X = Cl, Br, I) were synthesized by immersing them into their corresponding 0.1 M KX solution against Cu foil as an anode; demonstrates a high defect density and low roughness favors the formation of C_2 products particularly ethylene (FE = 72%). The maximum FE of C_{2+} at Cu foil was 25% (Fig. 8b) which was increased to 51% using Cu–KBr (Fig. 8c). The overall C_{2+} products faradaic efficiency obtained at −1.20 V (vs RHE) was 75%. The enhanced C_{2+} product was ascribed to the elevated active site density on the surface and the elevated roughness factor resulting from the extended halogenation process [227].

Later Wang et al. [228] synthesized various types of nanostructures (Fig. 8d) using three different halide precursors (Cu nanocubes using CuCl, Cu nano-dendrites using CuBr, Cu nanofibers using CuI) to check the halide effect on product selectivity [228]. The nanostructured Cu halide catalysts exhibited superior performance compared to Cu foil, achieving a higher Faradaic efficiency (FE) of 42% towards formates at −0.82 V vs RHE. FE_{C2+} was less than 10% for Cu foil at −0.75 V vs RHE but increased to 60% on Cu nanofibers (Cu-NFs) (Fig. 8e). Furthermore, the stability of Cu-NFs was tested for 8.5 h (Fig. 8f) with a current density of −30 mA cm^{-2} and FE_{C2H6} = 30%. The improved electrochemical performance of the nanostructured Cu halide catalyst can be attributed to rough structure and their distinct morphologies [228]. Furthermore, theoretical calculations and experimental findings concluded that halide may directly affect the binding strength ability of the intermediate species thus directing the reaction pathways of C_2 product. For instance, Ma et al. investigated hydrogen-assisted halogen-modified copper catalysts, which revealed that fluoride ion on Cu catalysts accelerates *CO to *CHO hydrogenation, reducing the Gibbs free energy of *CHO formation by 0.31 eV. *CHO species further undergo through C–C coupling, resulting in C_{2+} products(80%) at a higher current density of −1 600 mA cm^{-2} [229]. Although substantial progress has been made in halide-derived Cu catalysts, still optical areas like identifying key mechanisms of halide-based catalysts and modulation of electronic structure need more depth-profiling analysis. Thirdly, metal halide remains unstable; to encounter this issue, halide-doped carbon material could be employed with electrocatalysts to improve its stability in an alkaline environment.

4.5. Heteroatom doping of Cu-based catalyst

The addition of molecules or coating of an element on Cu surface has significant importance in altering the binding energy for an intermediate and improving the hydrophobicity of the catalyst to enhance mass transportation. The stabilization of CO_2RR intermediates by the adsorption of certain molecules to the Cu surface improves the stability and selectivity of the intended products [54]. Besides Cu^+ species stability, the dopant enriches the active site as well as strengthens the binding energy of *CO towards C_{2+} product reduction. For instance, the insertion of a p-block element i.e., Gallium (Ga) into Cu results in p-d hybridization which not only enriches the active sites on Cu surface but also strengthens the *CO intermediate, thus facilitating C–C coupling for C_{2+} products. The CuGa exhibited excellent electrochemical performance with 81.5% C_{2+} FE at a remarkable current density of 900 mA cm^{-2} as shown in (Fig. 9a and b). The highest current density shows the fast reaction kinetics of the Ga-doped Cu catalyst. Density functional theory calculation confirmed that $*CO_2$ adsorption energy (−0.73 eV) on CuGa is much lower than that on pure Cu (−0.37 eV), indicating CO_2 molecules to be adsorbed easier on CuGa than on Cu surface. The free energies of *CO and *OCCO formations on CuGa were found to be 0.31 and 0.72 eV, while those for Cu surface were 0.66 and 1.24 eV respectively. These C–C coupling calculated values on the CuGa surface are almost half of the pure Cu surface value, indicating the significant impact of dopant on Cu catalyst activity and productivity [230]. Tandem electrocatalyst or heteroatomic catalyst decouples the chemically complicated pathway of C_{2+} generation especially at high rates. For instance, Ag enhances to convert CO_2 reduction to CO in the first step and then CO enriched environment over Cu catalyst favors C–C coupling for C_{2+} products in Cu-Ag tandem catalyst. Fig. 9c shows that the partial current density of C_{2+} products at −0.7 V vs RHE increased from 37 to 160 mA cm^{-2} for Cu_{500}-Ag_{1000} tandem catalyst, which is almost 4 times higher than a single Cu catalyst. Similarly, the partial current density enhancement factor for ethylene, and ethanol on Cu_{500}-Ag_{1000} catalyst increased up to 3.5, and 5.5 times for ethylene, and ethanol respectively (Fig. 9d) [231].

Ding et al. reported a C_{2+} product with FE above 70% at −60 mA cm^{-2} and – 0.80 V having 130 h stability using potassium dopant (11.2%) Cu_2Se array nanosheets. Potassium was reported as an electron donor to Cu catalyst, making the intermediate easier to provide an adsorption site. Moreover, DFT studies showed that the Cu_2Se compound's bond length increased from 2.516 to 2.629 Å when a Cu atom was substituted with a K atom, stretching the lattice parameter. K–doping led to enhanced adsorption of key intermediates over the catalyst surface such as linear $*CO_L$ and bridge $*CO_B$, thereby promoting C–C coupling for ethanol production, even at a higher current density of −97.3 mA cm^{-2} [232]. Similarly, Sun et al. [233] used a flow cell to produce the single liquid product ethanol on a vanadium-doped (V–dopant) Cu_2Se nanotube catalyst. The current density effectively increased from −187.0 to −628.3 mA cm^{-2} on the $Cu_{1.22}V_{0.19}Se$ catalyst as the applied potential rose from −0.60 to −1.30 V (Fig. 10a) [234]. Meanwhile, ethanol formation on $Cu_{1.22}V_{0.19}Se$ catalyst occurred with a FE of 68.3% and a partial current density of −207.9 mA cm^{-2} at lower applied potential of −0.80 V, accompanied by negligible H_2 production. In contrast, no ethanol was observed for CuSe catalyst, with an abundance of H_2 being observed instead (Fig. 10b) [235]. The modification of active sites and the prevention of Cu^+ species from being reduced to CuO during CO_2RR were credited with the enhanced electrochemical performance that followed the insertion of V^{4+} doping ions into Cu_2Se lattice.

Similarly, the effect of Cu traces with various compositions (0 to 0.20%) was determined by introducing it into $Pd_{10}Te_3$ nanowires. The pure $Pd_{10}Te_3$ catalyst enabled the total current density to elevate CD from −2.70 mA cm^{-2} to a peak value of −18.7 mA cm^{-2} at 0.10% Cu loading using −0.98 V (vs. RHE) (Fig. 10(b–c)), which displays the FE_{CO} to 92% (6.57 times greater than undoped nanowires); with the suppression of HER at low Cu loading (Fig. 10d). FE_{CO} is maximum at 0.1% Cu loading with least HER.

The effect of Cu amount traces on pure and doped nanowires was investigated and found that Cu traces enhanced the current density and FE of the reduced products. The dopant component not only increases the electrochemical performance by increasing its electrochemical surface area (ECSA) and morphology of the active catalyst but also the stability of the catalyst for a long time. The effect of nitrogen doping in Cu_2O was proposed by Yan et al. [236], which reveals the higher current density and product selectivity. The cubic morphology retains the abundance of pores making its surface area larger than pristine Cu_2O; thus making it more favorable for higher CO_2 adsorption. The HR-TEM images demonstrate the presence of (100) and (110) facets with a lattice distance

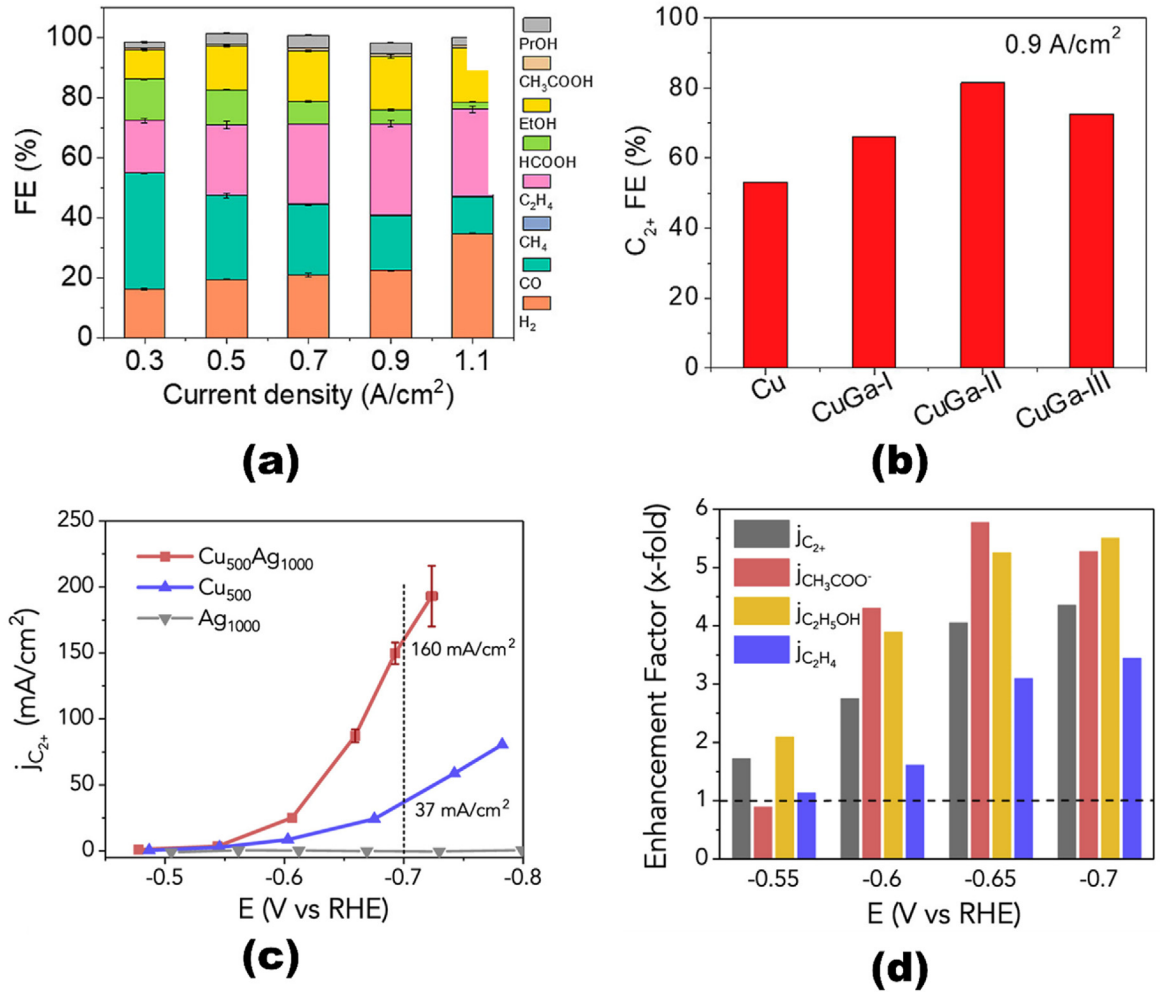

Fig. 9. (a) Product distributions of CO_2RR on Cu at various current densities,(b) C_{2+} FE values on different catalysts at 900 mA cm^{-2} current density [230], Copyrights ACS ©2023, (c) C_{2+} products partial current density over Cu_{500}-Ag_{1000}, Cu_{500} and Ag_{1000} catalysts and (d) Enhancement factor for total C_{2+} and individual products over different potentials (Enhancement factor: the ratio of tandem Cu_{500}-Ag_{1000} partial current density to Cu_{100} partial current density) [231], Copyrights Elsevier ©2020.

of 0.21 nm which indicates that Cu_2O structure is retained after CO_2RR [237].

The electrochemical performance enhancement was investigated by the formation of AgO_x and bimetallic AgO_x/Cu_2O surface. The bimetallic catalyst has a rough surface and the cluster of AgO_x NPs was equally distributed on its surface which was further verified by EDX (energy dispersive X-ray spectroscopy) mapping. The bimetallic catalyst demonstrated the maximum FE of 35% towards C_{2+} at −150 $mAcm^{-2}$ and −1.0 V having 20 h (Fig. 10e). The effect of dispersed Ag in Cu catalyst, was examined by Qi et al. [238] and reported that dispersed Ag particles on Cu surface is having a significant impact on strengthening C–O bond and lowering the activation energy for intermediates, and thus results in 2-propanol synthesis [238]. Although Cu exhibits medium adsorption energy for *CO (−0.78 V) which is suitable binding energy for C_{2+} selectivity. However, the sluggish kinetics of C–C coupling renders tremendous obstacles to its further application due to low FE and low current density. To overcome these obstacles, core-shell Ag-Cu composite catalysts with various amounts of Cu particles (2%, 5%, and 10%) have been examined. It was observed that FE of C_{2+} products particularly ethanol was 80.2% at a current density of −320 mA cm^{-2} and −1.0 V (vs. RHE) with significant stability of 60 h [160]. TEM (transmission electron microscope) and SEM (scanning electron microscope) images described the migration of Cu particles from the core part to the outer surface [160]. The optimized loading amount of 5% was used over Ag NPs which reveals the FE of C_2 = 60% at −1.0 V and −400 mA cm^{-2} (Fig. 10f). The combination of Cu catalyst with Ag-NPs enhances C_2 product concentration. In addition, CO production at a higher current density shows that Ag plays a significant role in its catalytic activity [231,160,239]. The sensitivity of the Cu surface plays a crucial role in its performance, influencing phenomena such as surface reconstruction or evolution during CO_2RR. These processes may result in altered atomic configurations, surface oxidation states, and electronic structures [161,240]. Copper has moderate *CO binding energy (−0.78 eV) on its surface and has the disadvantage of poor selectivity among the C_2 products [241].

4.6. Copper facets

The effect of various facets and grain boundaries affects the catalyst's performance and morphology. The correlation between the various morphologies and facets of Cu_2O catalysts (Fig. 11a to f) has been presented by Yang et al. [212]. The highest number of facets and grain boundaries have large CO_2 reduction peaks and the smallest Tafel slope value, indicating the reactivity towards CO_2RR. In addition, CO_2RR requires low energy and high reaction kinetics. Cu facets including (100), and (111) (Fig. 11g and h) are active for higher ethylene (FE = 57%) production and low hydrogen evolution reaction with higher kinetics (low Tafel slope) [212]. These facets have specific morphologies and are selective towards specific product selectivity. This study emphasized the

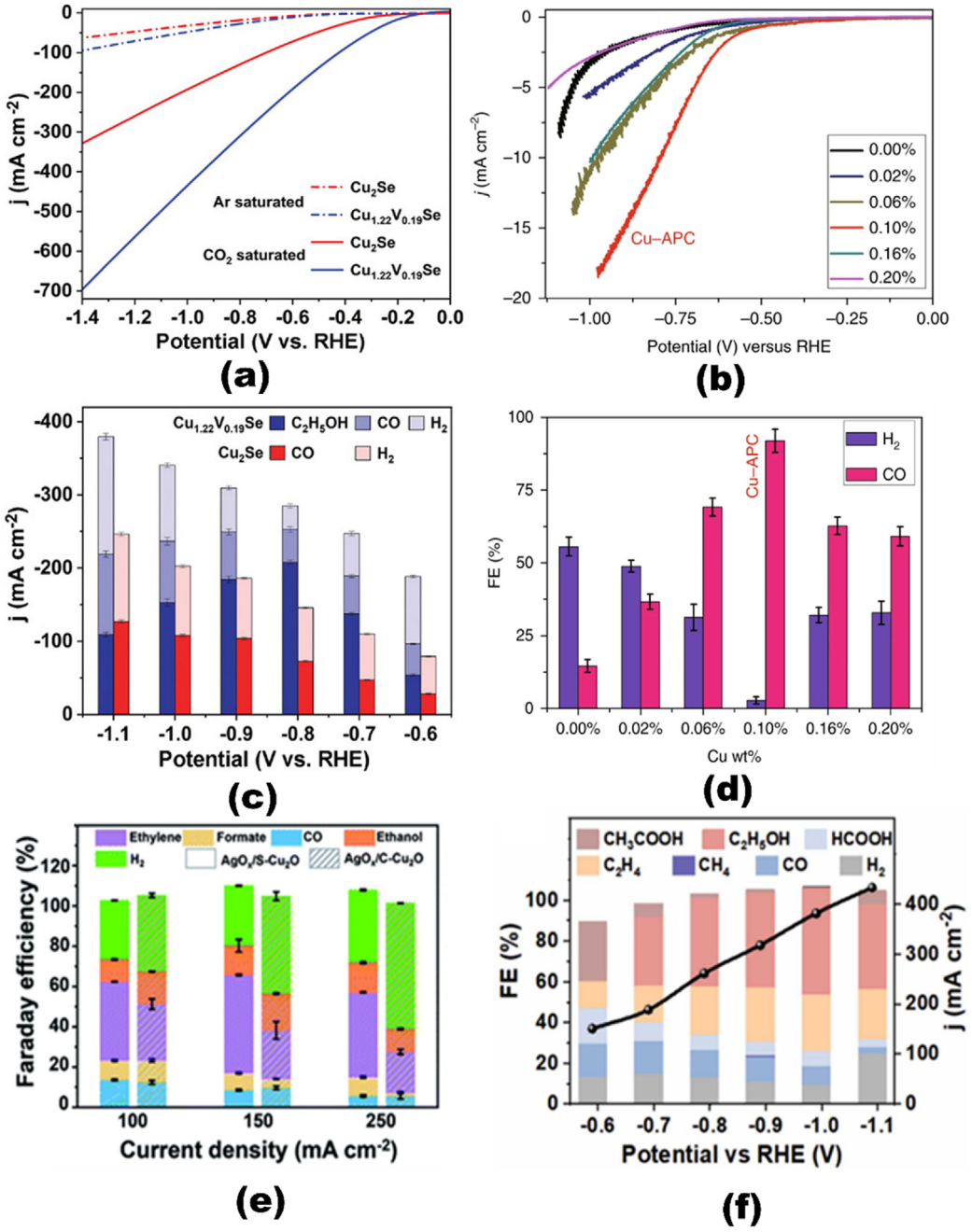

Fig. 10. (a) Effect of Cu traces on current density at various potentials in Ar- and CO_2–saturated conditions [220], (b) Correlation of optimized Cu traces with current density at various potentials [221], Copyrights Wiley ©2022, (c) Effect of current density at various potentials [220], (d) Correlation of various Cu traces with FE [221], (e) FEs of the AgO_x/S-Cu_2O under various current densities [164], Copyrights RCS ©2021,and (f) Products FEs and CD at several applied potentials for $Ag_{0.95}$-$Cu_{0.05}$ catalyst [160], Copyrights ACS ©2023.

creation of active facets through an etching process to synthesize Cu nanocrystals for CO_2RR. These facets have the potential to adsorb *CO on its surface with the minimum possible binding energy. Experimental adsorption studies have revealed that Cu(111) can stabilize CO* coverage up to 0.44 monolayers (ML), which is comparatively lower than the values of 0.57 ML and 0.60 ML observed on different facets of Cu (100) and(110), respectively. Thus high coverage of *CO was likely to create larger probabilities of C–C coupling and subsequently larger C_2 product selectivity [242]. Since CO dimerization is one of the dominant pathways for C_2 formation, Cu (100) has the lowest electronic energy barrier for the dimerization of CO, which is consistent with *CO coverage findings, whereas Fig. 11i to j illustrates CO_2 on Cu surface at different stages of the reaction (initial, transition and final) with required energy path diagram.

It has been observed that Cu (100) facet catalyzes the conversion of CO_2RR to C_{2+} product significantly faster than Cu (111) while being less stable in the crystalline phase [246]. Similarly, Bingqain et al. prepared various Cu crystal facets forming different morphologies including cubic, octahedron, urchin, and truncated Cu_2O nanostructures to figure out the product selectivity and FEs of these nanostructure crystal facets. Each of these nanoparticles has different product selectivity since each of them is enclosed by various crystal facets like cubic (100) facets, octahedron (111) facets, truncated (100), and (111) facets, and urchin-like morphology (222) crystal facets [247]. The comparison of these facets

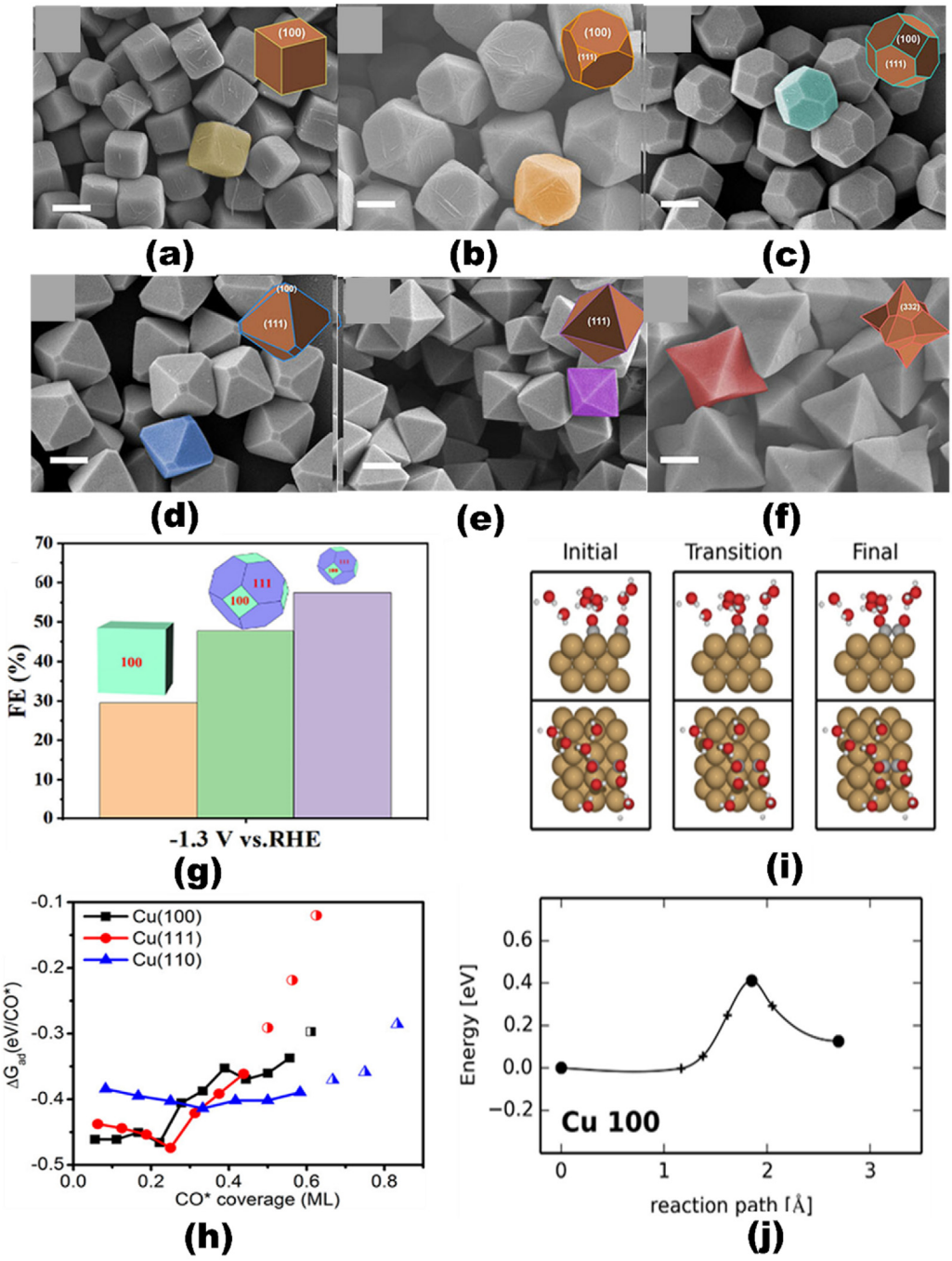

Fig. 11. SEM image of different shapes of Cu_2O catalysts named (a–f) Cu_2O, (a) Cubic (a-Cu_2O), (b) Corner-cut cubic (b-Cu_2O), (c) Truncated octahedral (c–Cu_2O), (d) Octahedral (d-Cu_2O) (e) Star-shaped (e-Cu_2O), (f) Star-shaped (f-Cu_2O) [243], Copyrights Wiley ©2022. (g) FE_{C2H4} of the prepared catalyst at −1.30 V vs. RHE [244], Copyrights Elsevier ©2023, (h) CO adsorption energy calculations over Cu (100), Cu (111), and Cu (110) surfaces as a function of CO* coverage [242], Copyrights ACS ©2017 and (i–j) CO dimerization on Cu (100) for the energy barrier calculations [245], Copyrights Elsevier ©2016.

indicates the fragmentation process during the reaction enhanced grain boundary formation and lattice fringes; subsequently leading to enhanced CO_2RR performance [248] and stability [30].

Durand et al. [249] investigated various Cu facets and found that intermediates in CO_2 reduction are stable by the decreasing order of FCC (211) > FCC (100) > FCC (111) facets. Initially, methane was identified as a major product when using the (211) facet, accompanied by minor production of H_2, CO, and formic acid. Later research revealed that Cu (111) facets contributed to the generation of an intermediate COH*, which promotes the synthesis of ethylene and methane. The applied potential and the CO* coverage are both necessary for the creation of this intermediate. For example, Cu(100), primarily promotes the synthesis of CHO* intermediate at low overpotentials, which in turn causes the C–C coupling of two CHO* species to produce ethylene, which is then followed by a sequence of reactions leading to C_2 species formation [98,250].

5. Reaction mechanism for C_2 products

Generally, the reaction mechanism to produce C_2 and C_{2+} products is extremely complex due to the multiple proton-electron transfer pathways, high energy barrier for C–C coupling reaction, wide range of intermediates, physicochemical properties of the active catalyst surface, nature of electrolyte and reaction environment. More specifically, CO_2 molecule is first reduced to *CO intermediate which is the key intermediate followed by *CHO, *COH, *COCO, *OCCHO, or *OCCOH, while the final product is determined by their binding strength on Cu surface [82]. The suitable Cu catalyst is the one that lowers the energy barrier by stabilizing the intermediates. The first intermediate species *CO dimerization is rate determining step during CO_2RR to C_{2+} due to *CO–*CO coupling. Thus, stable, and high coverage of *CO binding on the catalyst surface is crucial for C_{2+} which suggests that *CO is a prerequisite for

further intermediates such as *COCO, *OCCHO, or *OCCOH. Regarding C_1 products, the adsorption of CO_2 onto the catalyst surface has been observed, leading to the transformation of the gas into *COOH or *OCHO intermediates, which are important for the synthesis of CO and HCOOH, respectively [86]. *CO species can either participate in a C–C coupling process with other *CO species to make C_{2+} products like ethanol, ethylene, and n-propanol, or it can strongly adsorb on the catalyst surface to produce C_1 products through hydrogenation to CH_4 [86]. The initial adsorption of CO_2 molecules occurs in two possible ways i.e., proton-electron-coupled transfer (Eq 2) or electron-initiated CO_2 binding step (Eq 3).

$$*CO_2 + e^- + H^+ \rightarrow *COOH \quad (2)$$

$$*CO_2 + e^- \rightarrow *CO_2^- \quad (3)$$

$$*COOH + e^- + H^+ \rightarrow *CO \quad (4)$$

The CO_2 activation follows Eq. (2) on copper catalyst. Then *COOH intermediate is reduced to CO in the following step (Eq. (4)). According to the binding strength of *CO, it is either desorbed to form CO product or undergoes hydrogenation to *CHO or dimerization to *COCO to form C_2 or C_3. Recently, propanol was synthesized by CO_2/CO co-feed mechanism. In-situ Raman spectroscopy confirmed the unique CO–CO_2 coupling path toward propanol (FE: 25.7%) formation [251]. In similar work, Fan et al. investigated C–C coupling step between adsorbed *CO and *CHO species was more energetically favorable with barrier energy −0.83 V on a positive strain of +4% Cu (111) surface. On the contrary, the barrier energy for C-C coupling between adsorbed *CO and *COH was −0.47 eV on the negative strain of −4% Cu(111) surface [252]. Similarly, ions in electrolytes, especially halogen (F^-, Cl^-, I^- etc.), have been shown to improve CO_2RR performance of copper catalysts. The extended X-ray fine structure spectra (EXAFS) presented a Cu-O bond length of 2.15 Å, which matches the bond length of adsorbed ethoxy intermediate (Cu–OCH_2CH_3). Using potential-dependent Raman spectra, symmetric –CH_2 and –CH_3 stretching was identified at 2890 and 2920 cm^{-1} [253]. Such intermediate participated in a selectivity-determining step that occurred later in ethane or ethanol production. Furthermore, the authors proposed that fluorine on the surface of the copper catalyst lowered the energy barrier of C–C coupling through two *CHO dimerizations and that the rate-determining step is the hydrogenation of *CO to *CHO, which is arguably not common. The in situ FTIR (Fourier transform infrared spectroscopy) reveals that the band at 1 754 cm^{-1} could be attributed to *CHO species. Fluorine was also effective in assisting water activation and enhancing CO adsorption [253].

Among C_{2+} products, ethylene, ethanol, and ethane are very important owing to their higher energy density and their wide applications [140]. Four general steps can be used to describe the formation of C_2 products: (i) adsorption of CO_2 resulting in the formation of *CO; (ii) coupling reactions forming C–C bonds; (iii) additional post C–C coupling reactions; and (iv)desorption of products. Because of the occurrence of the undesirable hydrogen evolution reaction (HER) and the large activation energy needed for C–C coupling, the generation of C_{2+} or C_2 products is complicated. Numerous review articles have provided an overview of this complexity [90,233,157]. C–C coupling could be explained by two mechanisms; the Eley–Rideal mechanism (E–R) [254], and the Langmuir-Hinshelwood (L–H) mechanism [255]. The reactant in the former mechanism is CO while the catalyst surface adsorbs CO in the latter mechanism.

The energy barrier for C–C coupling is higher for the Ethylene-Ruthenium mechanism compared to that of the Leffler-Hammond mechanism, leading to the formation of C_{2+} products. L-H process, associated with these products, entails the creation of an easily hydrated $*C_2O_2$ intermediate [256,257]. There is still a debate regarding the C–C coupling mechanism, which is affected by several variables such as the applied potential, the presence of cations, tensile strain, and *CO partial pressure. The *CO coverage is especially significant since it is essential in lowering the activation energy required for *CO dimerization [257–259]. Although C_1 products are comparatively easier to form; owing to their low energy barrier and convenient reaction pathway, C_2 products are more important around the world due to their higher energy density and market demand. For instance, ethane (65.8 MJ/m^3) has surpassed methane (35.6 MJ/m^3), ethylene (1.32 MJ/mol), and ethanol (1.24 MJ/mol), owing to their higher energy density aforementioned products can be used as hydrocarbon fuel [223]. Cu catalyst has been extensively investigated for C_2 products, which can produce versatile products including hydrocarbons, oxygenates, and alcohols. Kuhl et al. [81] synthesized sixteen products via CO_2RR on Cu catalyst using a traditional H-cell reactor which strengthens the versatility feature of the Cu catalyst regarding product selectivity. Among all those products, ethylene, ethanol, ethane, and acetaldehyde are particularly important C_2 products due to their significant and widespread applications.

The mechanism of ethylene formation in CO_2RR is still under debate. However, there are two proposed pathways based on overpotential on a single Cu atom. It was assumed in the earliest studies [56] that ethylene formation occurs mostly due to direct coupling of CH_2–CH_2, while recent investigations revealed that *CO dimerization leads to ethylene formation. The local *CO concentration in the Cu-Ag catalyst was attributed to the low free energy of *COOH which facilitated the *CO production and the *CO spillover effect led to ethylene formation. It is observed on Cu-Ag tandem catalyst that the energy barrier(−0.61 eV) of $*CH_2CHO$ to $*CH_2CH_2$ (ethylene reaction pathway) is lower than the energy barrier (−0.19 eV) of $*CH_2CHO$ to $*CH_3CHO$ (ethanol reaction path), thus favoring ethylene formation instead of ethanol on CuAg Nano wires catalyst [260]. Furthermore, multiple reports have consistently indicated that the formation of ethylene is not influenced by pH [56]. This indicates that the rate-determining step of ethylene formation does not involve multiple electron protons interaction, unlike methane; which is confirmed by differential electrochemical mass spectrometry (DEMS) techniques used to investigate C–C coupling step [79]. They concluded that the first step of C_2 pathway was CO–CO coupling, followed by protonation (CO–CHO) to produce a surface-bonded enediol or enediolate, or an ox-metallacycle species, which explains the selectivity toward C_2H_4. Using differential electrochemical mass spectrometry (DEMS), they put forth two different processes for the synthesis of C_2H_4 with different overpotentials. The rate-determining step (RDS) of CO–CO coupling on the Cu (100) facet participates in the low-overpotential pathway, but the high-overpotential pathway uses the same RDS intermediate as CH_4, which occurs on both Cu (100) and (111) facets. Furthermore, the presence of Cu facets (111) or (110) enhanced selectivity towards ethylene. FE of ethylene was influenced by the Cu_2O crystal size; as the crystal size decreased from 41 nm to 18 nm, FE of ethylene increased from 10% to 43%, demonstrating the particle size impact on CO_2RR [261].

To explore further deep insights into the various morphology and facets that could affect the performance and hence the reaction mechanism. Cu (100) facets promote ethylene production by *CO dimerization and Cu (111) favors methane formation [262]. For instance, Yao et al. [263] stabilized Cu(100) facets with thiol molecule (CuO-SH), owing to its stronger binding ability. The Thiol-modified CuO(CuO-SH) resulted in 4 times more C_{2+} products (FE_{C2+} = 79.5%) than the original CuO electrode (FE_{C2+} = 16.9%) with a remarkable current density of −304 mA cm^{-2} at −1.2 V potential. In addition, Koolen et al. reported a non-equilibrium synthesis of nano-surface alloys (NSAs) with adjustable size, shape, and composition, even at temperatures below or equal to 80 °C, without considering miscibility [264]. Density functional theory (DFT) calculation of activation energy barriers of asymmetrical C–C coupling occurring between *CO and *CHO attributed this significant increase in FEs to the thiol-stabilized Cu(100). Regarding Cu morphological effect, density functional theory revealed that the defective Cu(111) surface results in a lower energy barrier of up to 110 meV during the *CO+*CO→ *OCCO step than that of the non-defective Cu(111) surface. Thus, the lower energy barrier for defective Cu(111) results in

higher ethylene formation (FE: 83%) than non-defective Cu(111) [176]. Numerous morphologies of Cu catalysts have been reported yet but the three morphologies including spherical, cubical, and octahedral are presented in Fig. 12a to c [265]. The cubic nanocrystals with Cu (100) facets exhibited ethylene production with FE of 57%, whereas Cu nanocrystals with Cu (111) facets achieved FE of 51% towards methane formation (Fig. 12d). XRD (X-ray diffraction) analysis of the corresponding catalyst verified that Cu(cubes) has the highest quantity of the Cu (100) facets (Fig. 12e), which could be attributed for higher production of ethylene. Therefore, it is evident that the development of favorable Cu facets plays a critical role in enhancing ethylene production during CO_2RR. Furthermore, with the addition of an Al_2O_3 layer to cover the competing facets Cu (111) and Cu (100), the relative surface area of Cu (100) is enhanced, resulting in a significant increase in ethylene production, resulting in an FE of 60.4% which is 22 times higher ethylene/methane ratio compared to pristine Cu-NCs (Fig. 12f). Later Wang et al. explained the remarkable increase in the production of ethylene using various copper facets through the electrodeposition (Fig. 12g) under CO_2 atmosphere as compared to the electrodeposition of Cu–HER catalyst in an N_2 atmosphere [30].

Based on density functional theory (DFT) calculations, it has been determined that the transfer of the first electron necessitates a large negative potential energy, making it the rate-determining step in the process. The potential pathways for ethylene formation include (i) The adsorption of *CO which undergoes hydrogenation, resulting in the formation of a carbene ($*CH_2$) which then undergoes dimerization, leading to the production of ethylene. (ii) The other pathway commenced with the dimerization of the adsorbed CO, which was subsequently followed by an electron-proton transfer yielded ethylene formation [267]. Three widely accepted pathways for the formation of ethylene are the dimerization of *CO, the coupling of two $*CH_2$ species (carbene mechanism), and the insertion of CO in *CHO species. These insights into the

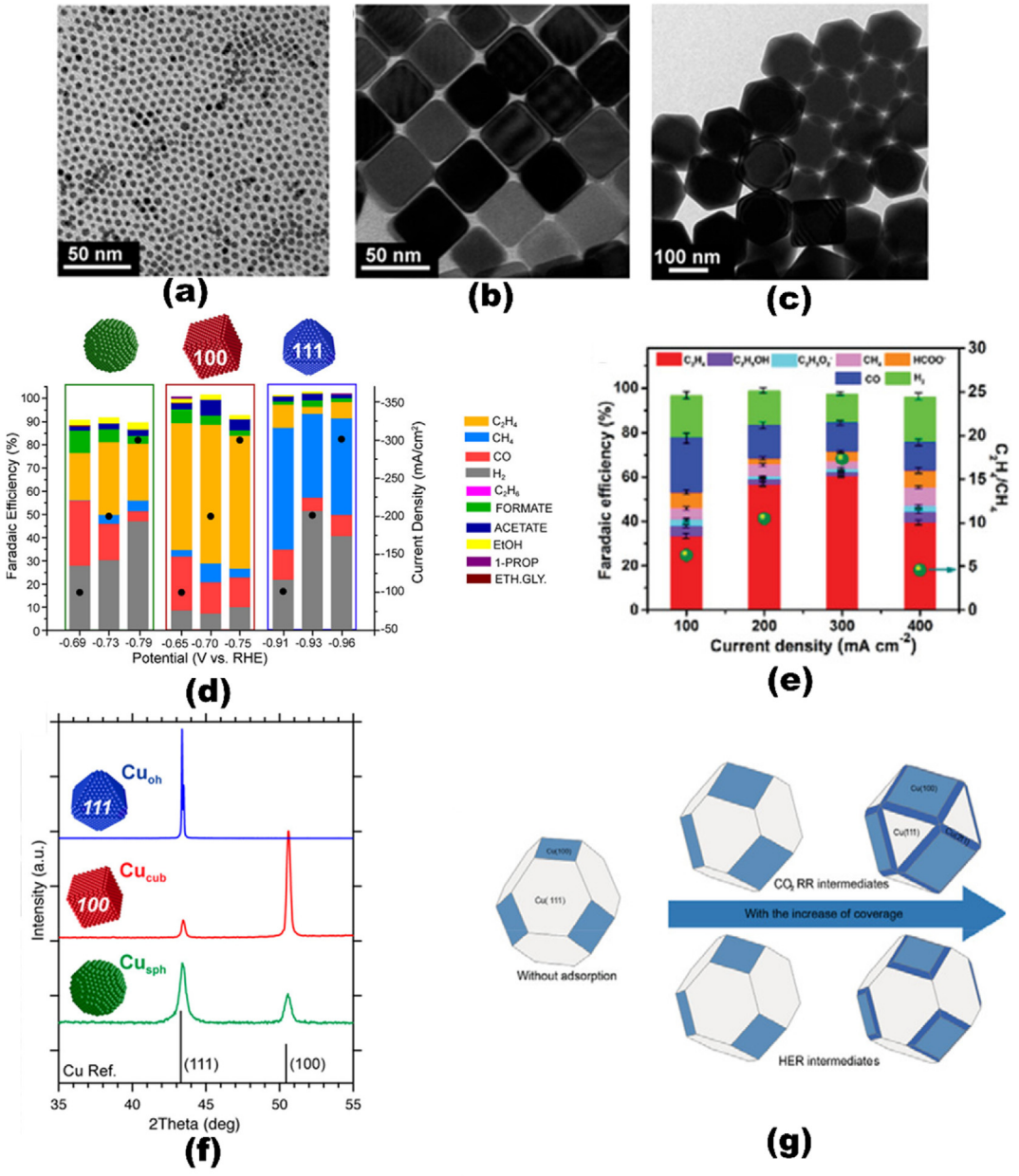

Fig. 12. (a–c) TEM images of Cu_{sph} (sphere = 200 μg cm^{-2}), Cu_{cub} (cube = 250 μg cm^{-2}), and Cu_{och} (octahedral = 50 μg cm^{-2}), (d) FEs vs. the potential for Cu_{sph}, Cu_{cub}, and Cu_{och}, (e) XRD of corresponding catalysts facets [265], Copyrights ACS ©2020, (f) Product distribution over Cu-NCs covered with Al_2O_3, and (g) CO_2RR intermediates adsorption over Cu(100) [266], Copyrights Springer Nature ©2020.

CO_2 reduction mechanism towards C_2 products are based on DFT and advanced operando spectroscopy as below in Fig. 13a [268]. Fig. 13b depicts two reaction pathways to produce ethylene based on the difference in the pH value. The pH-independent pathway, which has only one intermediate to form the selective product, and has higher energy barriers offers advantages in the reaction kinetics [269].

The synthesis of ethylene and ethanol is represented by a mechanistic computational model (Fig. 13c), in which the proton-electron transfer is the initial step leading to the surface moiety *COOH. *CO species is produced by further reducing the adsorbed species, and this moderately adsorbed *CO species is then hydrogenated to produce methane or dimerized to produce *$C_2H_xO_2$, which creates ethylene and ethanol [67].

Goodpaster et al. [100] revealed that ethanol is more favorable on Cu (100) at low overpotentials, whereas ethylene and methane are formed at higher overpotentials. In contrast, ethylene and methane are produced on Cu (111) surface at all potentials. DFT calculations revealed that *COCO dimer formation drives low overpotential C–C coupling, while *CO with *CHO enhances high overpotential C–C formation (Fig. 13d) [270]. The work on ethanol production from CO_2RR reported previously is summarized in Table 6.

Several strategies have been adopted to determine the ethane formation mechanism. The effect of grain boundaries on the production of ethylene and ethanol was investigated by Chen et al. [72] and the reaction mechanism using ATR-FTIR. The hydrogenation of C_2H_4 to C_2H_6 is

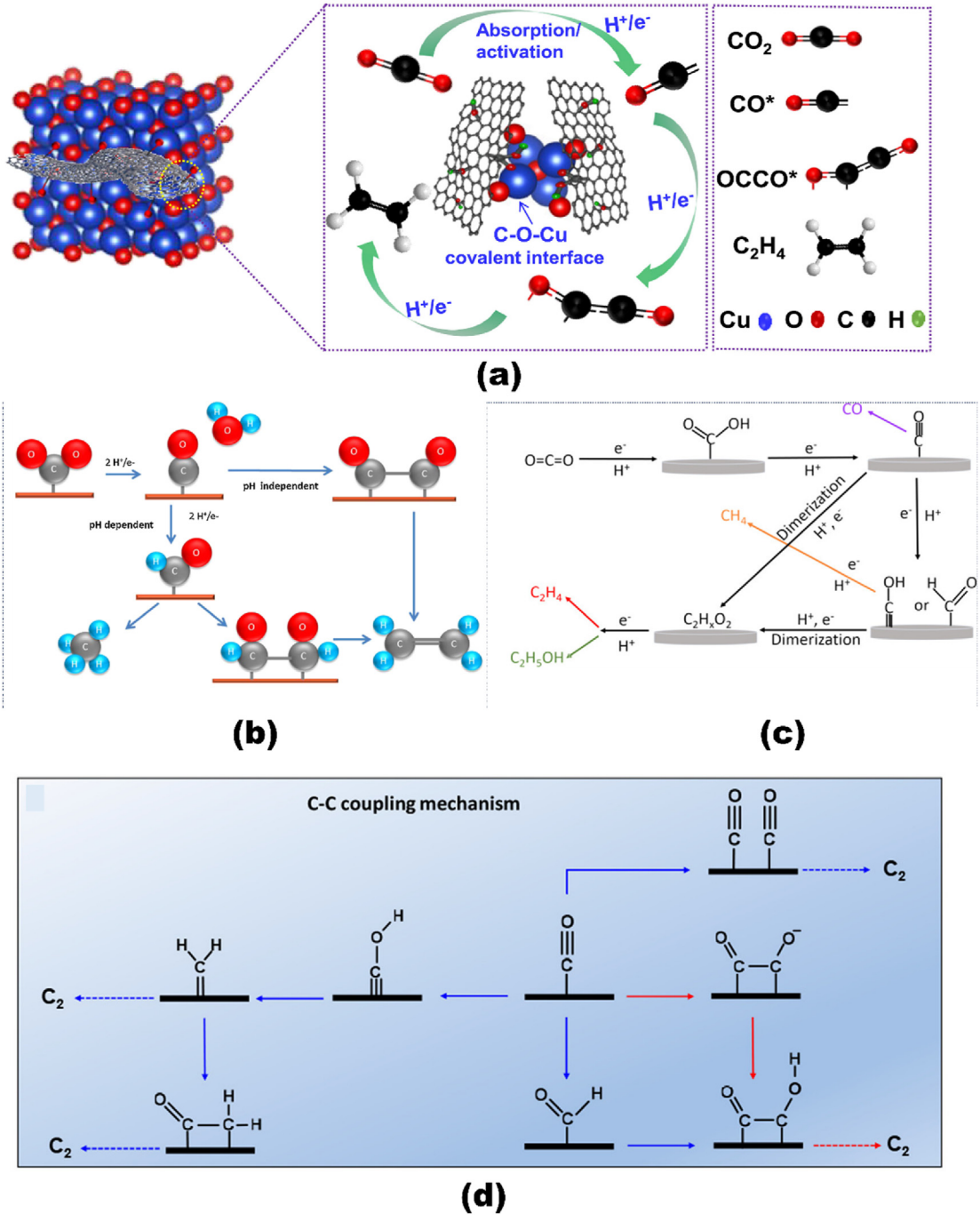

Fig. 13. Graphical representation of the proposed mechanism for ethylene production using Cu_2O/O–CNTs [268], Copyrights Elsevier ©2023, (b) Proton–dependent mechanism and proton-independent pathway [269], Copyrights Elsevier ©2016, (c) Proposed mechanism for eCO_2RR to ethylene and ethanol on Cu [67], Copyrights ACS ©2015, and (d) Possible mechanisms on the surface of Cu from *CO (red color indicates the most suitable mechanism) [270], Copyrights ACS ©2019.

Table 5
Summary of CO_2RR based on Cu nanocrystal catalyst for the formation of ethylene.

Catalysts	Electrolyte	Ethylene FE (%)	Current Density (mA/cm^2)	Potential (vs RHE) V	Ref.
Cu (711) foil	0.1 M $KHCO_3$	51.0	2.55	–0.54	[210]
Cu_2O/ILGS	0.1 M $KHCO_3$	31.	-	–1.15	[152]
240 nm Cu cubes pre-treated with O_2 plasma	0.1 M $KHCO_3$	45.0	34.8	–1.0	[95]
Truncated-octahedral Cu_2O	0.5 M $KHCO_3$	59.0	37.0	–1.10	[266]
Nano defective Cu nanosheets	0.1 M K_2SO_4	83.2	58.8	–1.18	[176]
ZrO_2/Cu-Cu_2O	0.1 M KCl	62.5	24.0	–1.28	[271]
44 nm Cu nano-cubes	0.1 M $KHCO_3$	41.0	3.0	–1.10	[99]
Cu_3N nano-cube	0.1 M $KHCO_3$	60.0	30.0	–1.60	[272]
Electro redeposited Cu	0.1 M $KHCO_3$	38.0	22.0	–1.0	[92]
Graphite/carbon NPs/Cu/PTFE electrodes)	7.0 M KOH	70.0	100	–0.55	[273]
Cu_2O nano-cube	0.25 M $KHCO_3$	32.0	N.A.	–1.10	[266]
Cu nanocrystals	1.0 M KOH	67.0	217	–0.63	[274]
Cu-oleyl amine NPs	1.0 M KOH	54.0	186	–1.0	[275]
Cu/'CeO_2 nanotubes	1.0 M KOH	65.5	50.0	–1.50	[276]
CuO nanoplate	0.5 M KCI	84.5	200	–0.81	[277]
Cu-Ag	0.1 M $KHCO_3$	60.0	300	–0.70	[278]
Cu hollow multi-shell structure	0.5 M $KHCO_3$	77 .0	513.7	–0.90	[279]
Au @ Cu	0.1 M $KHCO_3$	44.9	32.1	–1.11	[280]
Ag 65-Cu35	0.1 M $KHCO_3$	54.0	15.1	–1.20	[259]
Cu_2O/NRGO	0.1 M $KHCO_3$	19.7	12.0	–1.40	[256]
Electrochemical fragmented Cu_2O nanoparticles	0.1 M $KHCO_3$	27.0 – 57.3	17.5	–1.10	[91]
Cu_2O/NCS	0.1 M $KHCO_3$	24.7	10.3	–1.30	[281]
Cu_2O film on Cu	0.1 M $KHCO_3$	40.0	N.A.	–0.99	[67]
CuO/Al_2CuO_4	0.1 M $KHCO_3$	82.4	421	–0.99	[282]
Branched CuO nanoparticles	0.1 M $KHCO_3$	68.0	25.3	–1.05	[25]
250 nm Cu cubes on Cu foils	0.1 M $KHCO_3$	48.0	N.A.	–1.03	[283]

NA* = not available.

increased from 16% to 45% when Cu_2O-derived Cu is applied in the presence of potential (Fig. 14a). The ethane production was further analyzed using several experiments (Fig. 14b) at various current densities [77]. The selectivity of ethane formation is almost negligible, and ethanol is the dominant product. Song et al. [267] investigated the mechanism of ethanol production using DFT calculation. The selectivity switched to ethylene, ethane, n-propanol, and ethanol at constant potential by varying the length and density of nanowires (Fig. 14c to d)). However, Yang et al. [187] prepared Cu mesopore electrodes with controlled morphology (Fig. 14e to i) and found higher ethane selectivity on Cu mesopore electrodes having higher pore size and enhanced depth [187]. The reaction kinetics behind the proposed morphology were analyzed by specific activities and further confirmed by thermodynamic studies. The morphology affects the C–C coupling reactions and the pH of the reaction [187].

6. Conclusion and future perspective

The eCO_2RR via Cu catalyst into hydrocarbons including C_1 and C_{2+} has gained significant importance in maintaining carbon neutrality. However, commercialization has been limited because of the following challenges.

- A higher amount of energy (−1.90 V vs SHE) is required to adsorb CO_2 molecules on the surface of the catalyst to form a CO^{2-} intermediate which is considered a rate-determining step to initiate the reaction resulting in the large overpotential for the reaction.
- The limited mass transfer in electrolytes and sluggish reaction kinetics of CO_2 reduce its reaction rate.
- eCO_2RR produces a mixture of liquid and gaseous products, which makes it challenging to separate the products economically. The stability of the electrocatalyst so far reported is less than 100 h but there are limited catalysts that show higher stability owing to the blockage or poisoning of active sites, and formation of by-products (HER or carbonate/bicarbonate formation).
- OER (oxygen evolution reaction) and ORR (oxygen reduction reaction) occur easier than CO_2 reduction, which is difficult to quantify based on the reactor system, making it difficult to predict the actual mechanism behind the byproduct formation.

Considering the practical applications and commercialization of CO_2RR, the following requisites should be considered during the catalyst design strategies: (i) higher current densities (>-200 mA cm^{-2}) and fast reaction rates which allow one to produce large quantities of products with a small electrode size; (ii) increased product selectivity which is beneficial for improving feedstock utilization and lowers the downstream separation costs; owing to the high FE; (iii) high energy efficiencies yielding low onset potential which reduces the energy consumption and operating costs; (iv) high single-pass conversion is a promising parameter to determine the cost of product separation and recovery; (v) long-term stability for the practical applications, which is typically required in the CO_2RR process. The mechanism behind the C_2 product formation involves multi-proton electron transfer during CO_2RR making it more complicated by yielding other side products over the Cu surface. Advances in the in-situ techniques including ATR-FTIR, XAS (X-ray absorption spectroscopy), and Raman spectroscopy might be considered for the determination of intermediates. One of the major hurdles in electrochemical CO_2RR is the production of the products at higher potential (>-3.0 V) and low current density (<-100 mA cm^{-2}). Although Cu catalysts can produce a wide range of products, the FE of these products is not enough for practical applications. One of the reasons is the production of hydrogen which is the only competitive reaction occurring at lower potential. To suppress HER, different strategies could be adopted, including high pressure, appropriate membrane selection, electrolyte concentrations, cationic size of the electrolyte, and local pH values. In addition, the development of certain materials including MOFs, SACs, interfaces, and polymer-incorporated Cu catalysts would be effective for the conversion of CO_2 into hydrocarbons which would increase the FE towards C_{2+} products. In addition, understanding the reaction mechanism for C_2 products could be effective through DFT calculations and in-situ characterizations, which could explain the active sites for efficient electrochemical reactions.

Plenty of work has been invested into creating the best catalysts for CO_2RR, but much more research is required to comprehend the mechanism of degradation, morphological modifications, and working mechanisms. Due to the complexity of CO_2RR, it is difficult to understand the inconceivable variations by the ex-situ characterizations in the

Table 6
Summarized paper on ethanol production on Cu-based catalysts.

Catalysts	Electrolyte	Potential (V vs RHE)	Current density (mA/cm^2)	Ethanol FE (%)	Reactor type	Reference
Cu-DAT-wire	1.0 M KOH	−0.69	275	27.3	Flow cell	[284]
HKUST-1/CAU-17 blend	0.5 M $KHCO_3$	−0.21	20.0	28.3	H-type	[285]
Cu_4Zn	0.1 M $KHCO_3$	−1.05	28.2	29.1	H-type	[286]
Electrodeposited Cu_4Zn	0.1 M $KHCO_3$	−1.05	8.20	29.1	H-type	[287]
Fe-TPP[Cl] immobilized on Cu	1.0 M $KHCO_3$	−0.82	124	41.2	Flow	[266]
Cu_2O NWs/Ag NPs composites	0.1 M $KHCO_3$	−1.10	25.1	16.5	H-type	[288]
Cu-Ag alloy film	1.0 M KOH	−0.70	310.8	25.9	Flow cell	[278]
O_2-plasma-treated Cu nanocubes on Cu foil	0.1 M $KHCO_3$	−1.05	50.0	22.0	H-type	[289]
Cu_2O nanocubes on Cu foil	0.25 M $KHCO_3$	−0.96	68.0	12.5	H-type	[221]
Cu_2O film	0.1 M $KHCO_3$	−0.99	35.0	16.3	H-type	[290]
Fast-cooled CuO	1.0 M KOH	−1.05	356	35.7	Flow cell	[291]
Densely packed Cu NP ensemble	0.1 M $KHCO_3$	−0.86	20.4	16.6	H-type	[292]
N-doped carbon coated on CuO)	1.0 M KOH	−0.68	10.0	52.3	Flow cell	[280]
Cu (310)	0.1 M $KHCO_3$	−1.42 vs SHE	5.0	29.9	H-type	[63]
RuPC/NPC	0.5 M $KHCO_3$	−0.97	0.80	27.5	H-type	[258]
Cu NPs/N-doped nanodiamond	0.5 M $KHCO_3$	−0.50	0.70	28.9	H-type	[293]
Phase-blended Ag–Cu_2O	0.2 M KCl	−1.20	3.0	34.1	H-type	[187]
HKUST-1	0.5 M $KHCO_3$	−0.9 V vs Ag/AgCl	10.0	10.3	H-type	[96]
Cu (Ag-20)20	0.1 M $KHCO_3$	−1.10	25.1	16.5	H-type	[288]
Grain-boundary-rich CuO	1.0 M KOH	−1.30	45.0	31.7	H-type	[294]
Cu NPs on N-doped carbon nano spikes	0.1 M $KHCO_3$	−1.20	NA	63.0	H-type	[267]
Cu@AIL	1.0 M KOH	−1.31	1800	38.6	Flow cell	[295]

NA* = not available.

morphology and oxidation states on exposure to the air. The identification of active sites increases as the electrode's surface area increases, potentially leading to an increase in the interactions between the electrode and electrolyte as well as an increase in current density. Moreover, the cost of separating products may be decreased by using solid electrolytes between the AEM and CEM. Since this structure permits $HCOO^-$ and H^+ to migrate toward the center solid electrolyte, no extra purification or separation procedure is required. Although the separation is not needed in ionic forms; it is still challenging to separate the rest of the products which still needs more research and effort in the future. The reactor configuration is another factor that might be decisive in considering the catalyst design, along with the operando characterizations. Several studies focused on the in-situ characterization to understand the reaction mechanism and active sites. For instance, the direct correlation between the Cu^+ species and ethylene production has been explained by the in-situ XAFs analysis. The correlation towards the selectivity of C_{2+} products with the Cu^+ species was explained by the quasi-in-situ XPS analysis, which can further understand the stabilization of Cu^+ species over Cu surface. In addition, the selectivity of C_{2+} products might be enhanced by the presence of subsurface oxygen species, halides, and electrolyte cations.

eCO_2RR is typically conducted under ambient conditions (25 °C and 1 atm), resulting in a limited solubility of CO_2 at different operating variables. This low solubility leads to a reduced concentration of CO_2 both in the electrolyte as well as on the catalyst surface, leading to slow kinetics and hence poor electrochemical performance. The solubility of CO_2 increases with increasing the partial pressure of the CO_2, resulting in a higher concentration of CO_2 in the electrolyte as well as on catalyst surfaces, which could be effective for suppressing HER and hence higher C_2 product selectivity. Higher pressure of CO_2 up to 60 atm yields five times higher selectivity, and current density. This strategy could open a new avenue for synthesizing higher hydrocarbons from eCO_2RR, thereby providing a practical approach for addressing the intermittent of renewable energy fuels. Furthermore, recent advancements in the electrochemical conversion of CO_2 into C_2 products using Cu catalysts, which focus on major challenges, catalyst and interface engineering, and mechanistic insight into synthesizing C_2 products. The challenges in commercializing the reduction of CO_2 to C_2 products have been addressed. Considering such factors including morphology, facets, oxidation states, particle size, and active sites could enhance catalyst engineering. Considering the cell configuration, regulation of electrode surface, structure, and electrolyte can greatly contribute to the increase of mass transfer, high catalytic activity, and enhancement of energy efficiency. Therefore, these parameters boost the potential and their CO_2RR performance towards the C_2 products. Although much progress has been made using copper catalysts to convert CO_2 into C_2 products including ethylene, ethanol, and ethane, however, the active sites and reaction mechanisms are still unclear.

This is believed that the electrochemical reduction of CO_2 at higher pressure in MEA cells will be a turning point toward CO_2RR industrialization. Because higher pressure results in higher current density up to -200 mA cm^{-2} at less than -3.0 V. Secondly, catalyst structure engineering has ample importance regarding CO_2RR optimization, product selectivity, and operational stability. For instance, it is observed that Cu^+/Cu^0 coexistence states affect CO_2RR activity. The electrocatalyst needs to modified in such a way that the copper oxidation state (Cu^+/Cu^{2+}) could be prolonged as much as possible to maintain CO_2RR activity and stability. However, Cu oxidation state and its specific facets cannot persist for a long time in high alkaline conditions as well as high current density. Halide adsorption on Cu surface is one way to maintain the positive oxidation state of Cu particles owing to the electronegative behavior of the halides. Another way is to utilize a core-shell electrocatalyst structure where the shell structure would protect the core catalyst as a protecting layer. Apart from halides, particle size, oxygen vacancies, catalyst defects, and catalyst facets are very crucial for CO_2RR. It has been observed that Cu(111) favors ethylene and methane formation while Cu(100) results in C_{2+} products faster than Cu(111) owing to its low binding energy for *CO. Thus, controlled facets synthesis needs to be employed to prepare C_{2+} products. Similarly, a defective Cu surface is more active in adsorbing CO_2 compared to a polished or non-defective Cu surface; thus, producing higher ethylene regarding Cu-tandem catalyst has the potential to produce C_2 products at higher FE and Current density such as Cu-Co and Cu-Ag tandem catalyst owing to their low activation energy and higher reaction kinetics. In Cu-Ag tandem catalyst, Ag catalyst favors CO formation readily which is further converted to C_{2+} products by the C–C coupling mechanism. Similarly, the incorporation of carbon-based material as a substrate with Cu catalyst enhances its C_{2+} selectivity as well as the operational stability of the catalyst. Secondly, catalyst stability could be improved with PTFE (Poly tetrafluoro ethylene) (Polytetrafluoroethylene) binder during the catalyst ink preparation where PTFE protects GDL (gas diffusion layer) from delamination owing to its hydrophobic nature. Furthermore, the optimization of MEA

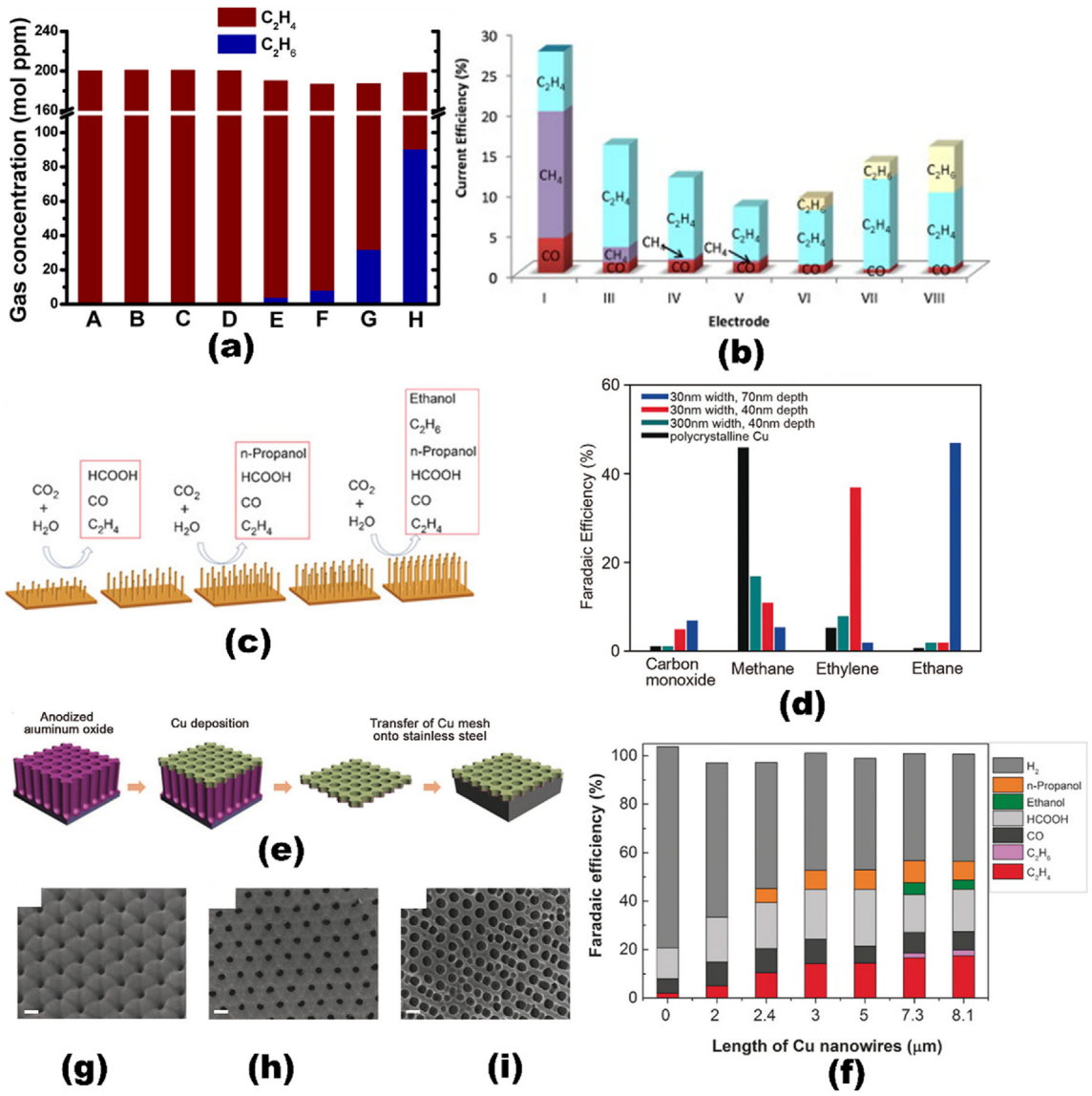

Fig. 14. (a) Product analysis of C_2H_4 in an electrochemical cell under various parameters A–H (working electrode, added particles, and potential) [72]. Copyrights ACS ©2015, (b) FEs of gaseous products for different electrodes (Potentials) [77], Copyrights Elsevier ©2013, (c) Schematic of gaseous products selectivity on various NWs length and density [296], (d) FEs of various products on different NWs length [267], Copyrights Wiley ©2016, (e) synthesis of Cu mesoporous electrode, (f) FEs of gaseous products at various porous lengths and depths, and SEM images of NWs with (g) 30 nm width/40 nm depth, (h) 30 nm width/70 nm depth, and (i) 300 nm width/40 nm [297], Copyrights Wiley ©2017.

membrane and strengthening of GDEs will enhance the operational stability of CO_2RR in the future and advance toward CO_2RR industrialization.

Acknowledgement

The authors are grateful for the financial support from International Society of Engineering Science and Technology (ISEST) UK.

References

[1] S.I. Seneviratne, M.G. Donat, A.J. Pitman, R. Knutti, R.L. Wilby, Allowable CO2 emissions based on regional and impact-related climate targets, Nature 529 (2016) 477–483.

[2] G. Luderer, Z. Vrontisi, C. Bertram, O.Y. Edelenbosch, R.C. Pietzcker, J. Rogelj, H.S. De Boer, L. Drouet, J. Emmerling, O. Fricko, S. Fujimori, P. Havlík, G. Iyer, K. Keramidas, A. Kitous, M. Pehl, V. Krey, K. Riahi, B. Saveyn, M. Tavoni, D.P. Van Vuuren, E. Kriegler, Residual fossil CO2 emissions in 1.5–2 °C pathways, Nat. Clim. Change 8 (2018) 626–633.

[3] M.S. Masnadi, H.M. El-Houjeiri, D. Schunack, Y. Li, J.G. Englander, A. Badahdah, J.-C. Monfort, J.E. Anderson, T.J. Wallington, J.A. Bergerson, Global carbon intensity of crude oil production, Science 361 (2018) 851–853.

[4] M.K. Khan, W. Kwek, J. Kim, Conversion of petroleum emulsion into light fraction-rich upgraded oil in supercritical methanol, Fuels 218 (2018) 78–88.

[5] M.K. Khan, W. Kwek, J. Kim, Upgrading heavy crude oils and extra heavy fractions in supercritical methanol, Energy Fuel. 31 (2017) 12054–12063.

[6] M.K. Khan, H.S. Cahyadi, S.-M. Kim, J. Kim, Efficient oil recovery from highly stable toxic oily sludge using supercritical water, Fuel 235 (2019) 460–472.

[7] W. Kwek, M.K. Khan, B. Sarkar, R. Insyani, M. Yi, J. Kim, A non-catalytic, supercritical methanol route for producing high-yield saturated and aromatic compounds from de-oiled asphaltenes, J. Supercrit. Fluids 120 (2017) 140–150.

[8] M.K. Khan, B. Sarkar, H. Zeb, M. Yi, J. Kim, Simultaneous breaking and conversion of petroleum emulsions into synthetic crude oil with low impurities, Fuels 199 (2017) 135–144.

[9] M.K. Khan, R. Insyani, J. Lee, M. Yi, J.W. Lee, J. Kim, A non-catalytic, supercritical methanol route for effective deacidification of naphthenic acids, Fuel 182 (2016) 650–659.

[10] O. Al-Juboori, F. Sher, A. Hazafa, M.K. Khan, G.Z. Chen, The effect of variable operating parameters for hydrocarbon fuel formation from CO2 by molten salts electrolysis, J. CO2 Util. 40 (2020) 101193.

[11] W. Kwek, M.K. Khan, B. Sarkar, J. Kim, Supercritical methanol as an effective medium for producing asphaltenes-free light fraction oil from vacuum residue, J. Supercrit. Fluids 133 (2018) 184–194.

[12] M.K. Khan, A. Riaz, M. Yi, J. Kim, Removal of naphthenic acids from high acid crude via esterification with methanol, Fuel Process. Technol. 165 (2017) 123–130.
[13] B. Sun, M. Dai, S. Cai, H. Cheng, K. Song, Y. Yu, H. Hu, Challenges and strategies towards copper-based catalysts for enhanced electrochemical CO2 reduction to multi-carbon products, Fuels 332 (2023) 126114.
[14] N. Zhou, L. Price, D. Yande, J. Creyts, N. Khanna, D. Fridley, H. Lu, W. Feng, X. Liu, A. Hasanbeigi, A roadmap for China to peak carbon dioxide emissions and achieve a 20% share of non-fossil fuels in primary energy by 2030, Appl. Energy 239 (2019) 793–819.
[15] M.K. Khan, P. Butolia, H. Jo, M. Irshad, D. Han, K.-W. Nam, J. Kim, Selective conversion of carbon dioxide into liquid hydrocarbons and long-chain α-olefins over Fe-amorphous AlOx bifunctional catalysts, ACS Catal. 10 (2020) 10325–10338.
[16] S. Ahmed, M. Irshad, W. Yoon, N. Karanwal, J.R. Sugiarto, M.K. Khan, S.K. Kim, J. Kim, Evaluation of MgO as a promoter for the hydrogenation of CO2 to long-chain hydrocarbons over Fe-based catalysts, Appl. Catal. B Environ. 338 (2023) 123052.
[17] M. Irshad, H.-J. Chun, M.K. Khan, H. Jo, S.K. Kim, J. Kim, Synthesis of n-butanol-rich C3+ alcohols by direct CO2 hydrogenation over a stable Cu–Co tandem catalyst, Appl. Catal. B Environ. 340 (2024) 123201.
[18] H. Jo, M.K. Khan, M. Irshad, M.W. Arshad, S.K. Kim, J. Kim, Unraveling the role of cobalt in the direct conversion of CO2 to high-yield liquid fuels and lube base oil, Appl. Catal. B Environ. 305 (2022) 121041.
[19] M.G. Sibi, M.K. Khan, D. Verma, W. Yoon, J. Kim, High-yield synthesis of BTEX over Na–FeAlOx/Zn–HZSM-5@ SiO2 by direct CO2 conversion and identification of surface intermediates, Appl. Catal. B Environ. 301 (2022) 120813.
[20] M.G. Sibi, D. Verma, H.C. Setiyadi, M.K. Khan, N. Karanwal, S.K. Kwak, K.Y. Chung, J.-H. Park, D. Han, K.-W. Nam, Synthesis of monocarboxylic acids via direct CO2 conversion over Ni–Zn intermetallic catalysts, ACS Catal. 11 (2021) 8382–8398.
[21] S. Ahmed, S.S. Bibi, M. Irshad, M. Asif, M.K. Khan, J. Kim, Synthesis of long-chain paraffins over bimetallic Na–Fe0. 9Mg0. 1Ox by direct CO2 hydrogenation, Top. Catal. 67 (2024) 363–376.
[22] Y. Xia, Z. Tian, T. Heil, A. Meng, B. Cheng, S. Cao, J. Yu, M. Antonietti, Highly selective CO2 capture and its direct photochemical conversion on ordered 2D/1D heterojunctions, Joule 3 (2019) 2792–2805.
[23] J. Lü, R. Cao, Unique heterostructures of ZnCdS nanoplates with Bi2S3− terminated edges for optimal CO2− to− CO photoconversion, Nano Mater. Sci (2022).
[24] B.Ó. Joensen, J.A. Zamora Zeledón, L. Trotochaud, A. Sartori, M. Mirolo, A.B. Moss, S. Garg, I. Chorkendorff, J. Drnec, B. Seger, Q. Xu, Unveiling transport mechanisms of cesium and water in operando zero-gap CO2 electrolyzers, Joule 8, 1–18 (2024).
[25] J. Kim, W. Choi, J.W. Park, C. Kim, M. Kim, H. Song, Branched copper oxide nanoparticles induce highly selective ethylene production by electrochemical carbon dioxide reduction, J. Am. Chem. Soc. 141 (2019) 6986–6994.
[26] Y. Lum, J.W. Ager, Evidence for product-specific active sites on oxide-derived Cu catalysts for electrochemical CO2 reduction, Nat. Catal. 2 (2019) 86–93.
[27] G. Wang, J. Chen, Y. Ding, P. Cai, L. Yi, Y. Li, C. Tu, Y. Hou, Z. Wen, L. Dai, Electrocatalysis for CO2 conversion: from fundamentals to value-added products, Chem. Soc. Rev. 50 (2021) 4993–5061.
[28] J. Yang, X. Kang, J. Jiao, X. Xing, Y. Yin, S. Jia, M. Chu, S. Han, W. Xia, H. Wu, M. He, B. Han, Ternary ionic-liquid-based electrolyte enables efficient electro-reduction of CO2 over bulk metal electrodes, J. Am. Chem. Soc. 145 (2023) 11512–11517.
[29] S. Hong, H.G. Abbas, K. Jang, K.K. Patra, B. Kim, B.U. Choi, H. Song, K.S. Lee, P.P. Choi, S. Ringe, Tuning the C1/C2 selectivity of electrochemical CO2 reduction on Cu–CeO2 nanorods by oxidation state control, Adv. Mater. 35 (2023) 2208996.
[30] A. Ozden, F. Li, F.P. García de Arquer, A. Rosas-Hernández, A. Thevenon, Y. Wang, S.-F. Hung, X. Wang, B. Chen, J. Li, J. Wicks, M. Luo, Z. Wang, T. Agapie, J.C. Peters, E.H. Sargent, D. Sinton, High-rate and efficient ethylene electrosynthesis using a catalyst/promoter/transport layer, ACS Energy Lett. 5 (2020) 2811–2818.
[31] X. Nie, M.R. Esopi, M.J. Janik, A. Asthagiri, Selectivity of CO2 reduction on copper electrodes: the role of the kinetics of elementary steps, Angew. Chem. Int. Ed. 125 (2013) 2519–2522.
[32] Y. Chen, Y. Zhao, Coupling captured CO2-to-fuel with plastic-to-chemical conversion using only sunlight, Joule 7 (2023) 1399–1402.
[33] P. Chen, Y. Zhang, Y. Zhou, F. Dong, Photoelectrocatalytic carbon dioxide reduction: fundamental, advances and challenges, Nano Mater. Sci 3 (2021) 344–367.
[34] Z. Wang, G. Zou, J.H. Park, K. Zhang, Progress in design and preparation of multi-atom catalysts for photocatalytic CO2 reduction, Sci. China Mater. (2024) 1–26.
[35] S. Ahmed, W.W. Kazmi, A. Hussain, M.Z. Khan, S. Bibi, M. Saleem, R.H. Song, Z. Sajid, A. Ullah, M.K. Khan, Facile and low-temperature synthesis approach to fabricate Sm0. 5Sr0. 5CoO3− δ cathode material for solid oxide fuel cell, J. Korean Ceram. Soc. 60 (2023) 272–282.
[36] S. Ahmed, W.W. Kazmi, F.N. Butt, M. Irshad, F. Sher, S.M.A. Kazmi, U.M. Chaudry, H. Zeb, T.-S. Jun, M.K. Khan, Fabrication of nanocage structured based electrocatalyst for oxygen evolution reactions, Mater. Lett. 331 (2023) 133416.
[37] F. Sher, N. Smječanin, M.K. Khan, I. Shabbir, S. Ali, M.R. Hatshan, I.U. Hai, Agglomeration behaviour of various biomass fuels under different air staging conditions in fluidised bed technology for renewable energy applications, Renew. Energy 227 (2024) 120479.
[38] U. Mushtaq, J. Park, A. Riaz, V. Ranaware, M.K. Khan, D. Verma, J. Kim, High-yield production of deoxygenated monomers from kraft lignin over ZnO-Co/N-CNTs in water, ACS Sustain. Chem. Eng. 9 (2021) 3232–3245.
[39] H. Han, T. Han, Y. Luo, M.A. Mushtaq, Y. Jia, C. Liu, Recent advances in α-Fe2O3-based photocatalysts for CO2 conversion to solar fuels, J. Ind. Eng. Chem. 128 (2023) 81–94.
[40] Y.Y. Birdja, E. Pérez-Gallent, M.C. Figueiredo, A.J. Göttle, F. Calle-Vallejo, M.T. Koper, Advances and challenges in understanding the electrocatalytic conversion of carbon dioxide to fuels, Nat. Energy 4 (2019) 732–745.
[41] W. Deng, P. Zhang, B. Seger, J. Gong, Unraveling the rate-limiting step of two-electron transfer electrochemical reduction of carbon dioxide, Nat. Commun. 13 (2022) 803.
[42] L. Wang, S.A. Nitopi, E. Bertheussen, M. Orazov, C.G. Morales-Guio, X. Liu, D.C. Higgins, K. Chan, J.K. Nørskov, C. Hahn, Electrochemical carbon monoxide reduction on polycrystalline copper: effects of potential, pressure, and pH on selectivity toward multicarbon and oxygenated products, ACS Catal. 8 (2018) 7445–7454.
[43] X. Cao, S. Ren, X. Zhang, Q. Fan, Q. Chen, J. Yang, J. Mao, Identification of Cu0/Cu+/Cu0 interface as superior active sites for CO2 electroreduction to C2+ in neutral condition, Chem 10 (2024) 2089–2102.
[44] D. Ren, J. Fong, B.S. Yeo, The effects of currents and potentials on the selectivities of copper toward carbon dioxide electroreduction, Nat. Commun. 9 (2018) 925.
[45] K. Xiang, F. Shen, Y. Fu, L. Wu, Z. Wang, H. Yi, X. Liu, P. Wang, M. Liu, Z. Lin, Boosting CO 2 electroreduction towards C 2+ products via CO* intermediate manipulation on copper-based catalysts, Environ. Sci.: Nano 9 (2022) 911–953.
[46] J. Wu, W. Li, K. Liu, A. Kucernak, H. Liu, L. Chai, M. Liu, Cation effects on electrochemical CO2 reduction reaction, Energy 1 (2023) 100032.
[47] Y. Hori, A. Murata, R. Takahashi, Formation of hydrocarbons in the electrochemical reduction of carbon dioxide at a copper electrode in aqueous solution, J. Chem. Soc., Faraday Trans. 85 (1989) 2309–2326.
[48] Y. Hori, A. Murata, R. Takahashi, S. Suzuki, Enhanced formation of ethylene and alcohols at ambient temperature and pressure in electrochemical reduction of carbon dioxide at a copper electrode, J. Am. Chem. Soc. (1988) 17–19.
[49] Y. Hori, K. Kikuchi, A. Murata, S. Suzuki, Production of methane and ethylene in electrochemical reduction of carbon dioxide at copper electrode in aqueous hydrogencarbonate solution, Chem. Lett. 15 (1986) 897–898.
[50] Y. Hori, K. Kikuchi, S. Suzuki, Production of carbon monoxide and methane in electrochemical reduction of carbon dioxide at metal electrodes in aqueous hydrogen carbonate solution, Chem. Lett. 14 (1985) 1695–1698.
[51] S. Kapusta, N. Hackerman, The electroreduction of carbon dioxide and formic acid on tin and indium electrodes, J. Electrochem. Soc. 130 (1983) 607.
[52] P. Russell, N. Kovac, S. Srinivasan, M. Steinberg, The electrochemical reduction of carbon dioxide, formic acid, and formaldehyde, J. Electrochem. Soc. 124 (1977) 1329.
[53] W. Paik, T. Andersen, H. Eyring, Kinetic studies of the electrolytic reduction of carbon dioxide on the mercury electrode, Electrochim. Acta 14 (1969) 1217–1232.
[54] Z. Wei, J. Ding, X. Duan, G.-L. Chen, F.-Y. Wu, L. Zhang, X. Yang, Q. Zhang, Q. He, Z. Chen, Enhancing selective electrochemical CO2 reduction by in situ constructing tensile-strained Cu catalysts, ACS Catal. 13 (2023) 4711–4718.
[55] M.S. Kwon, J.Y. Lee, O2 plasma oxidation of sputter-deposited Cu thin film during photo resist ashing, Appl. Surf. Sci. 135 (1998) 101–106.
[56] P. Friebe, P. Bogdanoff, N. Alonso-Vante, H. Tributsch, A real-time mass spectroscopy study of the (electro) chemical factors affecting CO2reduction at copper, J. Catal. 168 (1997) 374–385.
[57] H. Noda, S. Ikeda, A. Yamamoto, H. Einaga, K. Ito, Kinetics of electrochemical reduction of carbon dioxide on a gold electrode in phosphate buffer solutions, Bull. Chem. Soc. Jpn. 68 (1995) 1889–1895.
[58] K. Hara, A. Kudo, T. Sakata, M. Watanabe, High efficiency electrochemical reduction of carbon dioxide under high pressure on a gas diffusion electrode containing Pt catalysts, J. Electrochem. Soc. 142 (1995) L57.
[59] K. Hara, A. Kudo, T. Sakata, Electrochemical reduction of carbon dioxide under high pressure on various electrodes in an aqueous electrolyte, J. Electroanal. Chem. 391 (1995) 141–147.
[60] K. Hara, A. Tsuneto, A. Kudo, T. Sakata, Electrochemical reduction of CO 2 on a Cu electrode under high pressure: factors that determine the product selectivity, J. Electrochem. Soc. 141 (1994) 2097.
[61] A. Kudo, S. Nakagawa, A. Tsuneto, T. Sakata, Electrochemical reduction of high pressure CO 2 on Ni electrodes, J. Electrochem. Soc. 140 (1993) 1541.
[62] Y. Hori, A. Murata, Y. Yoshinami, Adsorption of CO, intermediately formed in electrochemical reduction of CO 2, at a copper electrode, J. Chem. Soc., Faraday Trans. 87 (1991) 125–128.
[63] Y. Hori, I. Takahashi, O. Koga, N. Hoshi, Electrochemical reduction of carbon dioxide at various series of copper single crystal electrodes, J. Mol. Catal. Chem. 199 (2003) 39–47.
[64] Y. Hori, I. Takahashi, O. Koga, N. Hoshi, Selective formation of C2 compounds from electrochemical reduction of CO2 at a series of copper single crystal electrodes, J. Phys. Chem. B 106 (2002) 15–17.
[65] H. Yano, T. Tanaka, M. Nakayama, K. Ogura, Selective electrochemical reduction of CO2 to ethylene at a three-phase interface on copper(I) halide-confined Cu-mesh electrodes in acidic solutions of potassium halides, J. Electroanal. Chem. 565 (2004) 287–293.
[66] J.L. White, M.F. Baruch, J.E. Pander III, Y. Hu, I.C. Fortmeyer, J.E. Park, T. Zhang, K. Liao, J. Gu, Y. Yan, T.W. Shaw, E. Abelev, A.B. Bocarsly, Light-Driven heterogeneous reduction of carbon dioxide: photocatalysts and photoelectrodes, Chem. Rev. 115 (2015) 12888–12935.

[67] A. Verdaguer-Casadevall, C.W. Li, T.P. Johansson, S.B. Scott, J.T. McKeown, M. Kumar, I.E. Stephens, M.W. Kanan, I. Chorkendorff, Probing the active surface sites for CO reduction on oxide-derived copper electrocatalysts, J. Am. Chem. Soc. 137 (2015) 9808–9811.
[68] D. Ren, Y. Deng, A.D. Handoko, C.S. Chen, S. Malkhandi, B.S. Yeo, Selective electrochemical reduction of carbon dioxide to ethylene and ethanol on copper (I) oxide catalysts, ACS Catal. 5 (2015) 2814–2821.
[69] M. Ma, K. Djanashvili, W.A. Smith, Selective electrochemical reduction of CO 2 to CO on CuO-derived Cu nanowires, Phys. Chem. Chem. Phys. 17 (2015) 20861–20867.
[70] R. Kas, R. Kortlever, H. Yılmaz, M.T. Koper, G. Mul, Manipulating the hydrocarbon selectivity of copper nanoparticles in CO2 electroreduction by process conditions, Chemelectrochem 2 (2015) 354–358.
[71] X. Feng, K. Jiang, S. Fan, M.W. Kanan, Grain-boundary-dependent CO2 electroreduction activity, J. Am. Chem. Soc. 137 (2015) 4606–4609.
[72] C.S. Chen, J.H. Wan, B.S. Yeo, Electrochemical reduction of carbon dioxide to ethane using nanostructured Cu2O-derived copper catalyst and palladium(II) chloride, J. Phys. Chem. C 119 (2015) 26875–26882.
[73] P. Bumroongsakulsawat, G. Kelsall, Tinned graphite felt cathodes for scale-up of electrochemical reduction of aqueous CO2, Electrochim. Acta 159 (2015) 242–251.
[74] R. Reske, H. Mistry, F. Behafarid, B. Roldan Cuenya, P. Strasser, Particle size effects in the catalytic electroreduction of CO2 on Cu nanoparticles, J. Am. Chem. Soc. 136 (2014) 6978–6986.
[75] R. Kas, R. Kortlever, A. Milbrat, M.T. Koper, G. Mul, J. Baltrusaitis, Electrochemical CO 2 reduction on Cu 2 O-derived copper nanoparticles: controlling the catalytic selectivity of hydrocarbons, Phys. Chem. Chem. Phys. 16 (2014) 12194–12201.
[76] J.H. Montoya, A.A. Peterson, J.K. Nørskov, Insights into C- C coupling in CO2 electroreduction on copper electrodes, ChemCatChem 5 (2013) 737–742.
[77] M.R. Gonçalves, A. Gomes, J. Condeço, T.R.C. Fernandes, T. Pardal, C.A.C. Sequeira, J.B. Branco, Electrochemical conversion of CO2 to C2 hydrocarbons using different ex situ copper electrodeposits, Electrochim. Acta 102 (2013) 388–392.
[78] F. Calle-Vallejo, M. Koper, Theoretical considerations on the electroreduction of CO to C 2 species on Cu (100) electrodes, Angew. Chem. Int. Ed. 52 (2013).
[79] K.J.P. Schouten, Z. Qin, E. Pérez Gallent, M.T. Koper, Two pathways for the formation of ethylene in CO reduction on single-crystal copper electrodes, J. Am. Chem. Soc. 134 (2012) 9864–9867.
[80] C.W. Li, M.W. Kanan, CO2 reduction at low overpotential on Cu electrodes resulting from the reduction of thick Cu2O films, J. Am. Chem. Soc. 134 (2012) 7231–7234.
[81] K.P. Kuhl, E.R. Cave, D.N. Abram, T.F. Jaramillo, New insights into the electrochemical reduction of carbon dioxide on metallic copper surfaces, Energy Environ. Sci. 5 (2012) 7050–7059.
[82] A.A. Peterson, F. Abild-Pedersen, F. Studt, J. Rossmeisl, J.K. Nørskov, How copper catalyzes the electroreduction of carbon dioxide into hydrocarbon fuels, Energy Environ. Sci. 3 (2010) 1311–1315.
[83] N. Gupta, M. Gattrell, B. MacDougall, Calculation for the cathode surface concentrations in the electrochemical reduction of CO2 in KHCO3 solutions, J. Appl. Electrochem. 36 (2006) 161–172.
[84] K. Ogura, R. Oohara, Y. Kudo, Reduction of CO2 to ethylene at three-phase interface effects of electrode substrate and catalytic coating, J. Electrochem. Soc. 152 (2005) D213.
[85] Z. Zhou, S. Liang, J. Xiao, T. Zhang, M. Li, W. Xie, Q. Wang, Surface modification of Cu2O with stabilized Cu+ for highly efficient and stable CO2 electroreduction to C2+ chemicals, J. Energy Chem. 84 (2023) 277–285.
[86] C.Y.J. Lim, M. Yilmaz, J.M. Arce-Ramos, A.D. Handoko, W.J. Teh, Y. Zheng, Z.H.J. Khoo, M. Lin, M. Isaacs, T.L.D. Tam, Surface charge as activity descriptors for electrochemical CO2 reduction to multi-carbon products on organic-functionalised Cu, Nat. Commun. 14 (2023) 335.
[87] Y. Ji, Z. Chen, R. Wei, C. Yang, Y. Wang, J. Xu, H. Zhang, A. Guan, J. Chen, T.-K. Sham, J. Luo, Y. Yang, X. Xu, G. Zheng, Selective CO-to-acetate electroreduction via intermediate adsorption tuning on ordered Cu–Pd sites, Nat. Catal. 5 (2022) 251–258.
[88] Z. Gu, H. Shen, Z. Chen, Y. Yang, C. Yang, Y. Ji, Y. Wang, C. Zhu, J. Liu, J. Li, Efficient electrocatalytic CO2 reduction to C2+ alcohols at defect-site-rich Cu surface, Joule 5 (2021) 429–440.
[89] H. Bao, Y. Qiu, X. Peng, J.-a. Wang, Y. Mi, S. Zhao, X. Liu, Y. Liu, R. Cao, L. Zhuo, Isolated copper single sites for high-performance electroreduction of carbon monoxide to multicarbon products, Nat. Commun. 12 (2021) 238.
[90] L. Fan, C. Xia, F. Yang, J. Wang, H. Wang, Y. Lu, Strategies in catalysts and electrolyzer design for electrochemical CO2 reduction toward C2+ products, Sci. Adv. 6 (2020) eaay3111.
[91] H. Jung, S.Y. Lee, C.W. Lee, M.K. Cho, D.H. Won, C. Kim, H.-S. Oh, B.K. Min, Y.J. Hwang, Electrochemical fragmentation of Cu2O nanoparticles enhancing selective C–C coupling from CO2 reduction reaction, J. Am. Chem. Soc. 141 (2019) 4624–4633.
[92] P. De Luna, R. Quintero-Bermudez, C.-T. Dinh, M.B. Ross, O.S. Bushuyev, P. Todorović, T. Regier, S.O. Kelley, P. Yang, E.H. Sargent, Catalyst electro-redeposition controls morphology and oxidation state for selective carbon dioxide reduction, Nat. Catal. 1 (2018) 103–110.
[93] C. Chen, X. Sun, L. Lu, D. Yang, J. Ma, Q. Zhu, Q. Qian, B. Han, Efficient electroreduction of CO 2 to C2 products over B-doped oxide-derived copper, Green Chem. 20 (2018) 4579–4583.
[94] R.G. Mariano, K. McKelvey, H.S. White, M.W. Kanan, Selective increase in CO2 electroreduction activity at grain-boundary surface terminations, Science 358 (2017) 1187–1192.
[95] D. Gao, F. Scholten, B. Roldan Cuenya, Improved CO2 electroreduction performance on plasma-activated Cu catalysts via electrolyte design: halide effect, ACS Catal. 7 (2017) 5112–5120.
[96] J. Albo, D. Vallejo, G. Beobide, O. Castillo, P. Castaño, A. Irabien, Copper-based metal–Organic porous materials for CO2 electrocatalytic reduction to alcohols, ChemSusChem 10 (2017) 1100–1109.
[97] H. Mistry, A.S. Varela, C.S. Bonifacio, I. Zegkinoglou, I. Sinev, Y.-W. Choi, K. Kisslinger, E.A. Stach, J.C. Yang, P. Strasser, Highly selective plasma-activated copper catalysts for carbon dioxide reduction to ethylene, Nat. Commun. 7 (2016) 12123.
[98] W. Luo, X. Nie, M.J. Janik, A. Asthagiri, Facet dependence of CO2 reduction paths on Cu electrodes, ACS Catal. 6 (2016) 219–229.
[99] A. Loiudice, P. Lobaccaro, E.A. Kamali, T. Thao, B.H. Huang, J.W. Ager, R. Buonsanti, Tailoring copper nanocrystals towards C2 products in electrochemical CO2 reduction, Angew. Chem. Int. Ed. 55 (2016) 5789–5792.
[100] J.D. Goodpaster, A.T. Bell, M. Head-Gordon, Identification of possible pathways for C–C bond formation during electrochemical reduction of CO2: new theoretical insights from an improved electrochemical model, J. Phys. Chem. Lett. 7 (2016) 1471–1477.
[101] H.M. Jeong, Y. Kwon, J.H. Won, Y. Lum, M.J. Cheng, K.H. Kim, M. Head-Gordon, J.K. Kang, Atomic-scale spacing between copper facets for the electrochemical reduction of carbon dioxide, Adv. Energy Mater. 10 (2020) 1903423.
[102] J. Hussain, H. Jónsson, E. Skúlason, Calculations of product selectivity in electrochemical CO2 reduction, ACS Catal. 8 (2018) 5240–5249.
[103] A. Handoko, F. Wei, B. Jenndy, Z. Yeo, N. Seh, Catalyst 1 (2018) 922–934; b) A, ACS Catal. 9 (2019) 10020–10043.
[104] X. Kang, G. Fu, X.-Z. Fu, J.-L. Luo, Copper-based metal-organic frameworks for electrochemical reduction of CO2, Chin. J. Chem. 34 (2023) 107757.
[105] S.A. Farooqi, A.S. Farooqi, S. Sajjad, C. Yan, A.B. Victor, Electrochemical reduction of carbon dioxide into valuable chemicals: a review, Environ. Chem. Lett. (2023) 1–39.
[106] S. Nitopi, E. Bertheussen, S.B. Scott, X. Liu, A.K. Engstfeld, S. Horch, B. Seger, I.E. Stephens, K. Chan, C. Hahn, Progress and perspectives of electrochemical CO2 reduction on copper in aqueous electrolyte, Chem. Rev. 119 (2019) 7610–7672.
[107] D. Raciti, C. Wang, Recent advances in CO2 reduction electrocatalysis on copper, ACS Energy Lett. 3 (2018) 1545–1556.
[108] H. Xie, T. Wang, J. Liang, Q. Li, S. Sun, Cu-based nanocatalysts for electrochemical reduction of CO2, Nano Today 21 (2018) 41–54.
[109] Z.-Z. Wu, P.-P. Yang, M.-R. Gao, Dynamic evolution of copper-based catalysts during CO2 electroreduction, Nano Mater. Sci (2024).
[110] K. Xu, Q. Zhang, X. Zhou, M. Zhu, H. Chen, Recent progress and perspectives on photocathode materials for CO2 catalytic reduction, Nanomaterials 13 (2023) 1683.
[111] S.A. Fors, C.A. Malapit, Homogeneous catalysis for the conversion of CO2, CO, CH3OH, and CH4 to C2+ chemicals via C–C bond formation, ACS Catal. 13 (2023) 4231–4249.
[112] L. Zhang, Z.J. Zhao, J. Gong, Nanostructured materials for heterogeneous electrocatalytic CO2 reduction and their related reaction mechanisms, Angew. Chem. Int. Ed. 56 (2017) 11326–11353.
[113] M. Abbas, M.A.Z.G. Sial, New Horizon in stabilization of single atoms on metal-oxide supports for CO2 reduction, Nano Mater. Sci 3 (2021) 368–389.
[114] F. Yu, P. Wei, Y. Yang, Y. Chen, L. Guo, Z. Peng, Material design at nano and atomic scale for electrocatalytic CO2 reduction, Nano Mater. Sci 1 (2019) 60–69.
[115] Z. Fang, X. Zhuang, Metal-free molecular catalysts for electrochemical CO2 reduction, Joule 7 (2023) 1101–1103.
[116] D.-H. Nam, P. De Luna, A. Rosas-Hernández, A. Thevenon, F. Li, T. Agapie, J.C. Peters, O. Shekhah, M. Eddaoudi, E.H. Sargent, Molecular enhancement of heterogeneous CO2 reduction, Nat. Mater. 19 (2020) 266–276.
[117] Q. Chen, X. Wang, Y. Zhou, Y. Tan, H. Li, J. Fu, M. Liu, Electrocatalytic CO2 reduction to C2+ products in flow cells, Adv. Mater. 36 (2024) 2303902.
[118] B. Rhimi, M. Zhou, Z. Yan, X. Cai, Z. Jiang, Cu-based materials for enhanced C2+ product selectivity in photo-/electro-catalytic CO2 reduction: challenges and prospects, Micro & Nano Lett. 16 (2024) 64.
[119] X. Hao, C. Ma, A. Mosallanezhad, J. Xue, C. Wei, N. Sun, Y. Wang, J. Feng, J. Liu, G. Wang, Evolution of catalyst structures and reaction intermediates during electroreduction CO2 toward C2+ product on Cu-based catalyst: an experimental and theoretical review, Mater. Sci. Semicond. Process. 169 (2024) 107906.
[120] S. Cui, S. Li, R. Deng, L. Wei, S. Yang, S. Dai, F. Wang, S. Liu, Y. Huang, Progress in Cu-based electrocatalysts for electrochemical CO 2 reduction to C 2+ products, Catal. Sci. Technol. 14 (2024) 2697–2716.
[121] M. Jun, J. Kundu, D.H. Kim, M. Kim, D. Kim, K. Lee, S.I. Choi, Strategies to modulate the copper oxidation state toward selective C2+ production in the electrochemical CO2 reduction reaction, Adv. Mater. (2024) 2313028.
[122] T. O'Carroll, X. Yang, K.J. Gordon, L. Fei, G. Wu, Ethylene electrosynthesis via selective CO2 reduction: fundamental considerations, strategies, and challenges, Adv. Energy Mater. (2024) 2401558.
[123] M. Zeng, W. Fang, Y. Cen, X. Zhang, Y. Hu, B.Y. Xia, Reaction environment regulation for electrocatalytic CO2 reduction in acids, Angew. Chem. Int. Ed. (2024) e202404574.
[124] M.S. Yesupatham, B. Honnappa, N. Agamendran, S.Y. Kumar, G. Chellasamy, S. Govindaraju, K. Yun, N.C.S. Selvam, A. Maruthapillai, W. Li, Recent developments in copper-based catalysts for enhanced electrochemical CO2 reduction, Adv. Sustain. Syst. (2024) 2300549.

[125] S. Liang, N. Altaf, L. Huang, Y. Gao, Q. Wang, Electrolytic cell design for electrochemical CO2 reduction, J. CO2 Util. 35 (2020) 90–105.
[126] O. Romiluyi, N. Danilovic, A.T. Bell, A.Z. Weber, Membrane-electrode assembly design parameters for optimal CO2 reduction, Electrochem. Sci. Adv. 3 (2023) e2100186.
[127] Y. Xie, Y. Wang, Expediting the technology readiness level of CO2 electrolysis, Joule 8 (2024) 879–881.
[128] S. Liu, C. Zhang, W. Yao, 3D modeling and numerical investigation of electrochemical CO2 reduction in microfluidic flow cells, Energy Technol. 11 (2023) 2300119.
[129] Y. Yin, W. Jing, F. Wang, Y. Liu, L. Guo, Electro-reduced copper on polymeric C3N4 for photocatalytic reduction of CO2, Carbon 214 (2023) 118317.
[130] C. Zhu, A. Chen, J. Mao, G. Wu, S. Li, X. Dong, G. Li, Z. Jiang, Y. Song, W. Chen, Cu–Pd bimetallic gas diffusion electrodes for electrochemical reduction of CO2 to C2+ products, Small Struct. 4 (2023) 2200328.
[131] Y. Liu, H. Liu, C. Wang, Y. Wang, J. Lu, H. Wang, Reconstructed Cu/Cu2O (I) catalyst for selective electroreduction of CO2 to C2+ products, Electrochem. Commun. 150 (2023) 107474.
[132] W. Guo, X. Tan, S. Jia, S. Liu, X. Song, X. Ma, L. Wu, L. Zheng, X. Sun, B. Han, Asymmetric Cu sites for enhanced CO2 electroreduction to C2+ products, CCS Chem. 6 (2024) 1231–1239.
[133] Q. Wu, R. Du, P. Wang, G.I. Waterhouse, J. Li, Y. Qiu, K. Yan, Y. Zhao, W.-W. Zhao, H.-J. Tsai, Nanograin-boundary-abundant Cu2O-Cu nanocubes with high C2+ selectivity and good stability during electrochemical CO2 reduction at a current density of 500 mA/cm2, ACS Nano 17 (2023) 12884–12894.
[134] M. Ye, T. Shao, J. Liu, C. Li, B. Song, S. Liu, Phase engineering of Cu@ Cu2O core-shell nanospheres for boosting tandem electrochemical CO2 reduction to C2+ products, Appl. Surf. Sci. 622 (2023) 156981.
[135] H. Cheng, S. Jia, J. Jiao, X. Chen, T. Deng, C. Xue, M. Dong, J. Zeng, C. Chen, H. Wu, Stabilization of Cu+ sites by amorphous Al 2 O 3 to enhance electrochemical CO 2 reduction to C 2+ products, Green Chem. 26 (2024) 2599–2604.
[136] Y.R. Du, X.Q. Li, X.X. Yang, G.Y. Duan, Y.M. Chen, B.H. Xu, Stabilizing high-valence copper (I) sites with Cu–Ni interfaces enhances electroreduction of CO2 to C2+ products, Small (2024) 2402534.
[137] C. Yang, R. Wang, C. Yu, J. Xiao, Z. Huang, B. Lv, H. Zhao, X. Wu, G. Jing, Engineering stable Cu+-Cu0 sites and oxygen defects in boron-doped copper oxide for electrocatalytic reduction of CO2 to C2+ products, J. Chem. Eng. 484 (2024) 149710.
[138] T. Deng, S. Jia, S. Han, J. Zhai, J. Jiao, X. Chen, C. Xue, X. Xing, W. Xia, H. Wu, Electrochemical CO2 reduction to C2+ products over Cu/Zn intermetallic catalysts synthesized by electrodeposition, Front. Energy 18 (2024) 80–88.
[139] Y. Yang, H. Fu, C. Xiao, X. Du, Z. Song, Efficient electrochemical CO2 reduction to C2+ hydrocarbons on Zn-doped Cu films, Appl. Surf. Sci. 646 (2024) 158866.
[140] L.-X. Liu, Y. Cai, H. Du, X. Lu, X. Li, F. Liu, J. Fu, J.-J. Zhu, Enriching the local concentration of CO intermediates on Cu cavities for the electrocatalytic reduction of CO2 to C2+ products, ACS Appl. Mater. Interfaces 15 (2023) 16673–16679.
[141] Z.-Y. Zhang, H. Tian, L. Bian, S.-Z. Liu, Y. Liu, Z.-L. Wang, Cu-Zn-based alloy/oxide interfaces for enhanced electroreduction of CO2 to C2+ products, J. Energy Chem. 83 (2023) 90–97.
[142] X. Meng, H. Huang, X. Zhang, L. Hu, H. Tang, M. Han, F. Zheng, H. Wang, Steering C–C coupling by hollow Cu2O@ C/N nanoreactors for highly efficient electroreduction of CO2 to C2+ products, Adv. Energy Mater. (2024) 2312719.
[143] R. Zhang, J. Zhang, S. Wang, Z. Tan, Y. Yang, Y. Song, M. Li, Y. Zhao, H. Wang, B. Han, Synthesis of N-propanol from CO2 electroreduction on bicontinuous Cu2O/Cu nanodomains, Angew. Chem. Int. Ed. (2024) e202405733.
[144] H. Wang, A. Gao, A. Bari, M. Gu, X. Zhang, G. Wang, Controllable active sites in Cu2–x Se/Cu/NC nanoparticles for efficient electroreduction to C2+ products, ACS Appl. Nano Mater. 7 (2024) 6810–6819.
[145] M. Wang, C. Chen, S. Jia, S. Han, X. Dong, D. Zhou, T. Yao, M. Fang, M. He, W. Xia, Enhancing C 2+ product selectivity in CO 2 electroreduction by enriching intermediates over carbon-based nanoreactors, Chem. Sci. 15 (2024) 8451–8458.
[146] T. Zhao, X. Zong, J. Liu, J. Chen, K. Xu, X. Wang, X. Chen, W. Yang, F. Liu, M. Yu, Functionalizing Cu nanoparticles with fluoric polymer to enhance C2+ product selectivity in membraned CO2 reduction, Appl. Catal. B Environ. 340 (2024) 123281.
[147] M. Hou, Y.X. Shi, J.J. Li, Z. Gao, Z. Zhang, Cu-Based organic-inorganic composite materials for electrochemical CO2 reduction, Chem. Asian J. 17 (2022) e202200624.
[148] W. Liu, P. Zhai, A. Li, B. Wei, K. Si, Y. Wei, X. Wang, G. Zhu, Q. Chen, X. Gu, R. Zhang, W. Zhou, Y. Gong, Electrochemical CO2 reduction to ethylene by ultrathin CuO nanoplate arrays, Nat. Commun. 13 (2022) 1877.
[149] Y. Lum, J.W. Ager, Stability of residual oxides in oxide-derived copper catalysts for electrochemical CO2 reduction investigated with 18O labeling, Angew. Chem. Int. Ed. 57 (2018) 551–554.
[150] I. Merino-Garcia, J. Albo, J. Solla-Gullón, V. Montiel, A. Irabien, Cu oxide/ZnO-based surfaces for a selective ethylene production from gas-phase CO2 electroconversion, J. CO2 Util. 31 (2019) 135–142.
[151] H. Xiang, S. Rasul, K. Scott, J. Portoles, P. Cumpson, H.Y. Eileen, Enhanced selectivity of carbonaceous products from electrochemical reduction of CO2 in aqueous media, J. CO2 Util. 30 (2019) 214–221.
[152] X. Wang, Z. Wang, T.-T. Zhuang, C.-T. Dinh, J. Li, D.-H. Nam, F. Li, C.-W. Huang, C.-S. Tan, Z. Chen, M. Chi, C.M. Gabardo, A. Seifitokaldani, P. Todorović, A. Proppe, Y. Pang, A.R. Kirmani, Y. Wang, A.H. Ip, L.J. Richter, B. Scheffel, A. Xu, S.-C. Lo, S.O. Kelley, D. Sinton, E.H. Sargent, Efficient upgrading of CO to C3 fuel using asymmetric C-C coupling active sites, Nat. Commun. 10 (2019) 5186.
[153] X. She, T. Zhang, Z. Li, H. Li, H. Xu, J. Wu, Tandem electrodes for carbon dioxide reduction into C2+ products at simultaneously high production efficiency and rate, Cell Rep. Phys. Sci. 1 (2020) 100051.
[154] Y. Yang, Z. Tan, J. Zhang, Electrocatalytic carbon dioxide reduction to ethylene over copper-based catalytic systems, Chem. Asian J. (2022) e202200893.
[155] J. Yin, Z. Gao, F. Wei, C. Liu, J. Gong, J. Li, W. Li, L. Xiao, G. Wang, J. Lu, Customizable CO2 electroreduction to C1 or C2+ products through Cu y/CeO2 interface engineering, ACS Catal. 12 (2022) 1004–1011.
[156] Z. Wei, S. Yue, S. Gao, M. Cao, R. Cao, Synergetic effects of gold-doped copper nanowires with low Au content for enhanced electrocatalytic CO2 reduction to multicarbon products, Nano Res. 16 (2023) 7777–7783.
[157] Y. Yang, Y. Zhang, J.-S. Hu, L.-J. Wan, Progress in the mechanisms and materials for CO2 electroreduction toward C2+ products, Acta Phys.-Chim. Sin 36 (2020) 1–13.
[158] L. Wang, D.C. Higgins, Y. Ji, C.G. Morales-Guio, K. Chan, C. Hahn, T.F. Jaramillo, Selective reduction of CO to acetaldehyde with CuAg electrocatalysts, Proc .Natl. Acad .Sci 117 (2020) 12572–12575.
[159] X. Wang, P. Ou, A. Ozden, S.-F. Hung, J. Tam, C.M. Gabardo, J.Y. Howe, J. Sisler, K. Bertens, F.P. García de Arquer, R.K. Miao, C.P. O'Brien, Z. Wang, J. Abed, A.S. Rasouli, M. Sun, A.H. Ip, D. Sinton, E.H. Sargent, Efficient electrosynthesis of n-propanol from carbon monoxide using a Ag–Ru–Cu catalyst, Nat. Energy 7 (2022) 170–176.
[160] Z. Cai, N. Cao, F. Zhang, X. Lv, K. Wang, Y. He, Y. Shi, H. Bin Wu, P. Xie, Hierarchical Ag-Cu interfaces promote C-C coupling in tandem CO2 electroreduction, Appl. Catal. B Environ. 325 (2023) 122310.
[161] Z. Chen, X. Liao, C. Sun, K. Zhao, D. Ye, J. Li, G. Wu, J. Fang, H. Zhao, J. Zhang, Enhanced performance of atomically dispersed dual-site Fe-Mn electrocatalysts through cascade reaction mechanism, Appl. Catal. B Environ. 288 (2021) 120021.
[162] Y. Pang, J. Li, Z. Wang, C.-S. Tan, P.-L. Hsieh, T.-T. Zhuang, Z.-Q. Liang, C. Zou, X. Wang, P. De Luna, Efficient electrocatalytic conversion of carbon monoxide to propanol using fragmented copper, Nat. Catal. 2 (2019) 251–258.
[163] T.-T. Zhuang, Y. Pang, Z.-Q. Liang, Z. Wang, Y. Li, C.-S. Tan, J. Li, C.T. Dinh, P. De Luna, P.-L. Hsieh, Copper nanocavities confine intermediates for efficient electrosynthesis of C3 alcohol fuels from carbon monoxide, Nat. Catal. 1 (2018) 946–951.
[164] J. Liu, L. Cheng, Y. Wang, R. Chen, C. Xiao, X. Zhou, Y. Zhu, Y. Li, C. Li, Dynamic determination of Cu+ roles for CO 2 reduction on electrochemically stable Cu 2 O-based nanocubes, J. Mater. Chem. 10 (2022) 8459–8465.
[165] P.-P. Yang, X.-L. Zhang, F.-Y. Gao, Y.-R. Zheng, Z.-Z. Niu, X. Yu, R. Liu, Z.-Z. Wu, S. Qin, L.-P. Chi, Y. Duan, T. Ma, X.-S. Zheng, J.-F. Zhu, H.-J. Wang, M.-R. Gao, S.-H. Yu, Protecting copper oxidation state via intermediate confinement for selective CO2 electroreduction to C2+ fuels, J. Am. Chem. Soc. 142 (2020) 6400–6408.
[166] Q. Fan, X. Zhang, X. Ge, L. Bai, D. He, Y. Qu, C. Kong, J. Bi, D. Ding, Y. Cao, Manipulating Cu nanoparticle surface oxidation states tunes catalytic selectivity toward CH4 or C2+ products in CO2 electroreduction, Adv. Energy Mater. 11 (2021) 2101424.
[167] P. Chen, Y. Wu, T.E. Rufford, L. Wang, G. Wang, Z. Wang, Organic molecules involved in Cu-based electrocatalysts for selective CO2 reduction to C2+ products, Mater. Today Chem. 27 (2023) 101328.
[168] X. Liu, J. Li, Y. Xue, M. Gong, C.R. Cabrera, L. Yao, Z. Hu, Electrochemical CO2 reduction to C2+ products with Cu-oleylamine based nanoparticles synthesized by simple thermal treatment, Fuels 348 (2023) 128498.
[169] A.R. Woldu, Z. Huang, P. Zhao, L. Hu, D. Astruc, Electrochemical CO2 reduction (CO2RR) to multi-carbon products over copper-based catalysts, Coord. Chem. Rev. 454 (2022) 214340.
[170] J. Zhang, C. Guo, S. Fang, X. Zhao, L. Li, H. Jiang, Z. Liu, Z. Fan, W. Xu, J. Xiao, Accelerating electrochemical CO2 reduction to multi-carbon products via asymmetric intermediate binding at confined nanointerfaces, Nat. Commun. 14 (2023) 1298.
[171] A. Bagger, W. Ju, A.S. Varela, P. Strasser, J. Rossmeisl, Electrochemical CO2 reduction: a classification problem, ChemPhysChem 18 (2017) 3266–3273.
[172] B. Chang, H. Pang, F. Raziq, S. Wang, K.-W. Huang, J. Ye, H. Zhang, Electrochemical reduction of carbon dioxide to multicarbon (C 2+) products: challenges and perspectives, Energy Environ. Sci. 16 (2023) 4714–4758.
[173] Y. Mi, S. Shen, X. Peng, H. Bao, X. Liu, J. Luo, Selective electroreduction of CO2 to C2 products over Cu3N-derived Cu nanowires, Chemelectrochem 6 (2019) 2393–2397.
[174] H. Ooka, M.C. Figueiredo, M.T. Koper, Competition between hydrogen evolution and carbon dioxide reduction on copper electrodes in mildly acidic media, Langmuir 33 (2017) 9307–9313.
[175] X. Wang, Q. Hu, G. Li, H. Yang, C. He, Recent advances and perspectives of electrochemical CO2 reduction toward C2+ products on Cu-based catalysts, Electrochem. Energy Rev. 5 (2022) 28.
[176] B. Zhang, J. Zhang, M. Hua, Q. Wan, Z. Su, X. Tan, L. Liu, F. Zhang, G. Chen, D. Tan, X. Cheng, B. Han, L. Zheng, G. Mo, Highly electrocatalytic ethylene production from CO2 on nanodefective Cu nanosheets, J. Am. Chem. Soc. 142 (2020) 13606–13613.
[177] Y. Piao, Q. Jiang, H. Li, H. Matsumoto, J. Liang, W. Liu, C. Pham-Huu, Y. Liu, F. Wang, Identify Zr promotion effects in atomic scale for co-based catalysts in Fischer–Tropsch synthesis, ACS Catal. 10 (2020) 7894–7906.
[178] C.A. Obasanjo, A.S. Zeraati, H.S. Shiran, T.N. Nguyen, S.M. Sadaf, M.G. Kibria, C.-T. Dinh, In situ regeneration of copper catalysts for long-term electrochemical CO 2 reduction to multiple carbon products, J. Mater. Chem. 10 (2022) 20059–20070.
[179] Z.-Z. Niu, L.-P. Chi, Z.-Z. Wu, P.-P. Yang, M.-H. Fan, M.-R. Gao, CO2-assisted formation of grain boundaries for efficient CO–CO coupling on a derived Cu catalyst, Open For. Sci. J. 2 (2023) 20220044.

[180] P.-C. Chen, C. Chen, Y. Yang, A.L. Maulana, J. Jin, J. Feijoo, P. Yang, Chemical and structural evolution of AgCu catalysts in electrochemical CO2 reduction, J. Am. Chem. Soc. 145 (2023) 10116–10125.
[181] R. An, X. Chen, Q. Fang, Y. Meng, X. Li, Y. Cao, Structure–activity relationship of Cu-based catalysts for the highly efficient CO2 electrochemical reduction reaction, Front. Chem. 11 (2023) 1141453.
[182] Z. Ma, T. Wan, D. Zhang, J.A. Yuwono, C. Tsounis, J. Jiang, Y.-H. Chou, X. Lu, P.V. Kumar, Y.H. Ng, Atomically dispersed Cu catalysts on sulfide-derived defective Ag nanowires for electrochemical CO2 reduction, ACS Nano 17 (2023) 2387–2398.
[183] F. Gou, H. Wang, M. Fu, Y. Jiang, W. Shen, R. He, M. Li, Boron-induced electron localization in Cu nanowires promotes efficient nitrate reduction to ammonia in neutral media, Appl. Surf. Sci. 612 (2023) 155872.
[184] M.Q. Alkoshab, E. Thomou, I. Abdulazeez, M.H. Suliman, K. Spyrou, W. Iali, K. Alhooshani, T.N. Baroud, Low overpotential electrochemical reduction of CO2 to ethanol enabled by Cu/CuxO nanoparticles embedded in nitrogen-doped carbon cuboids, Nanomaterials 13 (2023) 230.
[185] Y. Qu, W. Zheng, P. Wang, H. Huang, M. Huang, L. Hu, H. Wang, Q. Chen, Creating interfaces of Cu0/Cu+ in oxide-derived copper catalysts for electrochemical CO2 reduction to multi-carbon products, J. Colloid Interface Sci. 645 (2023) 735–742.
[186] K. Tran, Z.W. Ulissi, Active learning across intermetallics to guide discovery of electrocatalysts for CO2 reduction and H2 evolution, Nat. Catal. 1 (2018) 696–703.
[187] P. Gao, S. Li, X. Bu, S. Dang, Z. Liu, H. Wang, L. Zhong, M. Qiu, C. Yang, J. Cai, Direct conversion of CO2 into liquid fuels with high selectivity over a bifunctional catalyst, Nat. Chem. 9 (2017) 1019–1024.
[188] K.J.P. Schouten, E. Pérez Gallent, M.T. Koper, Structure sensitivity of the electrochemical reduction of carbon monoxide on copper single crystals, ACS Catal. 3 (2013) 1292–1295.
[189] K.J.P. Schouten, E.P. Gallent, M.T. Koper, The influence of pH on the reduction of CO and CO2 to hydrocarbons on copper electrodes, J. Electroanal. Chem. 716 (2014) 53–57.
[190] M. Sun, J. Cheng, M. Yamauchi, Gas diffusion enhanced electrode with ultrathin superhydrophobic macropore structure for acidic CO2 electroreduction, Nat. Commun. 15 (2024) 491.
[191] A. Inoue, T. Harada, S. Nakanishi, K. Kamiya, Ultra-high-rate CO2 reduction reactions to multicarbon products with a current density of 1.7 A cm−2 in neutral electrolytes, EES Catalysis 1 (2023) 9–16.
[192] L. Yuan, Q. Wan, W. Jiang, J. Hou, X. Zhuang, J. Zhang, C. Ke, Converting CO2 to multi-carbon products at >1 A/cm2 using gas diffusion electrode based on commercial materials via transfer process engineering, Electrochim. Acta 475 (2024) 143662.
[193] H. Xiao, W.A. Goddard III, T. Cheng, Y. Liu, Cu metal embedded in oxidized matrix catalyst to promote CO2 activation and CO dimerization for electrochemical reduction of CO2, Proc. Natl. Acad. Sci. USA 114 (2017) 6685–6688.
[194] S.Y. Lee, H. Jung, N.-K. Kim, H.-S. Oh, B.K. Min, Y.J. Hwang, Mixed copper states in anodized Cu electrocatalyst for stable and selective ethylene production from CO2 reduction, J. Am. Chem. Soc. 140 (2018) 8681–8689.
[195] Y. Lum, B. Yue, P. Lobaccaro, A.T. Bell, J.W. Ager, Optimizing C–C coupling on oxide-derived copper catalysts for electrochemical CO2 reduction, J. Phys. Chem. C 121 (2017) 14191–14203.
[196] C. Chen, X. Yan, Y. Wu, S. Liu, X. Sun, Q. Zhu, R. Feng, T. Wu, Q. Qian, H. Liu, The in situ study of surface species and structures of oxide-derived copper catalysts for electrochemical CO 2 reduction, Chem. Sci. 12 (2021) 5938–5943.
[197] J. Kochi, The mechanism of the copper salt catalysed reactions of peroxides, Tetrahedron 18 (1962) 483–497.
[198] M. Salavati-Niasari, F. Davar, N. Mir, Synthesis and characterization of metallic copper nanoparticles via thermal decomposition, Polyhedron 27 (2008) 3514–3518.
[199] T.-C. Chou, C.-C. Chang, H.-L. Yu, W.-Y. Yu, C.-L. Dong, J.-J.s. Velasco-Vélez, C.-H. Chuang, L.-C. Chen, J.-F. Lee, J.-M. Chen, Controlling the oxidation state of the Cu electrode and reaction intermediates for electrochemical CO2 reduction to ethylene, J. Am. Chem. Soc. 142 (2020) 2857–2867.
[200] R.G. Mariano, K. McKelvey, H.S. White, M.W. Kanan, Selective increase in CO_2 electroreduction activity at grain-boundary surface terminations, Science 358 (2017) 1187–1192.
[201] S. Ajmal, G. Yasin, A. Kumar, M. Tabish, S. Ibraheem, K.A. Sammed, M.A. Mushtaq, A. Saad, Z. Mo, W. Zhao, A disquisition on CO2 electroreduction to C2H4: an engineering and design perspective looking beyond novel choosy catalyst materials, Coord. Chem. Rev. 485 (2023) 215099.
[202] H. Mistry, A.S. Varela, C.S. Bonifacio, I. Zegkinoglou, I. Sinev, Y.-W. Choi, K. Kisslinger, E.A. Stach, J.C. Yang, P. Strasser, B.R. Cuenya, Highly selective plasma-activated copper catalysts for carbon dioxide reduction to ethylene, Nat. Commun. 7 (2016) 12123.
[203] J.-J. Velasco-Vélez, T. Jones, D. Gao, E. Carbonio, R. Arrigo, C.-J. Hsu, Y.-C. Huang, C.-L. Dong, J.-M. Chen, J.-F. Lee, P. Strasser, B. Roldan Cuenya, R. Schlögl, A. Knop-Gericke, C.-H. Chuang, The role of the copper oxidation state in the electrocatalytic reduction of CO2 into valuable hydrocarbons, ACS Sustain. Chem. Eng. 7 (2019) 1485–1492.
[204] Q. Lei, H. Zhu, K. Song, N. Wei, L. Liu, D. Zhang, J. Yin, X. Dong, K. Yao, N. Wang, X. Li, B. Davaasuren, J. Wang, Y. Han, Investigating the origin of enhanced C2+ selectivity in oxide-/hydroxide-derived copper electrodes during CO2 electroreduction, J. Am. Chem. Soc. 142 (2020) 4213–4222.
[205] R. Du, T. Li, Q. Wu, P. Wang, X. Yang, Y. Fan, Y. Qiu, K. Yan, P. Wang, Y. Zhao, W.-W. Zhao, G. Chen, In situ engineering of the Cu+/Cu0 interface to boost C2+ selectivity in CO2 electroreduction, ACS Appl. Mater. Interfaces 14 (2022) 36527–36535.
[206] Q. Wu, R. Du, P. Wang, G.I.N. Waterhouse, J. Li, Y. Qiu, K. Yan, Y. Zhao, W.-W. Zhao, H.-J. Tsai, M.-C. Chen, S.-F. Hung, X. Wang, G. Chen, Nanograin-boundary-Abundant Cu2O-Cu nanocubes with high C2+ selectivity and good stability during electrochemical CO2 reduction at a current density of 500 mA/cm2, ACS Nano 17 (2023) 12884–12894.
[207] S. Wang, D. Wang, B. Tian, X. Gao, L. Han, Y. Zhong, S. Song, Z. Wang, Y. Li, J. Gui, Synergistic Cu+/Cu0 on Cu2O-Cu interfaces for efficient and selective C2+ production in electrocatalytic CO2 conversion, Sci. China Mater. 66 (2023) 1801–1809.
[208] L. Diao, Y. Liu, F. Chen, H. Pan, D.P.d. Lara, H. Liu, Y. Cheng, F. Luo, Improving the activity of electrochemical reduction of CO2 to C1 products by oxidation derived copper catalyst, Mater. Reports, Energy. 3 (2023) 100180.
[209] S. Zhu, X. Ren, X. Li, X. Niu, M. Wang, S. Xu, Z. Wang, Y. Han, Q. Wang, Core-shell ZnO@ Cu2O as catalyst to enhance the electrochemical reduction of carbon dioxide to C2 products, Catalysts 11 (2021) 535.
[210] D. Zhong, Z.J. Zhao, Q. Zhao, D. Cheng, B. Liu, G. Zhang, W. Deng, H. Dong, L. Zhang, J. Li, Coupling of Cu (100) and (110) facets promotes carbon dioxide conversion to hydrocarbons and alcohols, Angew. Chem. Int. Ed. 60 (2021) 4879–4885.
[211] H. Ait Ahsaine, A. BaQais, Metal and metal oxide electrocatalysts for the electrochemical reduction of CO2-to-C1 chemicals: are we there yet? Green Chem. Lett. Rev. 16 (2023) 2160215.
[212] Y. Yang, S. Louisia, S. Yu, J. Jin, I. Roh, C. Chen, M.V. Fonseca Guzman, J. Feijóo, P.-C. Chen, H. Wang, C.J. Pollock, X. Huang, Y.-T. Shao, C. Wang, D.A. Muller, H.D. Abruña, P. Yang, Operando studies reveal active Cu nanograins for CO2 electroreduction, Nature 614 (2023) 262–269.
[213] L. Xu, J. Feng, L. Wu, X. Song, X. Tan, L. Zhang, X. Ma, S. Jia, J. Du, A. Chen, Identifying the optimal oxidation state of Cu for electrocatalytic reduction of CO 2 to C 2+ products, Green Chem. 25 (2023) 1326–1331.
[214] X. Lv, Q. Liu, J. Wang, X. Wu, X. Li, Y. Yang, J. Yan, A. Wu, H.B. Wu, Grain refining enables mixed Cu+/Cu0 states for CO2 electroreduction to C2+ products at high current density, Appl. Catal. B Environ. 324 (2023) 122272.
[215] Z. Gu, N. Yang, P. Han, M. Kuang, B. Mei, Z. Jiang, J. Zhong, L. Li, G. Zheng, Oxygen vacancy tuning toward efficient electrocatalytic CO2 reduction to C2H4, Small Methods 3 (2019) 1800449.
[216] Y. Zhou, Y. Yao, R. Zhao, X. Wang, Z. Fu, D. Wang, H. Wang, L. Zhao, W. Ni, Z. Yang, Stabilization of Cu+ via strong electronic interaction for selective and stable CO2 electroreduction, Angew. Chem. Int. Ed. 134 (2022) e202205832.
[217] X. Feng, K. Jiang, S. Fan, M.W. Kanan, A direct grain-boundary-activity correlation for CO electroreduction on Cu nanoparticles, ACS Cent. Sci. 2 (2016) 169–174.
[218] K.K. Patra, Z. Liu, H. Lee, S. Hong, H. Song, H.G. Abbas, Y. Kwon, S. Ringe, J. Oh, Boosting electrochemical CO2 reduction to methane via tuning oxygen vacancy concentration and surface termination on a copper/ceria catalyst, ACS Catal. 12 (2022) 10973–10983.
[219] K.P. Reddy, H. Choi, D. Kim, R. Ryoo, J.Y. Park, Cu oxide deposited on shape-controlled ceria nanocrystals for CO oxidation: influence of interface-driven oxidation states on catalytic activity, Catal. Sci. Technol. 11 (2021) 6134–6142.
[220] T.K. Pathak, E. Coetsee-Hugo, H.C. Swart, C.W. Swart, R.E. Kroon, Preparation and characterization of Ce doped ZnO nanomaterial for photocatalytic and biological applications, Mater. Sci. Eng. B. 261 (2020) 114780.
[221] K. Jiang, R.B. Sandberg, A.J. Akey, X. Liu, D.C. Bell, J.K. Nørskov, K. Chan, H. Wang, Metal ion cycling of Cu foil for selective C–C coupling in electrochemical CO2 reduction, Nat. Catal. 1 (2018) 111–119.
[222] D.L.T. Nguyen, M.S. Jee, H.-S. Oh, B.K. Min, Y.J. Hwang, Effect of halides on nanoporous Zn-based catalysts for highly efficient electroreduction of CO2 to CO, Catal. Commun. 114 (2018) 109–113.
[223] A. Vasileff, Y. Zhu, X. Zhi, Y. Zhao, L. Ge, H.M. Chen, Y. Zheng, S.Z. Qiao, Electrochemical reduction of CO2 to ethane through stabilization of an ethoxy intermediate, Angew. Chem. Int. Ed. 132 (2020) 19817–19821.
[224] A.S. Varela, W. Ju, T. Reier, P. Strasser, Tuning the catalytic activity and selectivity of Cu for CO2 electroreduction in the presence of halides, ACS Catal. 6 (2016) 2136–2144.
[225] X. Yan, C. Chen, Y. Wu, Y. Chen, J. Zhang, R. Feng, J. Zhang, B. Han, Boosting CO 2 electroreduction to C 2+ products on fluorine-doped copper, Green Chem. 24 (2022) 1989–1994.
[226] D. Raciti, M. Mao, J.H. Park, C. Wang, Local pH effect in the CO2 reduction reaction on high-surface-area copper electrocatalysts, J. Electrochem. Soc. 165 (2018) F799.
[227] T. Kim, G.T.R. Palmore, A scalable method for preparing Cu electrocatalysts that convert CO2 into C2+ products, Nat. Commun. 11 (2020) 3622.
[228] H. Wang, E. Matios, C. Wang, J. Luo, X. Lu, X. Hu, W. Li, Rapid and scalable synthesis of cuprous halide-derived copper nano-architectures for selective electrochemical reduction of carbon dioxide, Nano Lett. 19 (2019) 3925–3932.
[229] W. Ma, S. Xie, T. Liu, Q. Fan, J. Ye, F. Sun, Z. Jiang, Q. Zhang, J. Cheng, Y. Wang, Electrocatalytic reduction of CO2 to ethylene and ethanol through hydrogen-assisted C–C coupling over fluorine-modified copper, Nat. Catal. 3 (2020) 478–487.
[230] P. Li, J. Bi, J. Liu, Y. Wang, X. Kang, X. Sun, J. Zhang, Z. Liu, Q. Zhu, B. Han, –d orbital hybridization induced by p-block metal-doped Cu promotes the formation of C2+ products in ampere-level CO2 electroreduction, J. Am. Chem. Soc. 145 (2023) 4675–4682.
[231] C. Chen, Y. Li, S. Yu, S. Louisia, J. Jin, M. Li, M.B. Ross, P. Yang, Cu-Ag tandem catalysts for high-rate CO2 electrolysis toward multicarbons, Joule 4 (2020) 1688–1699.

[232] L. Ding, N. Zhu, Y. Hu, Z. Chen, P. Song, T. Sheng, Z. Wu, Y. Xiong, Over 70% faradaic efficiency for CO2 electroreduction to ethanol enabled by potassium dopant-tuned interaction between copper sites and intermediates, Angew. Chem. Int. Ed. 61 (2022) e202209268.
[233] F. Pan, X. Yang, T. O'Carroll, H. Li, K.J. Chen, G. Wu, Carbon catalysts for electrochemical CO2 reduction toward multicarbon products, Adv. Energy Mater. 12 (2022) 2200586.
[234] W. Sun, et al., V-doped Cu2Se hierarchical nanotubes enabling flow-cell CO2 electroreduction to ethanol with high efficiency and selectivity, Adv. Mater. 34 (50) (2022) 2207691.
[235] Copper atom-pair catalyst anchored on alloy nanowires for selective and efficient electrochemical reduction of CO2.
[236] C. Yan, W. Luo, H. Yuan, G. Liu, R. Hao, N. Qin, Z. Wang, K. Liu, Z. Wang, D. Cui, Stabilizing intermediates and optimizing reaction processes with N doping in Cu2O for enhanced CO2 electroreduction, Appl. Catal. B Environ. 308 (2022) 121191.
[237] B. Pan, Y. Wang, Y. Li, Understanding and leveraging the effect of cations in the electrical double layer for electrochemical CO2 reduction, Chem Catal. 2 (2022) 1267–1276.
[238] K. Qi, Y. Zhang, N. Onofrio, E. Petit, X. Cui, J. Ma, J. Fan, H. Wu, W. Wang, J. Li, J. Liu, Y. Zhang, Y. Wang, G. Jia, J. Wu, L. Lajaunie, C. Salameh, D. Voiry, Unlocking direct CO2 electrolysis to C3 products via electrolyte supersaturation, Nat. Catal. 6 (2023) 319–331.
[239] L. Luan, X. Ji, B. Guo, J. Cai, W. Dong, Y. Huang, S. Zhang, Bioelectrocatalysis for CO2 reduction: recent advances and challenges to develop a sustainable system for CO2 utilization, Biotechnol. Adv. (2023) 108098.
[240] S.H. Lee, J.C. Lin, M. Farmand, A.T. Landers, J.T. Feaster, J.E. Avilés Acosta, J.W. Beeman, Y. Ye, J. Yano, A. Mehta, R.C. Davis, T.F. Jaramillo, C. Hahn, W.S. Drisdell, Oxidation state and surface reconstruction of Cu under CO2 reduction conditions from in situ X-ray characterization, J. Am. Chem. Soc. 143 (2021) 588–592.
[241] S.Y. Lee, S.Y. Chae, H. Jung, C.W. Lee, D.L.T. Nguyen, H.-S. Oh, B.K. Min, Y.J. Hwang, Controlling the C2+ product selectivity of electrochemical CO 2 reduction on an electrosprayed Cu catalyst, J. Mater. Chem. 8 (2020) 6210–6218.
[242] Y. Huang, A.D. Handoko, P. Hirunsit, B.S. Yeo, Electrochemical reduction of CO2 using copper single-crystal surfaces: effects of CO* coverage on the selective formation of ethylene, ACS Catal. 7 (2017) 1749–1756.
[243] H. Luo, B. Li, J.G. Ma, P. Cheng, Surface modification of nano-Cu2O for controlling CO2 electrochemical reduction to ethylene and syngas, Angew. Chem. Int. Ed. 61 (2022) e202116736.
[244] Z.-x. Yang, X. Wen, L.-j. Gao, J. Zhang, R.-p. Wei, X.-m. Pan, G.-m. Xiao, Facilitating CO_2 electroreduction to C_2H_4 through facile regulating {100} & {111} grain boundary of Cu_2O, Catal. Comm. 174 (2023) 106595.
[245] R.B. Sandberg, J.H. Montoya, K. Chan, J.K. Nørskov, CO-CO coupling on Cu facets: coverage, strain and field effects, Surf. Sci. 654 (2016) 56–62.
[246] Z.-Z. Wu, X.-L. Zhang, Z.-Z. Niu, F.-Y. Gao, P.-P. Yang, L.-P. Chi, L. Shi, W.-S. Wei, R. Liu, Z. Chen, Identification of Cu (100)/Cu (111) interfaces as superior active sites for CO dimerization during CO2 electroreduction, J. Am. Chem. Soc. 144 (2021) 259–269.
[247] B. Liu, X. Yao, Z. Zhang, C. Li, J. Zhang, P. Wang, J. Zhao, Y. Guo, J. Sun, C. Zhao, Synthesis of Cu2O nanostructures with tunable crystal facets for electrochemical CO2 reduction to alcohols, ACS Appl. Mater. Interfaces 13 (2021) 39165–39177.
[248] D. Clark, H. Malerød-Fjeld, M. Budd, I. Yuste-Tirados, D. Beeaff, S. Aamodt, K. Nguyen, L. Ansaloni, T. Peters, P.K. Vestre, Single-step hydrogen production from NH3, CH4, and biogas in stacked proton ceramic reactors, Science 376 (2022) 390–393.
[249] W.J. Durand, A.A. Peterson, F. Studt, F. Abild-Pedersen, J.K. Nørskov, Structure effects on the energetics of the electrochemical reduction of CO2 by copper surfaces, Surf. Sci. 605 (2011) 1354–1359.
[250] T.K. Todorova, M.W. Schreiber, M. Fontecave, Mechanistic understanding of CO2 reduction reaction (CO2RR) toward multicarbon products by heterogeneous copper-based catalysts, ACS Catal. 10 (2019) 1754–1768.
[251] Y. Cai, R. Yang, J. Fu, Z. Li, L. Xie, K. Li, Y.-C. Chang, S. Ding, Z. Lyu, J.-R. Zhang, Self-pressurizing nanoscale capsule catalysts for CO2 electroreduction to acetate or propanol, Nat. Synth. (2024) 1–12.
[252] Q. Fan, P. Yan, F. Liu, Z. Xu, P. Liang, X. Cao, C. Ye, M. Liu, L. Zhao, S. Ren, H. Miao, X. Zhang, Z. Yang, X. Ding, J. Yang, C. Kong, Y. Wu, Compressive strain in Cu catalysts: enhancing generation of C2+ products in electrochemical CO2 reduction, Sci. Bull. (2024).
[253] W. Ma, S. Xie, T. Liu, Q. Fan, J. Ye, F. Sun, Z. Jiang, Q. Zhang, J. Cheng, Y. Wang, Electrocatalytic reduction of CO2 to ethylene and ethanol through hydrogen-assisted C–C coupling over fluorine-modified copper, Nat. Catal. 3 (2020) 478–487.
[254] C.Y.J. Lim, M. Yilmaz, J.M. Arce-Ramos, A.D. Handoko, W.J. Teh, Y. Zheng, Z.H.J. Khoo, M. Lin, M. Isaacs, T.L.D. Tam, Y. Bai, C.K. Ng, B.S. Yeo, G. Sankar, I.P. Parkin, K. Hippalgaonkar, M.B. Sullivan, J. Zhang, Y.-F. Lim, Surface charge as activity descriptors for electrochemical CO2 reduction to multi-carbon products on organic-functionalised Cu, Nat. Commun. 14 (2023) 335.
[255] F. Calle-Vallejo, M.T. Koper, Theoretical considerations on the electroreduction of CO to C2 species on Cu (100) electrodes, Angew. Chem. Int. Ed. 125 (2013) 7423–7426.
[256] H. Ning, Q. Mao, W. Wang, Z. Yang, X. Wang, Q. Zhao, Y. Song, M. Wu, N-doped reduced graphene oxide supported Cu2O nanocubes as high active catalyst for CO2 electroreduction to C2H4, J. Alloys Compd. 785 (2019) 7–12.
[257] O. Fernandez-Delgado, Synthesis of Fullerene Derivatives for Diverse Applications: from Catalysis to Photovoltaics, The University of Texas at El Paso, 2021.
[258] Y. Liu, X. Fan, A. Nayak, Y. Wang, B. Shan, X. Quan, T.J. Meyer, Steering CO2 electroreduction toward ethanol production by a surface-bound Ru polypyridyl carbene catalyst on N-doped porous carbon, Proc .Natl. Acad .Sci 116 (2019) 26353–26358.
[259] Y. Ma, J. Yu, M. Sun, B. Chen, X. Zhou, C. Ye, Z. Guan, W. Guo, G. Wang, S. Lu, Confined growth of silver–copper janus nanostructures with {100} facets for highly selective tandem electrocatalytic carbon dioxide reduction, Adv. Mater. 34 (2022) 2110607.
[260] D. Fan, S. Zhang, Y. Li, H. Bin, R. Li, Y. Li, M. An, P. Yang, J. Zhang, High selective electrocatalytic reduction of carbon dioxide to ethylene enabled by regulating the microenvironment over Cu-Ag nanowires, J. Colloid Interface Sci. 662 (2024) 786–795.
[261] A.D. Handoko, C.W. Ong, Y. Huang, Z.G. Lee, L. Lin, G.B. Panetti, B.S. Yeo, Mechanistic insights into the selective electroreduction of carbon dioxide to ethylene on Cu2O-derived copper catalysts, J. Phys. Chem. C 120 (2016) 20058–20067.
[262] T. Cheng, H. Xiao, W.A. Goddard III, Full atomistic reaction mechanism with kinetics for CO reduction on Cu (100) from ab initio molecular dynamics free-energy calculations at 298 K, Proc. Natl. Acad. Sci. USA 114 (2017) 1795–1800.
[263] Y. Yao, T. Shi, W. Chen, J. Wu, Y. Fan, Y. Liu, L. Cao, Z. Chen, A surface strategy boosting the ethylene selectivity for CO2 reduction and in situ mechanistic insights, Nat. Commun. 15 (2024) 1257.
[264] C.D. Koolen, E. Oveisi, J. Zhang, M. Li, O.V. Safonova, J.K. Pedersen, J. Rossmeisl, W. Luo, A. Züttel, Low-temperature non-equilibrium synthesis of anisotropic multimetallic nanosurface alloys for electrochemical CO2 reduction, Nat. Synth. 3 (2024) 47–57.
[265] G.L. De Gregorio, T. Burdyny, A. Loiudice, P. Iyengar, W.A. Smith, R. Buonsanti, Facet-dependent selectivity of Cu catalysts in electrochemical CO2 reduction at commercially viable current densities, ACS Catal. 10 (2020) 4854–4862.
[266] Y. Gao, Q. Wu, X. Liang, Z. Wang, Z. Zheng, P. Wang, Y. Liu, Y. Dai, M.H. Whangbo, B. Huang, Cu2O nanoparticles with both {100} and {111} facets for enhancing the selectivity and activity of CO2 electroreduction to ethylene, Adv. Sci. 7 (2020) 1902820.
[267] Y. Song, R. Peng, D.K. Hensley, P.V. Bonnesen, L. Liang, Z. Wu, H.M. Meyer III, M. Chi, C. Ma, B.G. Sumpter, High-selectivity electrochemical conversion of CO2 to ethanol using a copper nanoparticle/N-doped graphene electrode, ChemistrySelect 1 (2016) 6055–6061.
[268] W. Pan, L. Zhong, Z. Shi, C. Mao, J. Peng, S. Chen, J. Huang, Interfacial engineering of Copper(I) oxide nanocubes wrapped with functionalized carbon nanotubes toward carbon dioxide electroreduction to ethylene, Surface. Interfac. 37 (2023) 102708.
[269] A.S. Varela, M. Kroschel, T. Reier, P. Strasser, Controlling the selectivity of CO2 electroreduction on copper: the effect of the electrolyte concentration and the importance of the local pH, Catal. Today 260 (2016) 8–13.
[270] Y. Zheng, A. Vasileff, X. Zhou, Y. Jiao, M. Jaroniec, S.-Z. Qiao, Understanding the roadmap for electrochemical reduction of CO2 to multi-carbon oxygenates and hydrocarbons on copper-based catalysts, J. Am. Chem. Soc. 141 (2019) 7646–7659.
[271] P.-P. Guo, Z.-H. He, S.-Y. Yang, W. Wang, K. Wang, C.-C. Li, Y.-Y. Wei, Z.-T. Liu, B. Han, Electrocatalytic CO 2 reduction to ethylene over ZrO 2/Cu-Cu 2 O catalysts in aqueous electrolytes, Green Chem. 24 (2022) 1527–1533.
[272] Z. Yin, C. Yu, Z. Zhao, X. Guo, M. Shen, N. Li, M. Muzzio, J. Li, H. Liu, H. Lin, Cu3N nanocubes for selective electrochemical reduction of CO2 to ethylene, Nano Lett. 19 (2019) 8658–8663.
[273] C.-T. Dinh, T. Burdyny, M.G. Kibria, A. Seifitokaldani, C.M. Gabardo, F.P. García de Arquer, A. Kiani, J.P. Edwards, P. De Luna, O.S. Bushuyev, CO2 electroreduction to ethylene via hydroxide-mediated copper catalysis at an abrupt interface, Science 360 (2018) 783–787.
[274] Z. Li, Y. Fang, J. Zhang, T. Zhang, J.D. Jimenez, S.D. Senanayake, V. Shanov, S. Yang, J. Wu, Planar defect-driven electrocatalysis of CO 2-to-C 2 H 4 conversion, J. Mater. Chem. 9 (2021) 19932–19939.
[275] X. Liu, J. Li, Y. Xue, M. Gong, C.R. Cabrera, L. Yao, Z. Hu, Electrochemical CO2 reduction to C2+ products with Cu-oleylamine based nanoparticles synthesized by simple thermal treatment, Fuel 348 (2023) 128498.
[276] D. Tan, B. Wulan, X. Cao, J. Zhang, Strong interactions of metal-support for efficient reduction of carbon dioxide into ethylene, Nano Energy 89 (2021) 106460.
[277] T. Ahmad, S. Liu, M. Sajid, K. Li, M. Ali, L. Liu, W. Chen, Electrochemical CO2 reduction to C2+ products using Cu-based electrocatalysts: a review, Nano Res Energy 1 (2022) e9120021.
[278] T.T. Hoang, S. Verma, S. Ma, T.T. Fister, J. Timoshenko, A.I. Frenkel, P.J. Kenis, A.A. Gewirth, Nanoporous copper–silver alloys by additive-controlled electrodeposition for the selective electroreduction of CO2 to ethylene and ethanol, J. Am. Chem. Soc. 140 (2018) 5791–5797.
[279] C. Liu, M. Zhang, J. Li, W. Xue, T. Zheng, C. Xia, J. Zeng, Nanoconfinement engineering over hollow multi-shell structured copper towards efficient electrocatalytical C− C coupling, Angew. Chem. Int. Ed. 61 (2022) e202113498.
[280] Y. Chen, Z. Fan, J. Wang, C. Ling, W. Niu, Z. Huang, G. Liu, B. Chen, Z. Lai, X. Liu, Ethylene selectivity in electrocatalytic CO2 reduction on Cu nanomaterials: a crystal phase-dependent study, J. Am. Chem. Soc. 142 (2020) 12760–12766.
[281] H. Ning, X. Wang, W. Wang, Q. Mao, Z. Yang, Q. Zhao, Y. Song, M. Wu, Cubic Cu2O on nitrogen-doped carbon shells for electrocatalytic CO2 reduction to C2H4, Carbon 146 (2019) 218–223.
[282] S. Sultan, H. Lee, S. Park, M.M. Kim, A. Yoon, H. Choi, T.-H. Kong, Y.-J. Koe, H.-S. Oh, Z. Lee, Interface rich CuO/Al 2 CuO 4 surface for selective ethylene

production from electrochemical CO 2 conversion, Energy Environ. Sci. 15 (2022) 2397–2409.
[283] F. Scholten, I. Sinev, M. Bernal, B. Roldan Cuenya, Plasma-modified dendritic Cu catalyst for CO2 electroreduction, ACS Catal. 9 (2019) 5496–5502.
[284] T. Hoang, S. Ma, J. Gold, P. Kenis, A. Gewirth, Nanoporous copper films by additivecontrolled electrodeposition: CO2 reduction catalysis, ACS Catal. 7 (2017) 3313–3321.
[285] J. Albo, M. Perfecto-Irigaray, G. Beobide, A. Irabien, Cu/Bi metal-organic framework-based systems for an enhanced electrochemical transformation of CO2 to alcohols, J. CO2 Util. 33 (2019) 157–165.
[286] L.R.L. Ting, O. Pique, S.Y. Lim, M. Tanhaei, F. Calle-Vallejo, B.S. Yeo, Enhancing CO2 electroreduction to ethanol on copper–silver composites by opening an alternative catalytic pathway, ACS Catal. 10 (2020) 4059–4069.
[287] L. Wan, X. Zhang, J. Cheng, R. Chen, L. Wu, J. Shi, J. Luo, Bimetallic Cu–Zn catalysts for electrochemical CO2 reduction: phase-separated versus core–shell distribution, ACS Catal. 12 (2022) 2741–2748.
[288] L. Ting, O. Piqué, S. Lim, M. Tanhaei, F. Calle-Vallejo, B. Yeo, Enhancing CO2 electroreduction to ethanol on copper-silver composites by opening an alternative catalytic pathway, ACS Catal. 10 (2020) 4059–4069.
[289] D. Gao, I. Zegkinoglou, N. Divins, F. Scholten, I. Sinev, P. Grosse, B.R. Cuenya, Plasma-Activated copper nanocube catalysts for efficient carbon dioxide electroreduction to hydrocarbons and alcohols, ACS Nano 11 (2017) 4825–4831.
[290] D. Ren, Y. Deng, A. Handoko, C. Chen, S. Malkhandi, B. Yeo, Selective electrochemical reduction of carbon dioxide to ethylene and ethanol on copper (I) oxide catalysts, ACS Catal. 5 (2015) 2814–2821.
[291] C. Yang, H. Shen, A. Guan, J. Liu, T. Li, Y. Ji, A.M. Al-Enizi, L. Zhang, L. Qian, G. Zheng, Fast cooling induced grain-boundary-rich copper oxide for electrocatalytic carbon dioxide reduction to ethanol, J. Colloid Interface Sci. 570 (2020) 375–381.
[292] D. Kim, C.S. Kley, Y. Li, P. Yang, Copper nanoparticle ensembles for selective electroreduction of CO2 to C2–C3 products, Proc .Natl. Acad .Sci 114 (2017) 10560–10565.
[293] H. Wang, Y.-K. Tzeng, Y. Ji, Y. Li, J. Li, X. Zheng, A. Yang, Y. Liu, Y. Gong, L. Cai, Synergistic enhancement of electrocatalytic CO2 reduction to C2 oxygenates at nitrogen-doped nanodiamonds/Cu interface, Nat. Nanotechnol. 15 (2020) 131–137.
[294] Z. Chen, T. Wang, B. Liu, D. Cheng, C. Hu, G. Zhang, W. Zhu, H. Wang, Z.-J. Zhao, J. Gong, Grain-boundary-rich copper for efficient solar-driven electrochemical CO2 reduction to ethylene and ethanol, J. Am. Chem. Soc. 142 (2020) 6878–6883.
[295] Z. Tan, J. Zhang, Y. Yang, J. Zhong, Y. Zhao, J. Hu, B. Han, Z. Chen, Alkaline ionic liquid microphase promotes deep reduction of CO2 on copper, J. Am. Chem. Soc. 145 (2023) 21983–21990.
[296] Controllable Hydrocarbon Formation from the Electrochemical Reduction of CO2 over Cu Nanowire Arrays.
[297] Yang, Ki Dong, et al., Morphology-directed selective production of ethylene or ethane from CO2 on a Cu mesopore electrode, Angewandte Chemie 129 (3) (2017) 814–818.